COUPLED INTEGRAL EQUATION SOLUTION FOR TWO DIMENSIONAL BISTATIC TE SCATTER FROM A CONDUCTING CAVITY-BACKED INFINITE PLANE

THESIS

Ronald R. Fairbanks, B.S.E.E
Captain, USAF
AFIT/MA/GE/88D-1

DEPARTMENT OF THE AIR FORCE
AIR UNIVERSITY
AIR FORCE INSTITUTE OF TECHNOLOGY
Wright-Patterson Air Force Base, Ohio

AFIT/MA/GE/88D-1

COUPLED INTEGRAL EQUATION SOLUTION FOR TWO DIMENSIONAL BISTATIC TE SCATTER FROM A CONDUCTING CAVITY-BACKED INFINITE PLANE

THESIS

Ronald R. Fairbanks, B.S.E.E
Captain, USAF
AFIT/MA/GE/88D-1

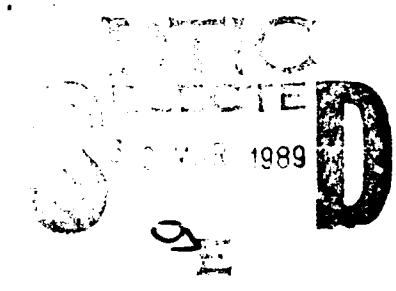

Approved For Public Release; Distribution Unlimited

AFIT/MA/GE/88D-1

Coupled Integral Equation Solution for Two Dimensional Bistatic TE Scatter From a Conducting Cavity-Backed Infinite Plane

THESIS

Presented to the Faculty of the School of Engineering

of the Air Force Institute of Technology

Air University

In Partial Fulfillment

of the Requirements for the Degree of

Master of Science in Electrical Engineering

Ronald R. Fairbanks, B.S.

Captain, USAF

December 1988

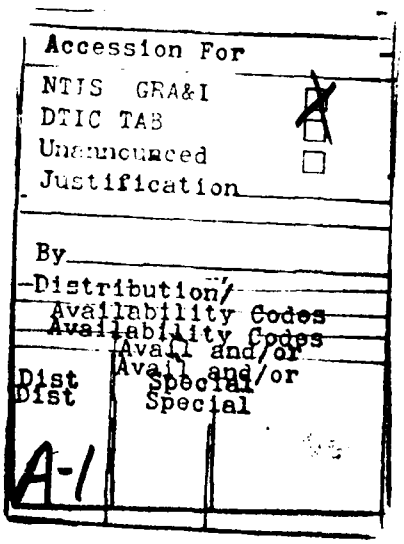

Approved for Public Release; distribution unlimited

Preface

The purpose of this thesis was to derive a set of equations that exactly determine the scattered EM fields from a cavity in an infinite conducting plane. The chosen approach was to use a set of integral equations for the field components inside the cavity and a set of integral equations for the field components outside the cavity and couple them together at the junction. A Green's function with Neumann boundary conditions was used outside the cavity. The thesis contains derivations of all the major equations used.

Three people gave me extensive mathematical consultation during the preparation of the thesis and I want to thank them for their contributions. They are: the sponsor, Dr. Arthur Yaghjian, without whom the singularities would not have been properly evaluated; Lt Col Baker, one of AFIT's finest instructors, who provided insight to several mathematical peculiarities within the thesis; and especially my advisor, Capt Greg Warhola, without whom this thesis may not have been completed error free. Capt Warhola's hard work and dedication and persistance upon perfection took their toll, but will always be remembered and appreciated.

I also wish to thank my parents who were the major contributors towards my bachelor's degree; I couldn't have done this if I hadn't earned my BSEE.

I especially want to thank the only person who gave more

than I did toward the completion of this thesis. The sacrifices and understanding my wife, Tina, contributed during this work are indescribable and her support kept me going.

Table of Contents

List of Figures

List of Figures Continued

List of Figures Continued

List of Figures Continued

List of Figures Continued

List of Tables

Abstract

The purpose of this thesis is to determine the scattered electromagnetic fields and radar cross section from a two-dimensional cavity in a perfectly electric conducting infinite plane. This is accomplished by deriving a coupled set of Fredholm integral equations of the second kind. A set of integral equations outside the cavity and a set of integral equations inside the cavity are coupled together at the interface. The Fredholm integral equations of the second kind for the outside of the cavity use a Green's function with Neumann boundary conditions to avoid an integration over the infinite plane for a transverse electric incident plane wave. An example problem is introduced and numerically solved to test the application of the newly derived equations.

Coupled Integral Equation Solutions for Two-Dimensional Bistatic TE Scatter From a Conducting Cavity-Backed Infinite Plane

I. Introduction

Electromagnetic (EM) waves exhibit the phenomena of reflection, transmission, absorption, interference, diffraction, and refraction (13, 11, 4). In free space, absorption, diffraction, and refraction may be ignored (14). With this single and precise assumption, EM energy (such as a radar pulse) propagates through space until it impinges upon an obstruction (such as an aircraft) in its path. The obstruction scatters the electromagnetic wave in many directions and the energy associated with the scattered portion of the EM wave then propagates in new directions. Though the energy is normally scattered in all directions, it is desirable to know the amount of energy scattered in various directions. Solutions to this problem in the form of the scattered electric and magnetic fields are of interest to many sectors of today's society, particularly to the military (6).

It is not a trivial problem to determine the exact solution for the scattered EM fields. The size and shape of the obstruction must be taken into account when solving for the scattered fields, but these are only two of the possible variables. The object's conductivity, the incident wave's frequency, and the permeability and permittivity of the space

surrounding the object all contribute to the solution of the scattered fields (6).

Closed form solutions of the EM scattering problem can be generated for only a very limited class of problems (12, 14). For general scattering objects, however, an approximate solution is needed to predict the scattered fields. With high speed computer systems (or low cost personal type computers) good numerical approximations are obtainable by solving the full scattered field equations (12).

The Problem

Modern jet aircraft use air intake and exhaust structures that can appear (to the EM wave) to be open ended wave guides or apertures. If one wishes to reduce the energy backscattered by these apertures, it is necessary to determine both the amount of EM energy scattered by them and the directions into which the energy is scattered. This thesis makes another step toward understanding this three-dimensional problem by determining the solution to a corresponding, but simpler, two-dimensional problem (26). One benefit from solving this simpler problem is the two-dimensional problem can be used to approximate the scattering from gaps and cracks in panels that comprise reflector antennas and radar targets.

The associated two-dimensional model of the problem that will be solved in this thesis is the determination of the bistatic EM fields scattered from an infinite plane containing a cavity (26). For example, if in three dimensions the

infinite plane is the xz plane and the coordinate axes are placed as in Figure 1, then the cross-sectional shape of the cavity is constant along the z-axis. This is the specific problem ultimately considered in this thesis.

Integral equations can be derived to describe the electromagnetic fields scattered in a problem of this type. These equations are developed in this thesis. Once derived, computer software will be described which numerically implements this formulation. In particular, predictions for two-dimensional scattering from an infinite plane containing a rectangular shaped cavity will be obtained.

Scope of the Problem

It is desired to determine the EM fields scattered from a perfectly electric conducting infinite plane containing a cavity of arbitrary cross section (i.e. a generic cavity). Surface integral equations have been derived by Stratton, Poggio and Miller and others (21, 15, 23, 24) that provide for the solution of scattered fields from objects of finite size using a free space Green's function as the kernel. To avoid integrations over the unbounded infinite plane, Green's functions which satisfy Dirichlet boundary conditions (the Green's function vanishes at the boundary) or Neumann boundary conditions (the normal derivative of the Green's function vanishes at the boundary) can be employed.

The integral equations using a Green's function with Neumann boundary equations will be derived and used in this

thesis. Once derived, these equations will be used to solve an example problem: a two dimensional rectangular cavity.

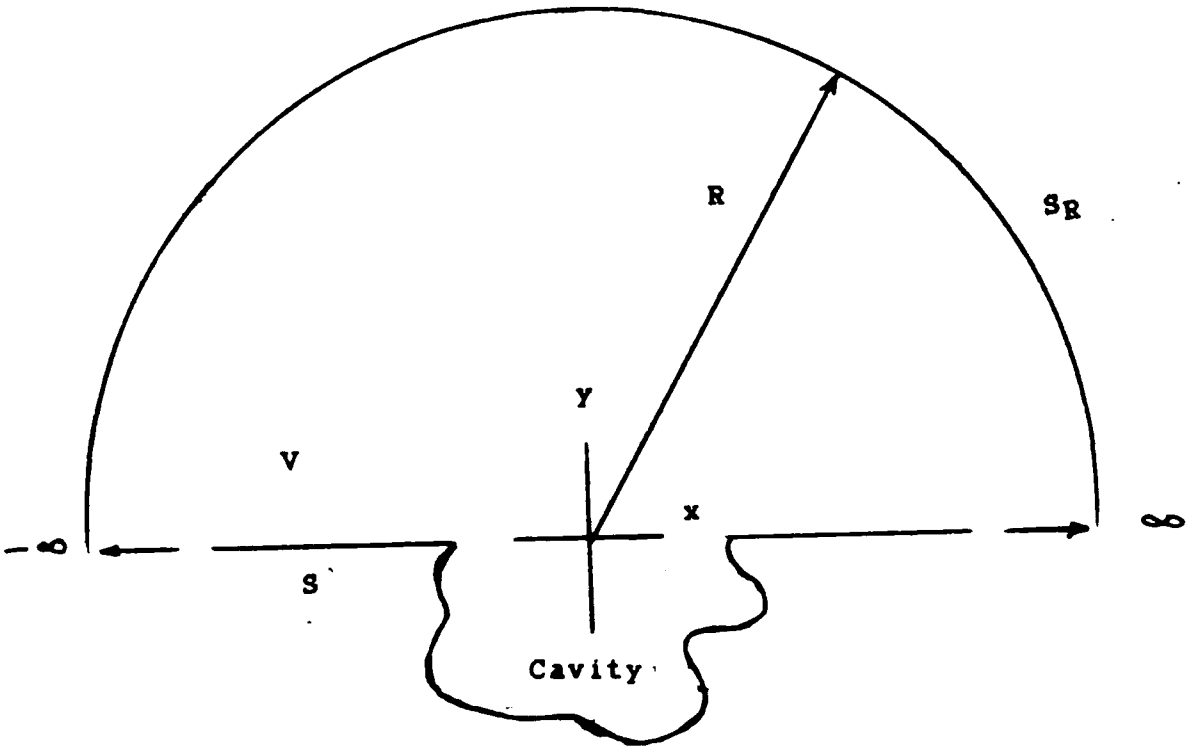

Figure 1. Cross Sectional View of a Generic Cavity in an Infinite Plane Closed at Infinity.

Assumptions

The problem is simplified by assuming that the infinite plane is a perfect electric conductor (i.e. the conductivity of the plane is infinite). The plane is suspended in free space where the incident wave will not be impeded (i.e. the relative permeability, μ_r, and the relative permittivity, ϵ_r are both equal to one, $\mu_r \equiv \epsilon_r \equiv 1$). Though a perfect conductor of this type does not actually exist, the mathematical assumption of a PEC (perfect electric conductor) is a good approximation and the amount of work involved in assuming the material is not perfect is considerably more difficult (6).

The assumption that the relative permeability and permittivity are exactly equal to one means that the medium through which the EM wave propagates does not impede the wave (14). In actuality, ϵ_r for air is approximately 1.0006 at atmospheric pressure and 24°C (11:58) and μ_r for air is approximately 1.0000004 at the same conditions (11:216). Since both ϵ_r and μ_r are functions of temperature, pressure, and material, they will be functions of position in space. It is not possible to determine the exact permittivity and permeability for all places at all times but it is known that for air, they will be very close to one (14).

One final assumption for solving this problem is that the source of EM waves is far enough away that the wave front is planar as it impinges upon the plane.

Approach

The general geometry initially considered in this problem is a three dimensional generic cavity in a PEC (perfectly electrically conducting) infinite plane (see Figure 1). Within the thesis the specific geometry of a two-dimensional rectangular channel is introduced as the cavity, the integral equations inside and outside of the cavity are then solved to produce the fields scattered from the channel. For purposes of derivation, the cavity will be considered generic. The chosen approach to solving this problem is to separate the upper half space from the cavity and allow the two regions to be coupled at their common boundary, hereafter referred to as the "aperture". This method was introduced by Harrington and Mautz in 1976 and lends itself well to this type of problem (5).

By considering the scatterer to be a PEC plane with a cavity, two sets of equations need to be derived: one set for the half space above the PEC plane and one set for the cavity. The first step used to solve this problem was to derive from Maxwell's Equations a set of integral equations needed to determine currents (field components) in the aperture and along the cavity walls. From the currents, the scattered fields are obtained by an integration. An integral equation formulation was used because it reduces, by one dimension, the dimensionality of the problem and represents an exact solution. Other theoretical approaches such as physical optics,

geometrical optics, and the geometrical theory of diffraction, etc., require major analytic approximations (6, 7, 18, 19).

Once the integral equations are derived, a computer program is introduced that solves the equations for the unknown magnetic surface current density, $\underline{M}$, from various aspect angles and scattered angles. With the magnetic surface current density in hand, the scattered fields are then determined by an integration of $\underline{M}$. An equation for the RCS (radar cross section) is then derived and evaluated to determine the RCS of the channel.

With the integral equation formulation and the computer program, data is generated and plotted to show the RCS as a function of several variables for a representative chosen geometry: that of a two-dimensional rectangular cavity. The AFIT computer facilities were used to run the computer program. A personal computer was used to plot the data generated from the computer program.

Before preceding to the development of the equations, a summarization of the current knowledge is necessary.

Summary of Current Knowledge

Integral equations for finding the electric and magnetic fields scattered from a three-dimensional object have been derived and used for several problems. Two of the most notable derivations are by J.A. Stratton (20) and Poggio and Miller (15). These equations are normally called the Electric Field

Integral Equation (EFIE) and the Magnetic Field Integral Equation (MFIE) (19).

In three dimensions, both the EFIE and the MFIE contain a singular kernel in convergent integrals; however the MFIE is normally more numerically stable and slightly less complicated to implement (22). For open conductors such as an antenna aperture, the MFIE becomes degenerate and the EFIE is normally used. In the early 1980's the EFIE and the MFIE were combined or augmented to eliminate spurious resonances which can pollute the solution of an exterior scattering problem (24, 23). These integral equations may be used to determine the scattered EM fields for many types of problems.

It has been possible to determine the scattered fields from some of the simplest geometries since just after the introduction of Maxwell's electromagnetic field equations (11). Only recently, high speed computers have allowed the use of the MFIE and EFIE to determine the fields scattered from more complicated geometries (12:2). Several computer codes have been written using the MFIE or EFIE to help determine the fields scattered from some specific geometries (6). Using these codes, the scattered fields from several geometries have been determined. Most of these are simple three dimensional bodies. The open literature does not provide any solutions to most of the more complex shapes. Some representations of scattered fields that have been obtained using surface integral equations are:

1) The perfectly conducting cube for monostatic scattering using both the MFIE and the EFIE (25).

2) An infinitely long, perfectly conducting circular cylinder for monostatic scattering using both the EFIE and the MFIE (21).

3) An infinite perfectly conducting half plane with short "bumps" (16) for monostatic scattering and using only the EFIE.

4) Various generic targets within stratified media (as opposed to free space) using only the MFIE (17).

5) Perfectly conducting bodies of revolution using both the EFIE and the MFIE in the monostatic case (8).

In order to use the MFIE or EFIE in our stated problem of interest, either an integration on an unbounded domain is necessary or else an approximation must be made by truncating the plane at some finite distance from the cavity. The necessary approximation is not considered valid in an "exact" solution. Therefore, a set of equations are derived herein that avoids the unbounded domain without the use of an approximation.

Preview

A coupled set of Fredholm integral equations of the second kind are derived in Chapter 2. Once obtained, these integral equations will be simplified in Chapter 3 by reducing them to two-dimensional space and providing a specific incident field. Chapter 4 provides a way to solve the coupled set of Fredholm integral equations numerically; the Method of Moments is used. In Chapter 5, a specific cavity is introduced to test

the equations. The specific cavity is a two-dimensional rectangular channel. A convenient representation of the scattered fields is the RCS (radar cross section) and an equation for RCS is derived in Chapter 6. Chapter 7 provides a quick description of the computer program used to approximate the equations derived in Chapters 2 and 3 to determine the RCS derived in Chapter 6. Chapter 8 gives the results of the tested cavity and Chapter 9 gives the overall conclusions and recommendations for future work. Three appendices are included at the end of the thesis. Appendix A contains the computer program written to numerically solve the integral equations and eventually determine the RCS from the test (rectangular) cavity. Appendix B consists of some of the output from running the computer program. A description of a model designed and built to further test the equations by making laboratory measurements of the scattered fields is in Appendix C.

The first major step, however is to derive the coupled set of Fredholm integral equations needed to solve for the surface currents and charges, and this is the subject of the next chapter.

II. Derivation of the Integral Equations

The Upper Half Space Region

The propagation of electromagnetic energy and the fundamental laws of electromagnetics are governed by Maxwell's equations (4, 11, 14, 20). To determine the magnetic and electric fields at any point $\underline{x} = (x, y, z)$ at a time, t, one may begin with Maxwell's equations and derive a more useful set of equations for the particular problem being considered (20). For this reason, the integral equations used to solve the stated problem will be derived from Maxwell's equations.

In time harmonic form with $\exp(-i\omega t)$ time dependence, Maxwell's equations are (11:376):

$$\nabla \times \underline{E} = i\omega\mu\underline{H} - \underline{I} \tag{1}$$

$$\nabla \times \underline{H} = -i\omega\epsilon\underline{E} + \underline{J} \tag{2}$$

$$\nabla \cdot \underline{E} = \rho/\epsilon \tag{3}$$

$$\nabla \cdot \underline{H} = \rho_m/\mu \tag{4}$$

where

$\underline{E}$ = Electric Field Vector
$\underline{H}$ = Magnetic Field Vector
$\underline{I}$ = Magnetic Current Volume Density
$\underline{J}$ = Electric Current Volume Density
ω = Operating Angular Frequency
μ = permeability of the medium
ϵ = permittivity of the medium
ρ = Electric Charge Volume Density
ρ_m = Magnetic Charge Volume Density

All of the fields ($\underline{E}$ and $\underline{H}$), currents ($\underline{I}$ and $\underline{J}$), and charges (ρ and ρ_m) in Eqs (1) through (4) are functions of position (i.e. $\underline{E}=\underline{E}(x, y, z)=\underline{E}(\underline{x})$, $\underline{H}=\underline{H}(x, y, z)=\underline{H}(\underline{x})$, etc.) For simplicity, the position variables will not be indicated until it is necessary to distinguish between separate positions in space.

At this point it should be noted that the magnetic current, $\underline{I}$, and the magnetic charge, ρ_m, are fictitious quantities that can exist mathematically, but have not yet been physically measured. The electric and magnetic fields in Eqs (1) through (4) are considered generated from the sources $\underline{J}$, $\underline{I}$, ρ_m, and ρ. The continuity equations relating currents and charges of Eqs (1) through (4) are (20:464):

$$\nabla \cdot \underline{J} = i\omega\rho \tag{5}$$

and

$$\nabla \cdot \underline{I} = i\omega\rho_m \tag{6}$$

Taking the curl of Eq (1) yields

$$\nabla \times \nabla \times \underline{E} = i\omega\mu(\nabla \times \underline{H}) - \nabla \times \underline{I} \tag{7}$$

Using Eq (2) in Eq (7) and simplifying the result gives an equation for the electric field without the magnetic field.

$$\nabla \times \nabla \times \underline{E} - k^2 \underline{E} = i\omega\mu \underline{J} - \nabla \times \underline{I} \tag{8}$$

where

$$k^2 = \omega^2\epsilon\mu$$

Similarly for the magnetic field,

$$\nabla \times \nabla \times \underline{H} - k^2 \underline{H} = i\omega\epsilon \underline{I} - \nabla \times \underline{J} \qquad (9)$$

An application of a vector Green's identity with the proper Kernel (or Green's Function) will yield two integral representations of the electric and magnetic fields in terms of volume and surface currents and charge densities. From these, integral equations are derived to obtain the surface current and charge densities. The vector analog to the scaler Green's second identity is (20:464):

$$\iiint_V (\underline{Q} \cdot \nabla \times \nabla \times \underline{P} - \underline{P} \cdot \nabla \times \nabla \times \underline{Q}) \, dv$$

$$= \iint_S (\underline{P} \times \nabla \times \underline{Q} - \underline{Q} \times \nabla \times \underline{P}) \cdot \hat{n} \, ds \qquad (10)$$

where $\hat{n}$ is the unit normal pointing out of a regular region, V, bounded by the surface, S. Eq (10) is valid for any vector functions of position $\underline{P}$ and $\underline{Q}$ having the proper regularity. Both $\underline{P}$ and $\underline{Q}$ need to be twice continuously differentiable on the surface and within the volume being considered (15:161).

For the vector $\underline{P}$, either $\underline{E}$ or $\underline{H}$ is chosen. Choosing the most advantageous vector $\underline{Q}$ depends upon the geometry being considered. A generic closed surface in free space lends itself well to the free space Green's function for $\underline{Q}$.

That is:

$$\underline{Q} = \bar{\bar{Q}}(\underline{x};\underline{x}')\ \hat{a} \tag{11}$$

where

$$\bar{\bar{Q}}(\underline{x};\underline{x}') = \frac{\exp(ikr)}{r} \tag{12}$$

$$r = |\ \underline{x} - \underline{x}'\ |$$

$$= \left[(x-x')^2 + (y-y')^2 + (z-z')^2\right]^{1/2} \tag{13}$$

$\hat{a}$ = arbitrary unit vector

The unit vector, $\hat{a}$, is arbitrary for two reasons: the free space Green's function is omnidirectional and the vector is common to all of the elements in Eq (10) (20:251-252). For the half space above the PEC plane, the vector $\underline{Q}$ is chosen to be the half space Green's function:

$$\underline{Q} = \bar{\bar{Q}}(\underline{x};\underline{x}')\ \hat{a} + \bar{\bar{Q}}(\underline{x};\tilde{\underline{x}}')\ \hat{a} = \bar{\bar{G}}(\underline{x};\underline{x}')\ \hat{a} \tag{14}$$

where

$$\tilde{\underline{x}}' = (x', -y', z') \tag{15}$$

and $\bar{\bar{Q}}(\underline{x};\underline{x}')$ is as defined in Eq (12).

Using Eq (14) for $\underline{Q}$ and $\underline{E}(\underline{x})$ for $\underline{P}$ in Eq (10) yields:

$$\iiint_V \left[G(\underline{x};\underline{x}')\hat{a} \cdot \nabla' \times \nabla' \times \underline{E}(\underline{x}') - \underline{E}(\underline{x}') \cdot \nabla' \times \nabla' \times G(\underline{x};\underline{x}')\hat{a} \right] dv'$$

$$= \iint_S \left[\underline{E}(\underline{x}') \times \nabla' \times G(\underline{x};\underline{x}')\hat{a} - G(\underline{x};\underline{x}')\hat{a} \times \nabla' \times \underline{E}(\underline{x}') \right] \cdot \hat{n}(\underline{x}')\, ds' \qquad (16)$$

in which ∇' represents differentiation with respect to $\underline{x}'$.

From Maxwell's equations, $\nabla' \times \underline{E}$ is known as a function of $\underline{H}$ and $\underline{I}$ and Eq (8) gives $\nabla' \times \nabla' \times \underline{E}$; the only other expressions that need to be analyzed are $\nabla' \times G(\underline{x};\underline{x}')\hat{a}$ and $\nabla' \times \nabla' \times G(\underline{x};\underline{x}')\hat{a}$. From basic vector identities:

$$\nabla' \times [G(\underline{x};\underline{x}')\hat{a}] = \nabla'[G(\underline{x};\underline{x}')] \times \hat{a} \qquad (17)$$

and

$$\nabla' \times \nabla' \times G(\underline{x};\underline{x}')\hat{a} = \nabla'[\nabla' \cdot (G(\underline{x};\underline{x}')\hat{a})] - \nabla'^2 [G(\underline{x};\underline{x}')\hat{a}] \qquad (18)$$

Dealing strictly with Eq (17) and the integrand in the left side of Eq (16) (recall that $\hat{a}$ is a constant unit vector):

$$[(\underline{E} \times \nabla' \times (G\,\hat{a})] \cdot \hat{n} = \hat{a} \cdot [(\hat{n} \times \underline{E}) \times \nabla' G] \qquad (19)$$

and

$$[G(\underline{x};\underline{x}')\hat{a} \times \nabla' \times \underline{E}(\underline{x}')] \cdot \hat{n} = \hat{a} \cdot [\nabla' \times \underline{E}(\underline{x}') \times \hat{n}]\, G(\underline{x};\underline{x}') \qquad (20)$$

Using Eq (1) in Eq (20) for $\nabla' \times \underline{E}(\underline{x}')$ and simplifying the result yields:

$$-G(\underline{x};\underline{x}')\hat{a} \times \nabla' \times \underline{E}(\underline{x}') \cdot \hat{n} = \hat{a} \cdot i\omega\mu[\hat{n} \times \underline{H}(\underline{x}')]\, G(\underline{x};\underline{x}') - \hat{a} \cdot [\hat{n} \times \underline{I}(\underline{x}')]\, G(\underline{x};\underline{x}') \qquad (21)$$

To further evaluate Eqs (18) and (19), it is necessary to determine $\nabla' G(\underline{x};\underline{x}')$ and $\nabla'^2 G(\underline{x};\underline{x}')$.

$$\nabla' G(\underline{x};\underline{x}') = \frac{\partial G(\underline{x};\underline{x}')}{\partial x'} \hat{x} + \frac{\partial G(\underline{x};\underline{x}')}{\partial y'} \hat{y} + \frac{\partial G(\underline{x};\underline{x}')}{\partial z'} \hat{z} \qquad (22)$$

$$= \left[\frac{d[\exp(ikr)]/r}{dr}\right]\left[\frac{\partial r}{\partial x'}\hat{x} + \frac{\partial r}{\partial y'}\hat{y} + \frac{\partial r}{\partial z'}\hat{z}\right]$$

$$+ \left[\frac{d[\exp(ik\tilde{r})]/\tilde{r}}{d\tilde{r}}\right]\left[\frac{\partial \tilde{r}}{\partial x'}\hat{x} + \frac{\partial \tilde{r}}{\partial y'}\hat{y} + \frac{\partial \tilde{r}}{\partial z'}\hat{z}\right] \qquad (23)$$

Breaking Eq (23) into its prominent pieces yields:

$$\frac{d[\exp(ikr)]/r}{dr} = \left[ik - \frac{1}{r}\right] Q(\underline{x};\underline{x}') \qquad (24)$$

$$\frac{d[\exp(ik\tilde{r})]/\tilde{r}}{d\tilde{r}} = \left[ik - \frac{1}{\tilde{r}}\right] Q(\underline{x};\tilde{\underline{x}}') \qquad (25)$$

and continuing,

$$\frac{\partial r}{\partial x'} = -\frac{(x-x')}{r} \tag{26}$$

$$\frac{\partial r}{\partial z'} = -\frac{(z-z')}{r} \tag{27}$$

where, in Eqs (26) and (27), r may replaced everywhere by $\tilde{r}$.

Continuing,

$$\frac{\partial r}{\partial y'} = -\frac{(y-y')}{r} \tag{28}$$

and

$$\frac{\partial \tilde{r}}{\partial y'} = \frac{(y+y')}{\tilde{r}} \tag{29}$$

Thus, combining Eqs (24) through (29) into Eq (23) yields:

$$\nabla' G(\underline{x};\underline{x}') = \left[ik - \frac{1}{r} \right] \frac{\bar{Q}(\underline{x};\underline{x}')}{r} \underline{r} + \left[ik - \frac{1}{\tilde{r}} \right] \frac{\bar{Q}(\underline{x};\tilde{\underline{x}})}{\tilde{r}} \left[2(y+y')\,\hat{y} - \underline{\tilde{r}} \right] \tag{30}$$

where

$$\underline{r} = \underline{x} - \underline{x}' = (x-x')\hat{x} + (y-y')\hat{y} + (z-z')\hat{z}$$

$$\underline{\tilde{r}} = \underline{x} - \tilde{\underline{x}}' = (x-x')\hat{x} + (y+y')\hat{y} + (z-z')\hat{z}$$

Similarly, without displaying all of the steps, the equation for $\nabla'^2 G(\underline{x};\underline{x}')$ is given by:

$$\nabla'^2[G(\underline{x};\underline{x}')\hat{a}] = \left[\frac{\partial^2 G(\underline{x};\underline{x}')}{\partial x'^2} + \frac{\partial^2 G(\underline{x};\underline{x}')}{\partial y'^2} + \frac{\partial^2 G(\underline{x};\underline{x}')}{\partial z'^2}\right]\hat{a}$$

$$= \left[\frac{\partial^2 \bar{Q}(\underline{x};\underline{x}')}{\partial x'^2} + \frac{\partial^2 \bar{Q}(\underline{x};\underline{x}')}{\partial y'^2} + \frac{\partial^2 \bar{Q}(\underline{x};\underline{x}')}{\partial z'^2}\right]\hat{a}$$

$$+ \left[\frac{\partial^2 \bar{Q}(\underline{x};\tilde{\underline{x}}')}{\partial x'^2} + \frac{\partial^2 \bar{Q}(\underline{x};\tilde{\underline{x}}')}{\partial y'^2} + \frac{\partial^2 \bar{Q}(\underline{x};\tilde{\underline{x}}')}{\partial z'^2}\right]\hat{a} \qquad (31)$$

since $\hat{a}$ is a constant unit vector.

Now,

$$\frac{\partial^2 \bar{Q}(\underline{x};\underline{x}')}{\partial x'^2} = \left[\frac{\partial r}{\partial x'}\right]^2 \left[\frac{\partial^2 \bar{Q}(\underline{x};\underline{x}')}{\partial r^2}\right] + \frac{\partial \bar{Q}(\underline{x};\underline{x}')}{\partial r}\frac{\partial^2 r}{\partial x'^2} \qquad (32)$$

Equations for the second derivatives of $\bar{Q}(\underline{x};\underline{x}')$ with respect to y' and z' and the second derivatives of $\bar{Q}(\underline{x};\tilde{\underline{x}}')$ with respect to x', y' and z' are all similar to Eq (32).

The component parts of Eq (32) are

$$\frac{\partial r}{\partial x'} = -\frac{(x-x')}{r} \qquad (33)$$

$$\frac{\partial^2 r}{\partial x'^2} = \frac{1}{r} - \frac{(x-x')^2}{r^3} \qquad (34)$$

and

$$\frac{\partial \bar{Q}(\underline{x};\underline{x}')}{\partial r} = \left[ik - \frac{1}{r} \right] \bar{Q}(\underline{x};\underline{x}') \tag{35}$$

and, finally,

$$\frac{\partial^2 \bar{Q}(\underline{x};\underline{x}')}{\partial r^2} = \left[ik - \frac{1}{r} \right]^2 \bar{Q}(\underline{x};\underline{x}') + \frac{\bar{Q}(\underline{x};\underline{x}')}{r^2} \tag{36}$$

Putting Eqs (33) through (36) into Eq (32) and simplifying the result gives:

$$\frac{\partial^2 \bar{Q}(\underline{x};\underline{x}')}{\partial x'^2} = \bar{Q}(\underline{x};\underline{x}') \left[-k^2 \frac{(x-x')^2}{r^2} - 3ik \frac{(x-x')^2}{r^3} + 3 \frac{(x-x')^2}{r^4} - \frac{1}{r^2} + \frac{ik}{r} \right] \tag{37}$$

Similarly,

$$\frac{\partial^2 \bar{Q}(\underline{x};\underline{x}')}{\partial y'^2} = \bar{Q}(\underline{x};\underline{x}') \left[-k^2 \frac{(y-y')^2}{r^2} - 3ik \frac{(y-y')^2}{r^3} + 3 \frac{(y-y')^2}{r^4} - \frac{1}{r^2} + \frac{ik}{r} \right] \tag{38}$$

and

$$\frac{\partial^2 \bar{Q}(\underline{x};\underline{x}')}{\partial z'^2} = \bar{Q}(\underline{x};\underline{x}') \left[-k^2 \frac{(z-z')^2}{r^2} - 3ik \frac{(z-z')^2}{r^3} + 3 \frac{(z-z')^2}{r^4} - \frac{1}{r^2} + \frac{ik}{r} \right] \quad (39)$$

for the y' and z' derivatives of $\bar{Q}(\underline{x};\underline{x}')$.

The second derivatives of $\bar{Q}(\underline{x};\tilde{\underline{x}}')$ with respect to x', y', and z' are nearly identical to Eqs (37), (38), and (39) respectively. These derivatives are:

$$\frac{\partial^2 \bar{Q}(\underline{x};\tilde{\underline{x}}')}{\partial x'^2} = \bar{Q}(\underline{x};\tilde{\underline{x}}') \left[-k^2 \frac{(x-x')^2}{\tilde{r}^2} - 3ik \frac{(x-x')^2}{\tilde{r}^3} + 3 \frac{(x-x')^2}{\tilde{r}^4} - \frac{1}{\tilde{r}^2} + \frac{ik}{\tilde{r}} \right] \quad (40)$$

$$\frac{\partial^2 \bar{Q}(\underline{x};\tilde{\underline{x}}')}{\partial y'^2} = \bar{Q}(\underline{x};\tilde{\underline{x}}') \left[-k^2 \frac{(y+y')^2}{\tilde{r}^2} - 3ik \frac{(y+y')^2}{\tilde{r}^3} + 3 \frac{(y+y')^2}{\tilde{r}^4} - \frac{1}{\tilde{r}^2} + \frac{ik}{\tilde{r}} \right] \quad (41)$$

$$\frac{\partial^2 \bar{Q}(\underline{x};\tilde{\underline{x}}')}{\partial z'^2} = \bar{Q}(\underline{x};\tilde{\underline{x}}') \left[-k^2 \frac{(z-z')^2}{\tilde{r}^2} - 3ik \frac{(z-z')^2}{\tilde{r}^3} + 3 \frac{(z-z')^2}{\tilde{r}^4} - \frac{1}{\tilde{r}^2} + \frac{ik}{\tilde{r}} \right] \quad (42)$$

Using Eqs (37) through (42) in Eq (31) and noting that $(x-x')^2 + (y-y')^2 + (z-z')^2 = r^2$ and $(x-x')^2 + (y+y')^2 + (z-z') = \tilde{r}^2$, gives the final, simple, result for $\nabla'^2 G(\underline{x};\underline{x}')$ as:

$$\nabla'^2 G(\underline{x};\underline{x}') = -k^2 \bar{g}(\underline{x};\underline{x}') - k^2 \bar{g}(\underline{x};\tilde{\underline{x}}') = -k^2 G(\underline{x};\underline{x}')$$
$$\text{for } \underline{x} \neq \underline{x}' \text{ and } \underline{x} \neq \tilde{\underline{x}}' \qquad (43)$$

Eq (43) is an important result. It allows the use of the half space Green's function, $G(\underline{x};\underline{x}')$, in the same equations used by J.A. Stratton in his derivation of the electric and magnetic field integral representations (20:465). The Stratton equations were developed with the free space Green's function, $\bar{g}(\underline{x};\underline{x}')$ which satisfies $\nabla' \times \nabla' \times \bar{g}\hat{a} = k^2 \bar{g}\hat{a} + \nabla'(\hat{a}\cdot\nabla'\bar{g})$ (20:465). Stratton's results are based on this relation which is now also satisfied by G as seen by combining Eq (43) with Eq (18):

$$\nabla' \times \nabla' \times G(\underline{x};\underline{x}')\hat{a} = \hat{a}k^2 G(\underline{x};\underline{x}') + \nabla'[\hat{a}\cdot\nabla' G(\underline{x};\underline{x}')]$$
$$\text{for } \underline{x} \neq \underline{x}' \text{ and } \underline{x} \neq \tilde{\underline{x}}' \qquad (44)$$

Using the results given in Eq (44) and the development of Eq (8), the two components for the right hand side of Eq (16) can now be cast in a more useful form. In particular,

$$G(\underline{x};\underline{x}')\hat{a} \cdot \nabla'x\ \nabla'x\ \underline{E}(\underline{x}') - \underline{E}(\underline{x}') \cdot \nabla'x\ \nabla'x\ G(\underline{x};\underline{x}')\hat{a}$$

$$= \hat{a}\cdot\left[i\omega\mu\underline{J}(\underline{x}') - \nabla'x\ \underline{I}(\underline{x}') + k^2\underline{E}(\underline{x}')\right]$$

$$- \hat{a}\cdot\left[k^2\underline{E}(\underline{x}') - \nabla G(\underline{x};\underline{x}')\ [\nabla'\cdot\ \underline{E}(\underline{x}')]\right]$$

$$+ \nabla'\cdot\ \underline{E}(\underline{x}')\ [\hat{a}\cdot\nabla'G(\underline{x};\underline{x}')] \qquad (45)$$

Eq (3) and Eq (45) are used in Eq (16) along with the following identity:

$$\iiint_V [\nabla'x\ \underline{I}(\underline{x}')]\ G(\underline{x};\underline{x}')\ dv' = \iint_S [\hat{n}(\underline{x}')\ x\ \underline{I}(\underline{x}')]\ G(\underline{x};\underline{x}')\ ds'$$

$$+ \iiint_V \underline{I}(\underline{x}')\ x\ \nabla'G(\underline{x};\underline{x}')\ dv' \qquad (46)$$

An application of the divergence theorem,

$$\iiint_V \nabla \cdot \underline{F}\ dv = \iint_S \underline{F}\ .\ \hat{n}(\underline{x}')\ ds' \qquad (47)$$

to that result yields:

$$\iiint_V \left[i\omega\mu\underline{J}(\underline{x}')G(\underline{x};\underline{x}') - [\nabla'x\ \underline{I}(\underline{x}')]G(\underline{x};\underline{x}')\right.$$

$$\left. + G(\underline{x};\underline{x}')\ \frac{\rho(\underline{x}')}{\epsilon}\right]\ dv'$$

$$= \iint_S \left[i\omega\mu[\hat{n}(\underline{x}')\ x\ \underline{H}(\underline{x}')]G(\underline{x};\underline{x}') + [\hat{n}(\underline{x}')\ x\ \underline{E}(\underline{x}')]\ x\ \nabla'G(\underline{x};\underline{x}')\right.$$

$$\left. +\ [\hat{n}(\underline{x}')\cdot\underline{E}(\underline{x}')]\ \nabla'G(\underline{x};\underline{x}')\right]\ ds' \qquad (48)$$

where the common factor of the arbitrary constant vector, $\hat{a}$ has been removed. (See Eqs (47), (45), (19), and (21).)

The integrand of Eq (48) is singular at $r = 0$, (i.e. when $(x, y, z) = (x', y', z')$). This violates the conditions for use of the vector Green's identity, Eq (10), unless the singular point is excluded from the volume, V. This singularity actually helps in the development of solvable equations. A small sphere of radius r_1 is circumscribed about

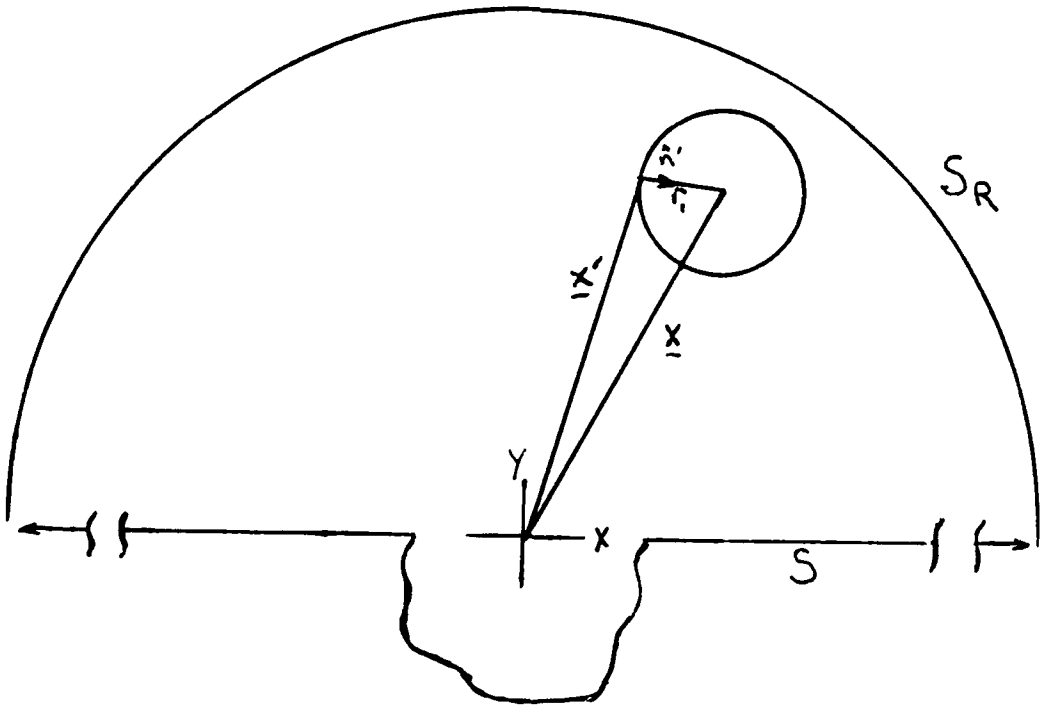

Figure 2. Exclusion of the Singularity by Enclosing It Within a Small Sphere of Radius r_1.

the point (x, y, z) (see Figure 2) to exclude this point from V. The outward pointing normal at the surface of this sphere points toward the center of the sphere (out of the volume) and along the radius, r_1. For points, $\underline{x}'$ on this small spherical surface

$$\hat{n}(\underline{x}') = \underline{r}/r$$

An element of surface area on the sphere is

$$ds' = r^2 \sin(\theta) d\theta d\varphi$$

with spherical coordinate system angles θ and φ. Using Eq (30) for $V'G(\underline{x};\underline{x}')$ and taking the limit as r_1 shrinks to zero, the integral over the surface of the sphere is:

$$\int_0^{2\pi}\int_0^{\pi} \Big[[\hat{n}(\underline{x}') \times \underline{E}(\underline{x}')] \times \hat{n}(\underline{x}') + [\hat{n}(\underline{x}')\cdot\underline{E}(\underline{x}')]\hat{n}(\underline{x}') \Big]\Big[\frac{1}{r_1} - ik \Big]\frac{\exp(ikr_1)}{r_1} r_1^2 \sin(\theta) d\theta d\varphi + O(r_1) \qquad (49)$$

which yields $4\pi\, \underline{E}(\underline{x})$ for vanishing R_1, since

$$\underline{E}(\underline{x}') = [\hat{n}(\underline{x}') \times \underline{E}(\underline{x}')] \times \hat{n}(\underline{x}') + [\hat{n}(\underline{x}')\cdot\underline{E}(\underline{x}')]\hat{n}(\underline{x}')$$

Thus, the contribution of the volume integral on the right hand side of Eq (48) is $4\pi\, \underline{E}(\underline{x})$ due to the volume integral about

the singular point. The electric field at the point $\underline{x} = (x, y, z)$ in the half space above the scatterer is given by:

$$\underline{E}(\underline{x}) = \frac{1}{4\pi} \iiint_V \left[i\omega\mu \underline{J}(\underline{x}') G(\underline{x};\underline{x}') - \underline{I}(\underline{x}') \times \nabla' G(\underline{x};\underline{x}') + \nabla' G(\underline{x};\underline{x}') \frac{\rho(\underline{x}')}{\epsilon} \right] dv'$$

$$- \frac{1}{4\pi} \iint_S \left[i\omega\mu [\hat{n}(\underline{x}') \times \underline{H}(\underline{x}')] G(\underline{x};\underline{x}') + [\hat{n}(\underline{x}') \times \underline{E}(\underline{x}')] \times \nabla' G(\underline{x};\underline{x}') + [\hat{n}(\underline{x}') \cdot \underline{E}(\underline{x}')] \nabla' G(\underline{x};\underline{x}') \right] ds' \quad (50)$$

Note that due to the singularity, the integral over the volume must be evaluated in the principle value sense, meaning that a vanishingly small spherical volume centered at $\underline{x}=\underline{x}'$ must be excluded.

With the choice of the half space Green's function as the kernel in Eq (16), the resulting equation for $\underline{E}(\underline{x})$ when $\underline{x}$ approaches the surface of the volume is the same as Eq (50), provided the surface integral is, too, a principal value integral. The volume integral remains unchanged since a small sphere can always be circumscribed about the point $\underline{x}$ as it approaches S. For the surface integration in Eq (50), a result due to Yaghjian (23, 24) is employed:

$$\lim_{x \to S} \iint_S \nabla' \bar{Q}(\underline{x};\underline{x}')ds' = \oiint_S \nabla' \bar{Q}(\underline{x};\underline{x}')ds' \pm 2\pi\hat{n}(\underline{x}') \qquad (50a)$$

where the + (-) sign corresponds to approaching S from the side into (out of) which $\hat{n}(\underline{x})$ points and the principal value integral employs a vanishingly small circular patch. For the half space Green's function, $G(\underline{x};\underline{x}')$, contributions with both signs cancel, leaving Eq (50) intact for $\underline{x}$ approaching S, with all integrals evaluated in the principal value sense.

A similar procedure may be used to find an equation for the magnetic field, $\underline{H}(\underline{x})$, where $\underline{H}(\underline{x}')$ is used for the $\underline{P}$ vector of Eq (10); an equation similar to Eq (50) may be developed. A decidedly simpler procedure is to use the concept of duality with Eq (50) (4). Based on the symmetry of Maxwell's Equations, Table I shows the quantities to be interchanged from Eq (50) to get an equation for $\underline{H}(\underline{x})$.

Table I. Duality Variable Interchanges

Quantities	
From $\underline{E}(\underline{x})$	To $\underline{H}(\underline{x})$
$\underline{E}$	$\underline{H}$
$\underline{H}$	$-\underline{E}$
μ	ϵ
ρ	$-\rho_m$
$\underline{J}$	$-\underline{I}$
$\underline{I}$	$-\underline{J}$

(4: 98, 99)

Using Table 1, the $\underline{H}(\underline{x})$ equation becomes:

$$\underline{H}(\underline{x}) = \frac{1}{4\pi} \iiint_V \left[i\omega\epsilon \underline{I}(\underline{x}')G(\underline{x};\underline{x}') + \underline{J}(\underline{x}') \times \nabla' G(\underline{x};\underline{x}') \right.$$

$$\left. + \nabla' G(\underline{x};\underline{x}') \frac{\rho_m(\underline{x}')}{\mu} \right] dv' + \frac{1}{4\pi} \iint_S \left[i\omega\epsilon[\hat{n}(\underline{x}') \times \underline{E}(\underline{x}')]G(\underline{x};\underline{x}') \right.$$

$$\left. - [\hat{n}(\underline{x}') \times \underline{H}(\underline{x}')] \times \nabla' G(\underline{x};\underline{x}') - [\hat{n}(\underline{x}') \cdot \underline{H}(\underline{x}')] \nabla' G(\underline{x};\underline{x}') \right] ds' \quad (51)$$

Eqs (50) and (51) may be further simplified in certain problems by noting that the volume integrals yield an incident field for a scattering problem and by defining surface current densities, $\underline{K}(\underline{x}')$ and $\underline{M}(\underline{x}')$, and surface charge densities, $\sigma(\underline{x}')$ and $\sigma_m(\underline{x}')$; based on the *outward pointing normal* for each region considered:

$$\underline{K}(\underline{x}') = \hat{n}(\underline{x}') \times \underline{H}(\underline{x}') \quad (52)$$

$$\underline{M}(\underline{x}') = \hat{n}(\underline{x}') \times \underline{E}(\underline{x}') \quad (53)$$

$$\sigma_m(\underline{x}')/\mu = \hat{n}(\underline{x}') \cdot \underline{H}(\underline{x}') \quad (54)$$

$$\sigma(\underline{x}')/\epsilon = \hat{n}(\underline{x}') \cdot \underline{E}(\underline{x}') \quad (55)$$

Using the simplifications noted above leaves:

$$\underline{E}(\underline{x}) = \frac{-1}{4\pi} \iint_S \left[i\omega\mu \underline{K}(\underline{x}')G(\underline{x};\underline{x}') + \underline{M}(\underline{x}') \times \nabla' G(\underline{x};\underline{x}') \right.$$

$$\left. + \frac{\sigma(\underline{x}')}{\epsilon} \nabla' G(\underline{x};\underline{x}') \right] ds' + \underline{E}^{inc}(\underline{x})$$

$\underline{x}$ not on S (56)

and

$$\underline{H}(\underline{x}) = \frac{1}{4\pi} \iint_S \left[i\omega\epsilon \underline{M}(\underline{x}') \, G(\underline{x};\underline{x}') - \underline{K}(\underline{x}') \times \nabla' G(\underline{x};\underline{x}') - \frac{\sigma_m(\underline{x}')}{\mu} \nabla' G(\underline{x};\underline{x}') \right] ds' + \underline{H}^{inc}(\underline{x})$$

$\underline{x}$ not on S (57)

where the superscript "inc" indicates and incident field. Eqs (56) and (57) are valid for all points within the volume in the upper have space of Figure 1. When the integrals are interpreted in the principal value sense, these equations are also valid for points on the bounding surface. However, this surface includes not only the plane between the upper and lower half spaces, but also includes the semicircular "cover", S_R, of the upper half space. Fortunately, the *Sommerfeld radiation* conditions (20) make the integrals over S_R vanish. The results for $\underline{x}$ approaching S are:

$$\underline{E}(\underline{x}) = \frac{-1}{4\pi} \iint_S \left[i\omega\mu \underline{K}(\underline{x}') G(\underline{x};\underline{x}') + \underline{M}(\underline{x}') \times \nabla' G(\underline{x};\underline{x}') + \frac{\sigma(\underline{x}')}{\epsilon} \nabla' G(\underline{x};\underline{x}') \right] ds' + \underline{E}^{inc}(\underline{x}), \quad \underline{x} \to S \tag{58}$$

and

$$\underline{H}(\underline{x}) = \frac{1}{4\pi} \iint_S \left[i\omega\epsilon \underline{M}(\underline{x}') \, G(\underline{x};\underline{x}') - \underline{K}(\underline{x}') \times \nabla' G(\underline{x};\underline{x}') - \frac{\sigma_m(\underline{x}')}{\mu} \nabla' G(\underline{x};\underline{x}') \right] ds' + \underline{H}^{inc}(\underline{x}), \quad \underline{x} \to S \tag{59}$$

Eqs (56) through (59) are the equations which represent the total electric or magnetic field at any point inside or on the surface of the upper half space of Figure 1 in terms of the surface charges, σ and σ_m, and the surface currents, $\underline{K}(\underline{x}')$ and $\underline{M}(\underline{x}')$. To find these currents and charges, equations must be developed to find the fields, currents, and charges inside the cavity of Figure 1 because the two spaces are coupled together at the interface between the surface. Recall, this interface has been named the aperture.

Inside the Cavity

Inside the cavity, the free space Green's function in the $\hat{a}$ direction may be used for $\underline{Q}$ (20) and $\underline{E}$ or $\underline{H}$ used for $\underline{P}$ in Eq (10). The volume in the integral is the volume of the cavity and the surface is the surface of the cavity. Again, no sources are found within the cavity and the surface currents and charges may be modeled as they were in Eqs (52) through (55). The fields incident to the aperture will induce surface currents and charges across the aperture. These surface currents and charges will generate the fields that are incident to the cavity. In this way, the cavity is coupled to the half space above the aperture. Using all of the above information, the electric and magnetic fields inside the cavity are

$$\underline{E}(\underline{x}) = \frac{-1}{4\pi} \iint_S \left[i\omega\mu\underline{K}(\underline{x}')\bar{Q}(\underline{x};\underline{x}') + \underline{M}(\underline{x}') \times \nabla'\bar{Q}(\underline{x};\underline{x}') + \frac{\sigma(\underline{x}')}{\epsilon} \nabla'\bar{Q}(\underline{x};\underline{x}') \right] ds'$$

for $\underline{x}$ not on the surface, S (60)

and

$$\underline{H}(\underline{x}) = \frac{1}{4\pi} \iint_S \left[i\omega\epsilon\underline{M}(\underline{x}')\,\bar{Q}(\underline{x};\underline{x}') - \underline{K}(\underline{x}') \times \nabla'\bar{Q}(\underline{x};\underline{x}') - \frac{\sigma_m(\underline{x}')}{\mu} \nabla'\bar{Q}(\underline{x};\underline{x}') \right] ds'$$

for $\underline{x}$ not on the surface, S (61)

To let the observation point approach the surface S bounding the cavity, Eq (50a) is again employed. The results are:

$$\underline{E}(\underline{x}) = \frac{-1}{4\pi} \iint\!\!\!\!\!\!- \left[i\omega\mu\underline{K}(\underline{x}')\bar{Q}(\underline{x};\underline{x}') + \underline{M}(\underline{x}') \times \nabla'\bar{Q}(\underline{x};\underline{x}') + \frac{\sigma(\underline{x}')}{\epsilon} \nabla'\bar{Q}(\underline{x};\underline{x}') \right] ds' - \frac{1}{2}\underline{M}(\underline{x}) \times \hat{n}(\underline{x}) - \frac{1}{2}\frac{\sigma(\underline{x})}{\epsilon}\hat{n}(\underline{x}')$$

for $\underline{x} \to S$ (62a)

and

$$\underline{H}(\underline{x}) = \frac{1}{4\pi} \iint_S \left[i\omega\epsilon \underline{M}(\underline{x}') \, \bar{Q}(\underline{x};\underline{x}') - \underline{K}(\underline{x}') \times \nabla' \bar{Q}(\underline{x};\underline{x}') \right.$$

$$\left. - \frac{\sigma_m(\underline{x}')}{\mu} \nabla' \bar{Q}(\underline{x};\underline{x}') \right] ds'$$

$$- \frac{1}{2} \underline{K}(\underline{x}) \times \hat{n}(\underline{x}) - \frac{1}{2} \frac{\sigma_m(\underline{x})}{\epsilon} \hat{n}(\underline{x}')$$

for $\underline{x} \rightarrow S$ (62b)

With Eqs (56) through (62) the fields at any point $\underline{x}$ can be determined if the incident fields and the surface charges and currents are known. The next step in the derivation of the integral equations, therefore, deals with finding the surface currents and charges.

Finding the Currents and Charges

The currents and charges needed to use Eqs (56) through (62) are found by the solution of a coupled set of second kind Fredholm integral equations which will be derived presently. To help in the computations, Eq (62a) is multiplied by $i\omega\epsilon$. This allows for the solution of $i\omega\epsilon\underline{M}(\underline{x}')$ instead of solving for $\underline{M}(\underline{x}')$ alone. Notice that $i\omega\epsilon$ multiplied by $i\omega\mu$ yields $-k^2$ by Eq (8). It is also more convenient to let the

constant $1/4\pi$ be part of the Green's functions so that $\bar{Q}(\underline{x};\underline{x}')/4\pi$ is referred to everywhere as $\bar{Q}(\underline{x};\underline{x}')$. Also, let σ_m/μ, from here on, be referred to as σ_m.

In the equations to follow, S_c refers to the surface of the cavity excluding the aperture and A refers to the aperture; as before, S refers to the surface of the upper half plane (which also includes the aperture). For the magnetic current across the aperture, Eqs (53) and (62a) along with the above simplifications yields a second kind Fredholm integral equation for the current $\underline{M}$ forced by integrals of the, as yet, unknown current $\underline{K}$ and charge σ:

$$\frac{1}{2}\, i\omega\epsilon\underline{M}(\underline{x}) = \hat{n}(\underline{x}) \times \left[\iint_{S_c \cup A} \left[k^2\, \underline{K}(\underline{x}')\bar{Q}(\underline{x};\underline{x}') - \underline{M}(\underline{x}') \times \nabla'\bar{Q}(\underline{x};\underline{x}')i\omega\epsilon - i\omega\sigma(\underline{x}')\, \nabla'\bar{Q}(\underline{x};\underline{x}') \right] ds' \right] \qquad (63)$$

where $\underline{x} \in A$.

Instead of using Eq (62a), Eq (58) could be used to find Eq (63). However, since Eq (58) is for the upper half space, the half space Green's function would be used in place of $\bar{Q}(\underline{x};\underline{x}')$ and the tangential component of the effective incident electric field across the aperture would be added. Eq (62a) is

chosen in place of Eq (58) since the former involves an integration over the bounded aperture, whereas the latter requires integration over the unbounded xz plane.

A further simplification is possible since $\underline{M}(\underline{x}) = \underline{0}$ when $\underline{x}$ is on a perfect electric conductor (4:34). The cavity walls are assumed to be PEC. Furthermore, to avoid confusion regarding the normal used in defining quantities in Eqs (52) through (55), the magnetic current is defined now to be $\underline{M}(\underline{x}') = -\hat{y} \times \underline{E}(\underline{x}')$, where $\hat{y}$ is the unit vector pointed in the positive direction along the y-axis. Using this definition, the equation for the magnetic current when $\underline{x}$ is on the aperture becomes:

$$\frac{1}{2} i\omega\epsilon\underline{M}(\underline{x}) = -\iint_{S_C \cup A} k^2 \left[\hat{y} \times \underline{K}(\underline{x}')\bar{Q}(\underline{x};\underline{x}') \right] ds'$$

$$- i\omega\epsilon \iint_{A} \hat{y} \times \left[\underline{M}(\underline{x}') \times \nabla'\bar{Q}(\underline{x};\underline{x}') \right] dx'$$

$$+ \iint_{S_C \cup A} \hat{y} \times i\omega\sigma(\underline{x}')\, \nabla'\bar{Q}(\underline{x};\underline{x}')\, ds' \qquad \underline{x} \in A \qquad (64)$$

To find the electric current across the aperture, Eqs (52) and (59) will be used with the current defined as $\underline{K}(\underline{x}') = \hat{y} \times \underline{H}(\underline{x}')$. The result is

$$\underline{K}(\underline{x}) = \hat{y} \times \underline{H}^{inc}(\underline{x}) + \hat{y} \times \iint_S \Big[i\omega\epsilon \underline{M}(\underline{x}') G(\underline{x};\underline{x}') - \underline{K}(\underline{x}') \times \nabla' G(\underline{x};\underline{x}') - \sigma_m \nabla' G(\underline{x};\underline{x}') \Big] ds'$$

with $\underline{x} \in A$ (65)

(Recall that σ_m/μ was earlier redefined as σ_m for simplicity of presentation.)

Although this, too, requires integration over the unbounded xz plane, some means of coupling the incident field into the problem must be employed. It will be explained in the next chapter how the judicious choice of Green's function, $G(\underline{x};\underline{x}')$, combined with other problem specifics is employed to eliminate the integrations over the plane.

For the electric current on the surface of the cavity (minus the aperture), Eq (62b) is used in conjunction with Eq (52). The equation for the electric current in the cavity becomes:

$$\frac{1}{2} \underline{K}(\underline{x}) = - \hat{n}(\underline{x}) \times \iint_{S_c \cup A} \Big[-i\omega\epsilon \underline{M}(\underline{x}') \underline{\underline{Q}}(\underline{x};\underline{x}') + \underline{K}(\underline{x}') \times \nabla' \underline{\underline{Q}}(\underline{x};\underline{x}') + \sigma_m \nabla' \underline{\underline{Q}}(\underline{x};\underline{x}') \Big] ds'$$

with $\underline{x} \in S_c$ (66)

To find an equation for the electric charge density on the surface of the cavity including the aperture, Eq (62a) is used in conjunction with Eq (55). Since σ is always multiplied by $i\omega$ in Eqs (58) through (62), it is appropriate to find an equation for $i\omega\sigma$. Again, $\underline{M}(\underline{x}) = \underline{0}$ when $\underline{x}$ is on the surface of a PEC, and $\hat{n}(\underline{x})$ is dependent upon the cavity surface. The equation for $i\omega\sigma$ is:

$$\frac{1}{2}\, i\omega\sigma(\underline{x}) = i\omega\epsilon \iint_{A} \hat{n}(\underline{x}) \cdot \left[\underline{M}(\underline{x}') \times \nabla' \underline{\underline{G}}(\underline{x};\underline{x}')\right] ds'$$

$$+ \iint_{S_C \cup A} \hat{n}(\underline{x}) \cdot k^2\, \underline{K}(\underline{x}')\underline{\underline{G}}(\underline{x};\underline{x}')\, ds'$$

$$- \iint_{S_C \cup A} \hat{n}(\underline{x}) \cdot i\omega\sigma(\underline{x}')\, \nabla' \underline{\underline{G}}(\underline{x};\underline{x}')\, ds'$$

$$\text{with } \underline{x} \in S_C \cup A \qquad (67)$$

An analogous equation for σ_m could be obtained from Eq (62b) but is not listed here. Eqs (64) through (67) and the equation for σ_m are the necessary equations for the surface current and charge densities. Each is a second kind Fredholm integral equation. The equations are coupled and may be viewed as a linear operator, L, acting on the vector of unknowns, $\underline{X} = [\underline{M}(\underline{x}), \underline{K}(\underline{x}), \sigma(\underline{x}), \sigma_m(\underline{x})]$, according to $L\underline{X} = \underline{B}$, where $\underline{B} = (\underline{0}, \hat{y} \times \underline{H}^{inc}(\underline{x}), \underline{0}, \underline{0})$. The operator, L, is a matrix of

linear operators having second kind Fredholm operators along the diagonal. Alternate, simpler, formulations which exclude charge densities are possible. In one such formulation, the resulting operator involves a first kind Fredholm operation, inversion of which is possibly ill-posed (2). Another formulation replaces $i\omega\sigma$ by $\nabla_s \cdot \underline{K}$ and $i\omega\sigma_m$ by $-\nabla_s \cdot \underline{M}$ in which ∇_s is the divergence operator in the surface. These relations follow directly from Maxwell's equations and are commonly employed (15) when using surface integral equations. However, the formulation herein is chosen to avoid numerical differentiation for approximate solutions obtained in a later chapter.

III. Reduction to a Two-dimensional Problem

The Cavity

For this problem, a two-dimensional cavity (Figure 1) of arbitrary shape is considered. Along the z-axis, the cross-sectional shape of the cavity is constant. For such a problem, the currents and charges, $\underline{M}$, $\underline{K}$, σ, and σ_m, as well as the resulting fields, are independent of z.

This simplification eliminates integration in the z direction from $-\infty$ to $+\infty$ for the surface currents and charges. It also allows the use of the half space Green's function in two-dimensions for $G(\underline{x};\underline{x}')$ and the two-dimensional free space Green's function for $\bar{Q}(\underline{x};\underline{x}')$. In two-dimensions these Green's functions are (13):

$$G(\underline{x};\underline{x}') = \pi i H_0^{(1)}(kr) + \pi i H_0^{(1)}(k\tilde{r}) \tag{68}$$

and

$$\bar{Q}(\underline{x};\underline{x}') = \pi i H_0^{(1)}(kr) \tag{69}$$

where, now

$$r = \left[(x-x')^2 + (y-y')^2\right]^{1/2} \tag{70}$$

$$\tilde{r} = \left[(x-x')^2 + (y+y')^2\right]^{1/2} \tag{71}$$

and

$H_0^{(1)}(kr)$ is a Hankel function of the first kind of order zero.

Dividing Eqs (68) and (69) by 4π will help simplify Eqs (58) through (61). Thus, the Green's functions are now redefined to be

$$G(\underline{x};\underline{x}') = \frac{i}{4} H_0^{(1)}(kr) + \frac{i}{4} H_0^{(1)}(k\tilde{r}) \tag{72}$$

and

$$\tilde{Q}(\underline{x};\underline{x}') = \frac{i}{4} H_0^{(1)}(kr) \tag{73}$$

In two-dimensions, the surface integrals of Eqs (58) through (61) are now line integrals for finding the "surface" currents and charges.

The Incident Fields

Assume that the field originates at a long distance from the aperture such that as it impinges upon the aperture the field is a plane wave. Further, let the incident field be a TE (Transverse Electric Field) plane wave. That is, the electric field is transverse to the $\hat{z}$ direction at all times. Also, let the medium above the plane be free space (this has already been assumed) and let both the electric and magnetic fields always be transverse to the direction of propagation. This is a TEM (Transverse Electromagnetic) plane wave. For a TE plane wave traveling in the TEM mode, the $\underline{H}$ field is in the $\hat{z}$ direction. Referring to Figure 3, θ_i is the positive angle measured clockwise from the y axis along which the wave propagates. Such an incident plane wave with $\exp(-i\omega t)$ time dependence (assumed at the outset) has spatial dependence governed by (4:146):

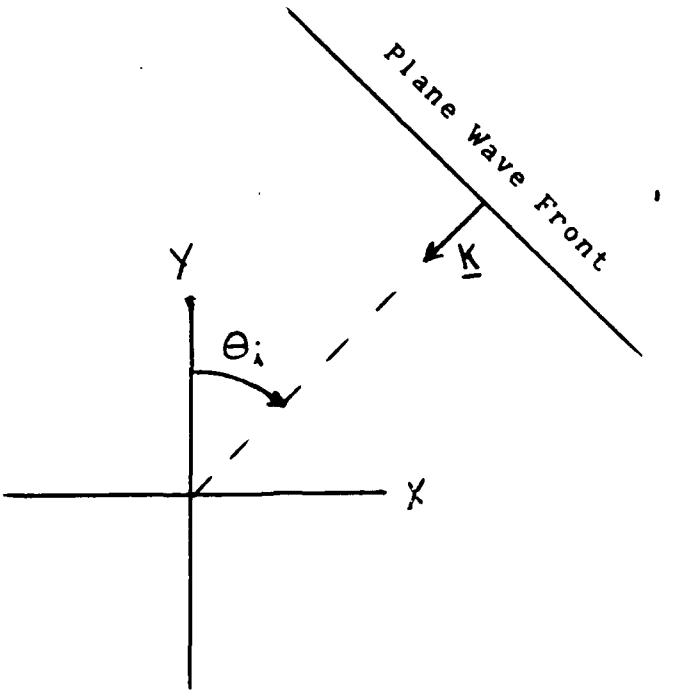

Figure 3. Incident Plane Wave with Incident Angle θ_i and Propagation Vector, $\underline{k}(\underline{x})$.

$$\underline{H}^{inc}(\underline{x}) = \hat{z}\, H_0 \exp(i\underline{k}\cdot\underline{r}) \tag{74}$$

where

H_0 = magnitude of the field

$\underline{k}(\underline{x}) = k\,\hat{k} = -k\,[\hat{x}\sin(\theta_i) + \hat{y}\cos(\theta_i)]$

$\underline{r}(\underline{x}) = x\,\hat{x} + y\,\hat{y}$

With unit magnitude, the incident field is:

$$\underline{H}^{inc}(\underline{x}) = \hat{z}\, \exp\{-ik[x \sin(\theta_i) + y \cos(\theta_i)]\} \qquad (75)$$

With this incident field and the two-dimensional cavity discussed above, Eqs (64) through (67) may be simplified. The simplifying observations are:

1. From Eq (54), the magnetic surface charge density, $\sigma_m(\underline{x})$, is zero for the TE plane wave considered above.

2. On the PEC, the magnetic surface current density, $\underline{M}(\underline{x})$, is zero.

3. The gradient, in primed coordinates, of the Green's function, $\nabla' G(\underline{x};\underline{x}')$, has only an $\hat{x}$ component when either y or y' equals zero. This is the Neumann boundary condition discussed in the introduction of the thesis. Therefore, $\underline{K}(\underline{x}') \times \nabla' G(\underline{x};\underline{x}') = \underline{0}$ when $\underline{x}'$ is on the x-axis.

4. The gradient of the Green's function never has a $\hat{z}$ component in this two-dimensional problem. Therefore, $\underline{H}(\underline{x}')\cdot\nabla' G(\underline{x};\underline{x}') = \underline{0}$ for all $\underline{x}'$.

5. The three-dimensional surface is now a two-dimensional contour. The equations to follow will reflect that; thus, S_C now indicates the contour around the cavity and A indicates the line across the aperture.

Using these simplifications, the five equations that will be approximated in the following analysis are:

$$\underline{H}(\underline{x}) = \underline{H}^{inc}(\underline{x}) + \int_A i\omega\epsilon \underline{M}(\underline{x}')G(\underline{x};\underline{x}')\, dx' \qquad (76)$$

$$\frac{1}{2}\, i\omega\epsilon \underline{M}(\underline{x}) = -\int\limits_{S_c \cup A} k^2 \left[\hat{y} \times \underline{K}(\underline{x}')\bar{Q}(\underline{x};\underline{x}') \right] dc'$$

$$+ \int\limits_{S_c \cup A} \hat{y} \times i\omega\sigma(\underline{x}')\, \nabla'\bar{Q}(\underline{x};\underline{x}')\, dc'$$

with $\underline{x} \in A$ (77)

$$\underline{K}(\underline{x}) = \hat{y} \times \underline{H}^{inc}(\underline{x}) + \hat{y} \times \int\limits_{A} i\omega\epsilon \underline{M}(\underline{x}')G(\underline{x};\underline{x}')\, dx'$$

with $\underline{x} \in A$ (78)

$$\frac{1}{2}\, \underline{K}(\underline{x}) = -\hat{n}(\underline{x}) \times \left[\int\limits_{A} i\omega\epsilon \underline{M}(\underline{x}')\bar{Q}(\underline{x};\underline{x}')\, dx' \right.$$

$$\left. + \int\limits_{S_c \cup A} \underline{K}(\underline{x}') \times \nabla'\bar{Q}(\underline{x};\underline{x}')\, dc' \right]$$

with $\underline{x} \in S_c$ (79)

and

$$\frac{1}{2}\, i\omega\sigma(\underline{x}) = -i\omega\epsilon \oint_A \hat{n}(\underline{x})\cdot\left[\underline{M}(\underline{x}') \times \nabla' \underline{\underline{G}}(\underline{x};\underline{x}')\right] dc'$$

$$+ \oint_{S_C \cup A} \hat{n}(\underline{x})\cdot k^2\, \underline{K}(\underline{x}')\underline{\underline{G}}(\underline{x};\underline{x}')\, dc'$$

$$- \oint_{S_C \cup A} \hat{n}(\underline{x})\cdot i\omega\sigma(\underline{x}')\, \nabla' \underline{\underline{G}}(\underline{x};\underline{x}')\, dc'$$

with $\underline{x} \in S_C \cup A$ (80)

Eqs (77) through (80) are a coupled set of Fredholm integral equations of the second kind for finding the currents and charges needed to solve for the scattered fields, using Eq (76), from the two-dimensional cavity introduced at the beginning of the chapter. Recall if $i\omega\sigma$ is replaced by $\nabla_s \cdot \underline{K}$, as described at the end of Chapter 2, Eq (80) is not needed. In either case, the equations are specifically designed for use with the TE plane wave of Eq (75). Solutions of these equations may be approximated numerically by any of several methods. The chosen method of approximating the solutions to Eqs (77) through (80) is introduced in the next chapter.

IV. Approximate Solution of the Integral Equations

In Eqs (77) through (80), linear operations (the integrals and vector operations) act on a set of unknowns (the currents and charges) and must be equal to a set of knowns (the incident fields). If the inverse of the linear operators can be found and applied to the set of knowns, the set of unknowns can be determined. The Method of Moments is a reasonably simple means by which one can approximate such an operator equation for numerical solution (3). Eqs (77) through (80) can be solved using moment methods by using the following approximations:

$$i\omega\epsilon\underline{M}(\underline{x}) \approx \sum_{n=1}^{M} \alpha_n \underline{f}_n(\underline{x})$$

$$\underline{K}(\underline{x}) \approx \sum_{n=1}^{N} \beta_n \underline{h}_n(\underline{x})$$

$$i\omega\sigma(\underline{x}) \approx \sum_{n=1}^{N} \tau_n p_n(\underline{x}) \qquad (81)$$

where α_n, β_n, and τ_n are constants and $\underline{f}_n(\underline{x})$, $p_n(\underline{x})$, and $\underline{h}_n(\underline{x})$ are functions to be described below.

The "$\approx$" sign in Eq (81) implies approximations because the numbers M and N are assumed to be finite. As M and N approach infinity, the summation (right hand side) approaches a smooth curve (left hand side) and the "$\approx$" can be replaced by an equal sign. In Eq (81), $\underline{f}_n(\underline{x})$, $\underline{h}_n(\underline{x})$, and $p_n(\underline{x})$ are basis functions

of position (3:42). The functions $\underline{f}_n(\underline{x})$ and $\underline{h}_n(\underline{x})$ are vectors because $\underline{M}(\underline{x})$ and $\underline{K}(\underline{x})$ are vectors. Using Eq (81) and the linear operators in Eqs (77) through (80) yields:

$$\frac{1}{2} i\omega\epsilon\underline{M}(\underline{x}) \approx \frac{1}{2}\sum_{n=1}^{M}\alpha_n\underline{f}_n(\underline{x}) = \sum_{n=1}^{M}\alpha_n L_1\underline{f}_n(\underline{x}') + \sum_{n=1}^{N}\beta_n L_2\underline{h}_n(\underline{x}') + \sum_{n=1}^{N}\tau_n L_3 p_n(\underline{x}')$$

with $\underline{x} \in A$ (82)

$$\underline{K}(\underline{x}) \approx \sum_{n=1}^{N}\beta_n\,\underline{h}_n(\underline{x}) = \sum_{n=1}^{M}\alpha_n L_4\underline{f}_n(\underline{x}') + \underline{H}^{inc}(\underline{x})$$

with $\underline{x} \in A$ (83)

$$\frac{1}{2}\underline{K}(\underline{x}) \approx \frac{1}{2}\sum_{n=1}^{N}\beta_n\,\underline{h}_n(\underline{x}) = \sum_{n=1}^{M}\alpha_n L_5\underline{f}_n(\underline{x}') + \sum_{n=1}^{N}\beta_n L_6\underline{h}_n(\underline{x}')$$

with $\underline{x} \in S_c$ (84)

$$\frac{1}{2} i\omega\sigma(\underline{x}) \approx \frac{1}{2}\sum_{n=1}^{N}\tau_n p_n(\underline{x}) = \sum_{n=1}^{M}\alpha_n L_7\underline{f}_n(\underline{x}') + \sum_{n=1}^{N}\beta_n L_8\underline{h}_n(\underline{x}') + \sum_{n=1}^{N}\tau_n L_9 p_n(\underline{x}')$$

with $\underline{x} \in Sc \cup A$ (85)

The linear operators L_1 through L_9 are all functions of position. That is, $L_1 = L_1(\underline{x})$, $L_2 = L_2(\underline{x})$, etc. Further, the linear operators may be determined by examining the equations from which they came: Eqs (77) through (80). For instance,

$$L_1 \underline{f}_n(\underline{x}') = \int_A \hat{y} \times \underline{f}_n(\underline{x}') \times \nabla' \underline{\underline{Q}}(\underline{x};\underline{x}') \, dx'$$

The method is employed by defining a weighting function, $W_m(\underline{x};\underline{x}_m)$, for the specific problem being solved, and taking the inner product of W_m with each of Eqs (77) through (80); where the inner product is defined as:

$$\langle W_m(\underline{x},\underline{x}_m), f(\underline{x})\rangle = \int_{S_c \cup A} W_m(\underline{x},\underline{x}_m) f(\underline{x}) \, dc' \tag{86}$$

This yields

$$\frac{1}{2}\sum_{n=1}^{M} \alpha_n \langle W_m, \underline{f}_n(\underline{x})\rangle = \sum_{n=1}^{M} \alpha_n \langle W_m, L_1 \underline{f}_n(\underline{x}')\rangle + \sum_{n=1}^{N} \beta_n \langle W_m, L_2 \underline{h}_n(\underline{x}')\rangle + \sum_{n=1}^{N} \tau_n \langle W_m, L_3 p_n(x')\rangle$$

with $\underline{x} \in A$, (87)

$$\sum_{n=1}^{N} \beta_n \langle W_m, \underline{h}_n(\underline{x})\rangle = \sum_{n=1}^{M} \alpha_n \langle W_m, L_4 \underline{f}_n(\underline{x}')\rangle + \langle W_m, \underline{H}^{inc}(\underline{x})\rangle$$

with $\underline{x} \in A$, (88)

and

$$1/2 \sum_{n=1}^{N} \beta_n \langle W_m, \underline{h}_n(\underline{x}) \rangle = \sum_{n=1}^{M} \alpha_n \langle W_m, L_5 \underline{f}_n(\underline{x}') \rangle + \sum_{n=1}^{N} \beta_n \langle W_m, L_6 \underline{h}_n(\underline{x}') \rangle$$

with $\underline{x} \in S_c$, (89)

$$1/2 \sum_{n=1}^{N} \tau_n \langle W_m, p_n(x_y) \rangle = \sum_{n=1}^{M} \alpha_n \langle W_m, L_7 \underline{f}_n(\underline{x}') \rangle + \sum_{n=1}^{N} \beta_n \langle W_m, L_8 \underline{h}_n(\underline{x}') \rangle + \sum_{n=1}^{N} \tau_n \langle W_m, L_9 p_n(x') \rangle$$

with $\underline{x} \in S_c \cup A$. (90)

Eqs (87) through (90) allow the currents and charges to be found using moment methods directly. No matter what the shape of the cavity's cross section, Eqs (87) through (90) should yield a reasonably accurate solution if M and N are chosen judiciously. However it is advantageous to deal with a specific cross section as opposed to a generic or arbitrary cross section. For this reason, the specific cavity cross section of interest is introduced in the next section.

V. The Rectangular Cavity

Figure 4 shows the cross section of the cavity whose scattering properties will be examined here. The rectangular cavity has a width, w, and a depth, d. For purposes of computation all lengths will be normalized to the width, w. Doing so gives an effective width of 1, a depth of d/w, a wavelength of λ/w, etc. The sides of the cavity are labeled S-, Sd, S+, and A which correspond to surfaces along x = -0.5, y = -d, x = +0.5, and the aperture, respectively.

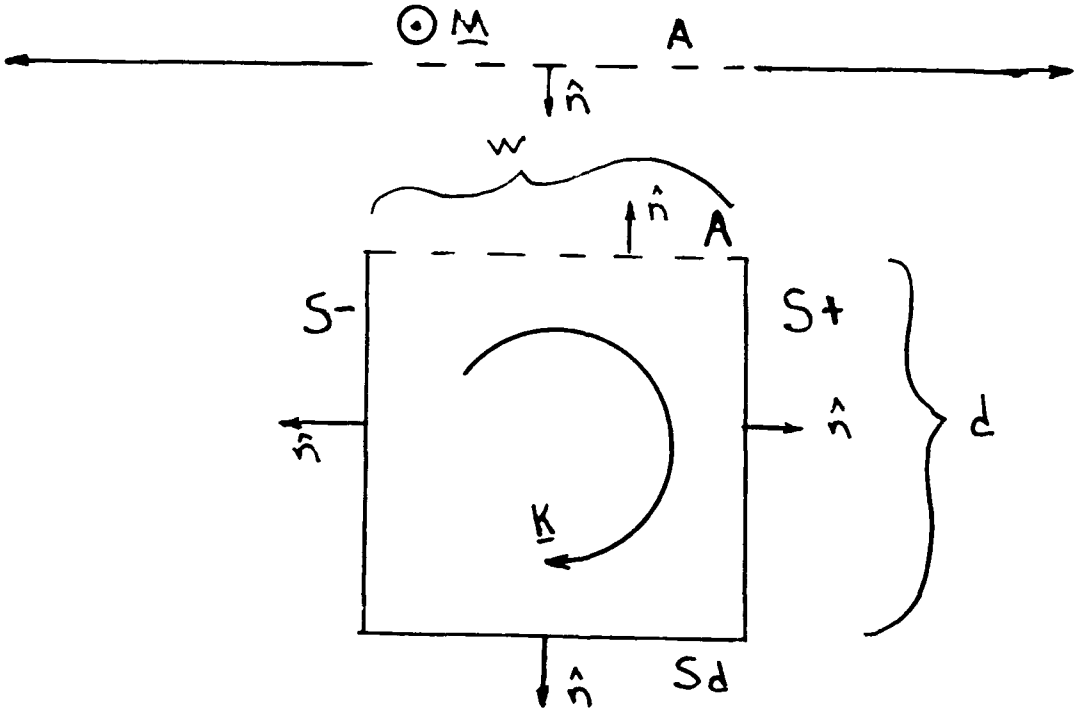

Figure 4. Cross Section of the Rectangular Cavity Showing Width, Depth, Coupling Aperture, Along with the Currents and Unit Normals and Their Directions.

On Figure 4, the outward pointing normals are indicated on each surface. Further, the electric current direction is also noted. The integrations within the linear operators of Eqs (87) through (90) are line integrals with respect to positive arc length around the cavity and across the aperture (21).

Table II gives a list of variables normalized to the width. The first column gives the original variable. The second column gives the normalized variable and the third column gives the name used in the computations.

Table II. Quantities Normalized to the Width

Original Variable	Normalized Variable	Used Quantity
w	w/w	1
x	x/w	x
y	y/w	y
z	z/w	z
d	d/w	d
λ	λ/w	λ
k	kw	k

With the geometry indicated in Figure 4, the cavity can be broken up into N equally sized segments with M of them across

the aperture. If the size of each segment is termed ΔC_n (actually normalized to w) where $\Delta C_1 = \Delta C_2 = \ldots = \Delta C_N$, the basis functions can be defined as:

$$\underline{f}_n(\underline{x}) = \begin{cases} 1\hat{e} \text{ if } \underline{x} \text{ is on } \Delta C_n \\ 0 \text{ elsewhere} \end{cases} \tag{91}$$

where the direction, $\hat{e}$, associated with $\underline{f}_n(\underline{x})$ is the same as that of the current for each particular segment. For instance, on the inside of the aperture $\underline{K}(\underline{x})$ is in the $\hat{x}$ direction. Similar basis functions are defined for $\underline{h}_n$ and p_n.

Using "point matching" for testing, the weighting function, $W_m(\underline{x};\underline{x}')$, is defined as (3:42)

$$W_m(\underline{x};\underline{x}') = W(\underline{x};\underline{x}_m) = \delta(\underline{x} - \underline{x}_m) \tag{92}$$

Eq (91) reduces the integrals within the linear operations $L_1(\underline{x})$, $L_2(\underline{x})$, ..., $L_9(\underline{x})$ to integrations over a small segment, ΔC. Eq (92) replaces the position vector $\underline{x}$ with the position vector $\underline{x}_m$ in Eqs (87) through (90). To illustrate, let $r(x;x')$ be any function that is continuous along the line L and let the line, L, be broken into M segments. Then

$$\int_L r(x;x')\,dx' = \sum_{n=1}^{M} \int_{\Delta C_n} r(x;x')\,dx'$$

Taking the inner product as defined above yields

$$\int_L \left[\sum_{n=1}^{M} \int_{\Delta C_n} r(x;x')dx' \right] \delta(x-x_m)\, dx = \sum_{n=1}^{M} \int_{\Delta C_n} r(x_m;x')\, dx'$$

If $r(x;x')$ is one of $\underline{f}$, $\underline{h}$, or p given in Eq (91), only those line segments ΔC_n survive on which r is non-zero.

Referring now to the problem at hand, by letting $\underline{x}_m$ be the midpoint of each line segment, ΔC_m, (as m goes from 1 to N) and $\underline{x}_n$ be the midpoint of each line segment ΔC_n (as n goes from 1 to N), the integrals over the line segment ΔC_n may be approximated by:

$$\int_{\Delta C_n} \underline{f}(\underline{x}_m;\underline{x}')\, d\underline{x}' \approx \underline{f}(\underline{x}_m;\underline{x}_n)\, \Delta C_n \qquad (94)$$

if ΔC_n is sufficiently small.

Using Eqs (91) through (94) and performing the inner products of W_m with the linear operators operating upon their appropriate functions, Eqs (87) through (90) may be cast in a more easily solvable form.

At either y or y' equal to zero, $G(\underline{x}_m;\underline{x}_n) = 2\underline{Q}(\underline{x}_m;\underline{x}_n)$. This fact is used to simplify the equations. It is important to note that the integrations are line integrals and are independent of direction across the small segment, ΔC.

Since ΔC_n is always a positive number, the line integration does not affect the sign of the approximation as defined in Eq (94). Further, the principle value of the integral over $\nabla'\bar{Q}(\underline{x}_m;\underline{x}_n)$ is identically zero (as will be shown) when n=m. When n=m, the segment ΔC_n is termed a self-patch. The principle value integrals over the self-patches will now be examined in more detail.

Self-Patch Integrations

In two-dimensions, $\nabla'\bar{Q}(\underline{x};\underline{x}')$ is

$$\nabla'\bar{Q}(\underline{x};\underline{x}') = \frac{\partial\bar{Q}}{\partial x'}\hat{x} + \frac{\partial\bar{Q}}{\partial y'}\hat{y}$$

$$= \frac{-H_1^{(1)}(kr)}{r}\left[(x-x')\hat{x} + (y-y')\hat{y}\right] \qquad (95)$$

In Eq (95) the Hankel function of the first kind order one and the 1/r term both produce singularities when x=x'. Performing the integrals in the principle value sense, however, does not produce singularities.

When integrating $\nabla'\bar{Q}(\underline{x};\underline{x}')\cdot\hat{x}$ along the y-axis, the term involving x-x' (or x_m-x_n in the approximation) will always multiply the integral by zero when x=x' (or $x_m=x_n$). The same situation is involved when integrating $\nabla'\bar{Q}(\underline{x};\underline{x}')\cdot\hat{y}$ along the x-axis, where the (y-y') term always multiplies the integral by zero when y=y'. Thus, those particular self-patches are identically zero.

For the self-patches involving integrations in the x direction of $\nabla'\underline{\underline{G}}(\underline{x};\underline{x}')\cdot\hat{x}$, a more rigorous proof is necessary. The same situation applies when integrating in the y direction of $\nabla'\underline{\underline{G}}(\underline{x};\underline{x}')\cdot\hat{y}$. In the following proof, the variable "x" may be replace by the variable "y" to achieve the same result as long as every "x" is replaced by a "y".

When integrating on a self-patch in the x direction (for the rectangular channel), y is always equal to y'. Thus,

$$\int_{\Delta C_m} \nabla'\underline{\underline{G}}(x_m;x')\cdot\hat{x}\,dx' = \frac{i}{4}\int_{x_m-\Delta C/2}^{x_m+\Delta C/2} \frac{H_1^{(1)}[k|x_m-x'|]}{|x_m-x'|}(x_m-x')\,dx' \qquad (96)$$

Eq (96) is a symmetrical integration of an odd function about the singularity x'=0. This integration is therefore identically zero.

The integrations over all self patches involving $\nabla'\underline{\underline{G}}(\underline{x};\underline{x}')$ have been shown to be equal to zero. All of the self-patches that do not involve a $\nabla'\underline{\underline{G}}(\underline{x};\underline{x}')$ term have, instead, only a $\underline{\underline{G}}(\underline{x};\underline{x}')$ term. These integrals do not reduce to zero. Again, the variable "x" may be replaced by the variable "y" in the following integrals.

$$\int_{\Delta C_m} \bar{Q}(x_m;x')\,dx' = \frac{i}{4}\int_{x_m-\Delta C/2}^{x_m+\Delta C/2} H_o^{(1)}(k|x_m-x'|)\,dx'$$

$$= \lim_{\epsilon \to 0} \int_{\epsilon}^{\Delta C/2} \frac{i}{2} H_o^{(1)}(kx)\,dx \qquad (97)$$

For small arguments, the asymptotic approximation for $H_o^{(1)}$ is (1:360)

$$H_o^{(1)}(z) \sim i\frac{2}{\pi}\ln(z/2) + 1 + i\frac{2}{\pi}\gamma - i\frac{z^2}{2\pi}\ln(z/2) + \left[i\frac{2}{\pi}(1-\gamma) - 1 \right]\frac{z^2}{4} + O[z^4\ln(z)] \qquad (98)$$

where γ = Euler's constant $\approx 0.5772156649015...$

Thus,

$$\int_{\Delta C_m} \bar{Q}(x_m;x')\,dx' \approx \frac{k\Delta C}{4}\left[\frac{i}{k} - \frac{2\gamma}{k\pi}\right] - \frac{\Delta C}{2\pi}\left[\ln(k\Delta C/4) - 1\right] + \left[\frac{k\Delta C}{4}\right]^3\left[\frac{2}{3k\pi}\right]\left[\ln(k\Delta C/4) - 1/3\right] \qquad (99)$$

All of the self-patch integrations have now been determined. Those line integrals over sections other than self-patches will be approximated using Eq (89).

Solving for the Currents and Charges

Most of the equations used thus far are vector valued. However, these equations can be broken into $\hat{x}$ and $\hat{y}$ components if necessary and a set of equations developed from each of Eqs (88) through (91) and their corresponding earlier equations, Eqs (77) through (80).

The set of equations corresponding to Eqs (77) and (88) are:

For $m = 1, 2, 3 \ldots M$ where $\hat{n}(\underline{x}_m) = -\hat{y}$

$$0 = \sum_{n=1}^{M} \alpha_n \left[\nabla' \bar{\bar{Q}}(\underline{x}_m; \underline{x}_n) \cdot \hat{y}\right] \Delta C_n - k^2 \sum_{n=1}^{M} \beta_n \bar{\bar{Q}}(\underline{x}_m; \underline{x}_n) \Delta C_n$$

$$+ k^2 \sum_{n=L+M}^{L+2M} \beta_n \bar{\bar{Q}}(\underline{x}_m; \underline{x}_n) \Delta C_n + \sum_{n=1}^{M+L} \gamma_n \left[\nabla' \bar{\bar{Q}}(\underline{x}_m; \underline{x}_n) \cdot \hat{x}\right] \Delta C_n$$

$$+ \sum_{n=M+L}^{N} \gamma_n \left[\nabla' \bar{\bar{Q}}(\underline{x}_m; \underline{x}_n) \cdot \hat{x}\right] \Delta C_n + \alpha_m/2 \qquad (100)$$

where

L = the number of segments along S- and S+
M = the number of segments along A and Sd

Eq (100) is actually a set of M equations because it applies for m=1, 2, . . . , M. There are only M equations because $\underline{x}_m$ is not

on the aperture when $m > M$; Eq (77), and therefore Eq (88), is only good when the observation point ($\underline{x}$ or $\underline{x}_m$) is on the aperture. The set of equations that correspond to Eqs (78) and (89) are:

For $m = 1, 2, 3, \ldots M$ where $\hat{n}(\underline{x}_m) = \hat{y}$

$$\frac{1}{2} H^{inc}(\underline{x}_m) = -\sum_{n=1}^{M} \alpha_n \, \bar{Q}(\underline{x}_m; \underline{x}_n) \, \Delta C_n + \beta_m/2 \qquad (101)$$

The set of equations that correspond to Eqs (79) and (90) are:

For $m = M+1, M+2, \ldots M+L$ where $\hat{n}(\underline{x}_m) = -\hat{x}$

$$0 = \sum_{n=1}^{M} \alpha_n \bar{Q}(\underline{x}_m; \underline{x}_n) \Delta C_n + \sum_{n=1}^{M} \beta_n \, [\nabla' \bar{Q}(\underline{x}_m; \underline{x}_n) \cdot \hat{y}] \Delta C_n + \beta_m/2$$

$$- \sum_{n=M+L}^{L+2M} \beta_n [\nabla' \bar{Q}(\underline{x}_m; \underline{x}_n) \cdot \hat{y}] \Delta C_n + \sum_{n=L+2M}^{N} \beta_n \, [\nabla' \bar{Q}(\underline{x}_m; \underline{x}_n) \cdot \hat{x}] \Delta C_n \qquad (102)$$

For $M+L < m \leq 2M+L$ where $\hat{n}(\underline{x}_m) = -\hat{y}$

$$0 = -\sum_{n=1}^{M} \alpha_n \bar{Q}(\underline{x}_m; \underline{x}_n) \Delta C_n - \sum_{n=1}^{M} \beta_n \, [\nabla' \bar{Q}(\underline{x}_m; \underline{x}_n) \cdot \hat{y}] \Delta C_n - \beta_m/2$$

$$+ \sum_{n=M}^{L+M} \beta_n [\nabla' \bar{Q}(\underline{x}_m; \underline{x}_n) \cdot \hat{x}] \Delta C_n - \sum_{n=L+2M}^{N} \beta_n \, [\nabla' \bar{Q}(\underline{x}_m; \underline{x}_n) \cdot \hat{x}] \Delta C_n \qquad (103)$$

For $2M+L < m \leq N$ where $\hat{n}(\underline{x}_m) = \hat{x}$

$$0 = -\sum_{n=1}^{M} \alpha_n \bar{Q}(\underline{x}_m;\underline{x}_n)\Delta C_n - \sum_{n=1}^{M} \beta_n [\nabla' \bar{Q}(\underline{x}_m;\underline{x}_n)\cdot\hat{y}]\Delta C_n - \beta_m/2$$

$$+ \sum_{n=M}^{L+M} \beta_n [\nabla' \bar{Q}(\underline{x}_m;\underline{x}_n)\cdot\hat{x}]\Delta C_n + \sum_{n=L+M}^{L+2M} \beta_n [\nabla' \bar{Q}(\underline{x}_m;\underline{x}_n)\cdot\hat{y}]\Delta C_n \tag{104}$$

And finally, the set of equations that correspond to Eqs (80) and (91) are:

For $0 < m \leq M$ where $\hat{n}(\underline{x}_m) = \hat{y}$

$$0 = \sum_{n=1}^{M} \alpha_n [\nabla' \bar{Q}(\underline{x}_m;\underline{x}_n)\cdot\hat{x}]\Delta C_n + \sum_{n=M}^{M+L} \tau_n [\nabla' \bar{Q}(\underline{x}_m;\underline{x}_n)\cdot\hat{y}]\Delta C_n$$

$$+ k^2 \sum_{n=M}^{M+L} \beta_n \bar{Q}(\underline{x}_m;\underline{x}_n)\Delta C - k^2 \sum_{n=2M+L}^{N} \beta_n \bar{Q}(\underline{x}_m;\underline{x}_n)\Delta C$$

$$- \sum_{n=M+L}^{N} \tau_n [\nabla' \bar{Q}(\underline{x}_m;\underline{x}_n)\cdot\hat{y}]\Delta C_n - \tau_m/2 \tag{105}$$

For $M < m \leq M+L$ where $\hat{n}(\underline{x}_m) = -\hat{x}$

$$0 = \sum_{n=1}^{M} \alpha_n [\nabla' \bar{Q}(\underline{x}_m;\underline{x}_n)\cdot\hat{y}]\Delta C_n + \sum_{n=1}^{M} \tau_n [\nabla' \bar{Q}(\underline{x}_m;\underline{x}_n)\cdot\hat{x}]\Delta C_n$$

$$- k^2 \sum_{n=1}^{M} \beta_n \bar{Q}(\underline{x}_m;\underline{x}_n)\Delta C + k^2 \sum_{n=M+L}^{2M+L} \beta_n \bar{Q}(\underline{x}_m;\underline{x}_n)\Delta C$$

$$+ \sum_{n=M+L}^{N} \tau_n [\nabla' \bar{Q}(\underline{x}_m;\underline{x}_n)\cdot\hat{x}]\Delta C_n - \tau_m/2 \tag{106}$$

For $M+L < m \leq L+2M$ where $\hat{n}(\underline{x}_m) = -\hat{y}$

$$0 = -\sum_{n=1}^{M} \alpha_n [\nabla' \bar{Q}(\underline{x}_m; \underline{x}_n) \cdot \hat{x}] \Delta C_n + \sum_{n=1}^{M+L} \tau_n [\nabla' \bar{Q}(\underline{x}_m; \underline{x}_n) \cdot \hat{y}] \Delta C_n$$

$$- k^2 \sum_{n=M}^{M+L} \beta_n \bar{Q}(\underline{x}_m; \underline{x}_n) \Delta C + k^2 \sum_{n=2M+L}^{N} \beta_n \bar{Q}(\underline{x}_m; \underline{x}_n) \Delta C$$

$$+ \sum_{n=2M+L}^{N} \tau_n [\nabla' \bar{Q}(\underline{x}_m; \underline{x}_n) \cdot \hat{y}] \Delta C_n - \tau_m/2 \qquad (107)$$

For $L+2M < m \leq N$ where $\hat{n}(\underline{x}_m) = \hat{x}$

$$0 = -\sum_{n=1}^{M} \alpha_n [\nabla' \bar{Q}(\underline{x}_m; \underline{x}_n) \cdot \hat{y}] \Delta C_n - \sum_{n=1}^{M+L} \tau_n [\nabla' \bar{Q}(\underline{x}_m; \underline{x}_n) \cdot \hat{x}] \Delta C_n$$

$$+ k^2 \sum_{n=1}^{M} \beta_n \bar{Q}(\underline{x}_m; \underline{x}_n) \Delta C - k^2 \sum_{n=M+L}^{2M+L} \beta_n \bar{Q}(\underline{x}_m; \underline{x}_n) \Delta C$$

$$- \sum_{n=M+L}^{2M+L} \tau_n [\nabla' \bar{Q}(\underline{x}_m; \underline{x}_n) \cdot \hat{x}] \Delta C_n - \tau_m/2 \qquad (108)$$

Eqs (100) through (108) represent 2N+M equations and 2N+M unknowns. The unknowns are α_1, α_2, ... α_M, β_1, β_2, ... β_N, τ_1, τ_2, ... and τ_N. Each of the unknowns appear in each of the equations, though several are multiplied by zero. Remember, each of Eqs (100) through (108) are valid for a given set of $\underline{x}_m$'s. The unknowns may be solved for using matrix techniques. This is easier to see if the equations are set in the following form:

$$\begin{bmatrix} l_{11} & l_{12} & \cdots & l_{1(2N+M)} \\ l_{21} & l_{22} & \cdots & \cdot \\ \cdot & \cdot & \cdots & \cdot \\ \cdot & \cdot & \cdots & \cdot \\ \cdot & \cdot & \cdots & \cdot \\ l_{(2N+M)1} & \cdot & \cdots & l_{(2N+M)(2N+M)} \end{bmatrix} \begin{bmatrix} \alpha_1 \\ \cdot \\ \alpha_M \\ \beta_1 \\ \cdot \\ \beta_N \\ \tau_1 \\ \cdot \\ \tau_N \end{bmatrix} = \begin{bmatrix} 0 \\ \vdots \\ 0 \\ g_{(M+1)} \\ \vdots \\ g_{(2M)} \\ 0 \\ \vdots \\ 0 \end{bmatrix} \tag{109}$$

Where l_{mn} are determined from Eqs (100) through (108) and represent the inner products in Eqs (88) through (91). The vector in Eq (109) with the coefficients α, β, and τ naturally represents the unknowns. The coefficients g_m represent the incident magnetic field in Eq (108) obtained from Eq (74). Representing Eq (109) as

$$[l_{mn}][\alpha_n] = [g_m]$$

the unknowns by can be found by the inverse operation (or its equivalent),

$$[\alpha_n] = [l_{mn}]^{-1}[g_m] \tag{110}$$

Once the unknowns, α's, β's, and τ's, are determined numerically, they may be used in Eq (81) to approximate the currents and charges as functions of position. These approximations may then be used to find the scattered and total electric and magnetic fields using Eqs (58) and (59),

respectively, for all points in the half space above the y=0 plane and Eqs (60) and (61), respectively, for all points inside the cavity. The same approximations used in the previous integrals may be used to approximate the integrals in Eqs (58) and (59). If the radar cross section of the cavity is desired instead of the scattered fields, an equation needs to be developed to produce it. The required equation is derived in the next chapter.

VI. Radar Cross Section

In three dimensional space, the RCS (radar cross section) of an obstacle, or scatterer, is defined as the area for which an "incident wave contains sufficient power to produce, by omnidirectional radiation, the same back-scattered power density" (4:116). Simply put, RCS is the cross sectional area that would normally be required to isotropically scatter the same power as the target radiates toward the receiver. The mathematical form for RCS can be in terms of the incident and scattered power, $\underline{P}^i$ and $\underline{P}^s$ respectively, as in (4:116):

$$\sigma = \lim_{r \to \infty} 4\pi r^2 \frac{|\underline{P}^s|}{|\underline{P}^i|} \tag{111}$$

RCS may also be determined from the field quantities, $\underline{E}$ and $\underline{H}$, as in (9:157):

$$\sigma = \lim_{r \to \infty} 4\pi r^2 \frac{|\underline{F}^s|^2}{|\underline{F}^i|^2} \tag{112}$$

where $\underline{F}$ refers to either $\underline{E}$ or $\underline{H}$.

Though other definitions are possible for RCS, Eqs (111) and (112) are the most widely used. The assumptions that are made in deriving Eqs (111) and (112) are that the scatterer is a three dimensional object and the distance, r, from the object approaches infinity to remove the dependence on range. The scattered fields decay as $1/r$ in the far field. The presence

of r^2 in the numerator of Eqs (111) and (112) effectively eliminates the effect of range on RCS.

For two-dimensional RCS problems, such as in the channel problem, the RCS is the area (or width) that would normally be required to scatter "isotropically", in two-dimensions, the same power radiated toward the receiver. A three dimensional isotropic radiator radiates into a sphere; a two-dimensional isotropic radiator radiates into a circle. The fields decay as $r^{-1/2}$ in two-dimensional problems. Though not actually a cross sectional area, the term RCS is still used in two-dimensions. Perhaps a more correct term would be a scattering width (9). The equation for RCS using the incident and scattered fields in two-dimensions becomes:

$$\sigma = \lim_{r \to \infty} 2\pi r \frac{|\underline{F}^s|^2}{|\underline{F}^i|^2} \tag{113}$$

The distance from the scatterer is again large enough to remove the dependence on range. Notice that if a two-dimensional scatterer could be seen in three dimensions, it would be infinitely long. If a two-dimensional scatterer of bounded cross sectional area could be viewed in three dimensions from a place a large distance r away, the scatterer would look like an infinite line.

To use Eq (113) on the channel problem, it must be noted that only the RCS of the cavity can be found. Since the cavity

is embedded in an infinite PEC plane, it would be impossible to reach a distance, r, such that the plane would appear as a point. Therefore, only the cavity's RCS can be determined. This is not at all bad. Determining the RCS of an infinite PEC plane is nearly useless.

The magnetic field scattered from the channel can be found using Eq (76) once the magnetic current is known. It appears as

$$\underline{H}^s(\underline{x}) = \frac{i\omega\epsilon}{4\pi} \int_A \underline{M}(\underline{x}')G(\underline{x};\underline{x}')\, dx' \tag{114}$$

Perhaps more precisely, using Eqs (70) through (73),

$$\underline{\underline{H}}^s(\underline{\underline{x}}) = -\frac{\omega\epsilon}{2} \int_{-1/2}^{1/2} \underline{\underline{M}}(\underline{\underline{x}}')H_0^{(1)}\{k[(x-x')^2 + y^2]^{1/2}\}\, dx' \tag{115}$$

Eq (113) refers to the limit as r approaches infinity. Since Eq (115) is in (x, y) coordinates, it needs to be converted to (r, θ) coordinates. If θ is the angle from the positive y axis measured positively clockwise and r is the distance from the origin, then the Hankel function of the first kind, order zero in Eq (115) becomes

$$H_0^{(1)}\{k[(x-x')^2 + y^2]^{1/2}\}$$
$$= H_0^{(1)}\{k[r^2\sin^2\theta - 2x'r\sin\theta + x'^2 + y^2\cos^2\theta]^{1/2}\}$$

or

$$H_0^{(1)}\{k[(x-x')^2 + y^2]^{1/2}\} = H_0^{(1)}\{k[r^2 - 2x'r\sin\theta + x'^2]^{1/2}\} \tag{116}$$

since

$$x = r\sin(\theta)$$
$$y = r\cos(\theta)$$

For large arguments, such as when r goes to infinity in Eq (116), the Hankel function of the first kind order zero behaves as

$$H_0^{(1)}(z) \sim \left[\frac{2}{\pi z}\right]^{1/2} \exp[i(z-\pi/4)], \quad z \to \infty \tag{117}$$

Using a binomial expansion on the argument of Eq (116) and discarding terms on the order of r^{-1}, a simpler form of Eq (115) is possible. In antenna theory it is common practice when going into the far field to expand the argument and keep the first term for magnitude purposes and the first two terms for phase purposes. This is what has been done here. The new form of Eq (115) is

$$\underline{H}^s(r,\theta) = i\omega\epsilon \int_{-1/2}^{1/2} \underline{M}(\underline{x}')\left[\frac{2}{\pi kr}\right]^{1/2} \exp[i(kr - x'k\sin\theta - \pi/4)]\, dx' \tag{118}$$

The integration in Eq (118) is in terms of x' so several of the constants may be removed to outside of the integral sign. Also, using Eq (81) to approximate $i\omega\epsilon\underline{M}(\underline{x}')$ and

breaking the integral from -1/2 to 1/2 into M integrals each over a width ΔC_n, Eq (114) may be further simplified as

$$\underline{H}^s(r,\theta) = \frac{i}{4}\left[\frac{2}{\pi kr}\right]^{1/2} \exp[i(kr-\pi/4)] \sum_{n=1}^{M} \alpha_n \int_{x_n-\Delta C/2}^{x_n+\Delta C/2} \exp[-ikx'\sin(\theta)]\, dx' \tag{119}$$

After performing the integration, the magnitude of the scattered field becomes

$$|\underline{H}^s| = \left[\frac{2}{\pi kr}\right]^{1/2} \left| \sum_{n=1}^{M} \alpha_n \exp[-ikx_n \sin(\theta)] \frac{\sin[k(\Delta C/2)\sin(\theta)]}{k \sin(\theta)} \right| \tag{120}$$

and k times the RCS becomes

$$k\sigma = 4 \left| \sum_{n=1}^{M} \alpha_n \exp[-ikx_n \sin(\theta)] \frac{\sin[k(\Delta C/2)\sin(\theta)]}{k \sin(\theta)} \right|^2 \tag{121}$$

Notice that when $\sin(\theta) = 0$, the ratio in Eq (121) is equal to $\Delta C/2$. Once the coefficients of Eq (81) have been determined (i.e. α's, β's, and τ's) the RCS of the cavity may be generated.

VII. The Computer Program

A FORTRAN computer program has been written to implement Eqs (100) through (108) and solve for the unknown coefficients in Eq (81). Using these coefficients, the program then evaluates Eq (121) for the RCS of the cavity. The fields scattered from the cavity or from both the PEC plane and the cavity are easily obtainable using Eqs (59) through (62), but have not been plotted. A copy of the program is contained in Appendix A.

The inputs to the program are the channel depth, normalized by the width, the incident angle of the incoming field, and the operating frequency in the form of the wave number, k. Here, the wave number is also normalized by the channel width, w. The output of the program is the RCS of the cavity excluding the PEC plane at all reflected angles from -90^{o} to $+90^{o}$, measured from the +y axis.

Appendix B provides some of the output from the program in a plotted form. The input angles for the plane wave are θ_i equal to 0^{o}, 22.5^{o}, 45^{o} and 67.5^{o}. The wave numbers used are k equal to 0.1, 1.0, and 10.0 which correspond to long wavelength, intermediate wavelength, and short wavelength respectively. The normalized depth of the channel, d, is either 0.25, 1.0, 4.0, or 8.0.

Using these numbers and subdividing the channel into pieces small enough so that the smallest length in the problem

(depth, wavelength, or width) is resolved by at least 12 patches, will yield systems of equations (2N+M by 2N+M) ranging in size from a minimum of 108 by 108 to a maximum of 440 by 440. The maximum number of equations and unknowns the program can reasonably solve is 450 due to storage constraints. A Gaussian elimination subroutine utilizing scaled partial pivoting and iterative improvement was used to solve the linear system of equations. Matrix inversion was tested as a possible method of solution and found to be as accurate as the Gaussian elimination subroutine (to eight significant digits) and much faster for more than one input angle.

Using the Gaussian elimination subroutine was slightly faster than the matrix inversion for one input angle and the output of both solutions was comparable. However, a single matrix inversion can be used to determine the RCS for many incident angles. With more than one input plane wave (i.e. θ_i=0°, 22.5°, 45°, and 67.5°), it was more efficient to use the matrix inversion technique. The output plotted in Appendix B was generated using the matrix inversion technique.

The program given in Appendix A can be easily modified to allow the variables K and d to vary while keeping the incident and reflected angles constant. Doing so requires a matrix inversion for each different K and d. This slows the program down since several inversions are necessary to get a good plot for the data. The plots obtained by varying K and d for specific input and output angles are presently more interesting

than those plots contained in Appendix B. Examples of varying k and d are given in the next chapter with a discussion of the results of the thesis.

Table III gives a quick list of the plots obtained by running the program. The plots generated from the program's data were obtained from the program inputs given in the table.

Table III. Summary of Inputs to the Plotted Data

Normalized Wave Number k	Normalized Channel Depth d	Plane Wave Incidence Angle θ_i	Matrix Size 2N+M
0.1	0.25	0, 22.5, 45, 67.5	288
0.1	1.0	" " "	108
0.1	4.0	" " "	252
0.1	8.0	" " "	444
1.0	0.25	" " "	288
1.0	1.0	" " "	108
1.0	4.0	" " "	252
1.0	8.0	" " "	444
10.0	0.25	" " "	288
10.0	1.0	" " "	144
10.0	4.0	" " "	336
0.2 — 10.0	1.0	0, 45	-
0.2 — 10.0	4.0	0, 45	-
1.0	0.25 — 8.0	0, 45	-
8.0	0.25 — 8.0	0, 45	-

Total Number of Plots = 60

The theory and equations derived earlier allow for determining the magnetic or electric field at any point $\underline{x}$ or the RCS at any bistatic angle. Notice that $\underline{x}$ may be inside the cavity, on the cavity, in the upper half space, or at any desired point in space. The plots given, however, are only for the RCS of the given input values; no plots were generated for the fields inside the cavity, though it is trivial to find them if desired. Discussion of the most prominent results is given in the next chapter.

VIII. Results

The most important contribution of this thesis is the development of the coupled set of Fredholm integral equations of the second kind. A set of equations was developed for the region above the cavity and a set of equations was developed for use within the cavity. These equations are coupled together by the aperture of the cavity. The coupled set (Eqs (64)through (67)) of Fredholm integral equations of the second kind can be used for any cavity in a PEC plane; they were later specialized for use with a two-dimensional cavity when a TE plane wave is the incident field. In this particular case, the equations can easily be solved numerically; or at least approximated numerically.

The resulting set of equations developed for the two-dimensional problem (Eqs (76) through (80)) reduced an integration over an infinite plane to an integration over an aperture and around the cavity within the plane. These specific equations can be used with any shape two-dimensional cavity. The scattered fields can be determined by using Eq (76) and the currents and charges found using Eqs (77) through (80).

A specific, rectangular, cavity was introduced and the RCS determined from that shaped cavity for several wavenumbers, K, and cavity depths, d. A computer program was written and used

to solve those equations. Most of the data generated by the computer program is given in Appendix B. Some of the most important observations of that data will be presented here.

Figure 5 shows three plots of RCS data for a wavenumber of 10, an incident angle of 0^{o}, and channel depths of 0.25, 1.0, and 4.0. Notice that the shape of the curves remains relatively constant while the peak magnitudes change. With incident angles of 0^{o}, all of the other sets of K and d produce plots similar to Figure 5. This indicates that a 0^{o} plane wave (with any wavelength) incident to any rectangular cavity produces a bistatic RCS of roughly the same shape given in Figure 5; only the magnitudes change with changing wavenumber and cavity size.

Figure 6 shows the same wavenumber and depths when the incident angle is 45^{o}. At this incident angle, the shape of the curves do not remain constant. This indicates that depth, wavenumber, and incident angle all contribute to RCS separately and are not tied specifically together.

Figures 7 and 8 give plots of k=1.0 and d=1.0 with incident angles of 22.5^{o}, 45^{o}, and 67.5^{o} and k=1.0 and d=8.0 with incident angles of 22.5^{o}, 45^{o}, and 67.5^{o}, respectively. With varying incident angles and a fixed K and d, the shape of the curves tend to change slowly. The relative magnitude of the plots also changes slowly. This type of plot occurs for every channel depth when k=0.1 and k=1.0. When k=10.0 (see Appendix B for the plots) the wavelength is much smaller and a

small change in input angle changes the ouput RCS by a much larger degree.

Allowing k to vary while holding the depth and incident and scattering angles constant produces some interesting plots. Figures 9, 10, and 11 are examples of this type of plot. Figures 9 and 10 are monostatic at 0^{o} with d=1.0, while Figure 11 is bistatic at 0^{o} and 45^{o}. Notice that Figure 11 contains two curves; one for an input angle of 0^{o} (output of 45^{o}) and one for an input angle of 45^{o} (output of 0^{o}). The concept of reciprocity (21) is represented quite well from the nearly exact coincidence of the two plots.

The plot in Figure 9 approaches zero at three points: all integer multiples of π. When $k=n\pi$, the wavelength, λ, is $2/n$. With a depth of 1.0 and an incident angle of 0^{o}, the monostatic RCS from this cavity approaches zero because an integer number of half wavelengths exactly fill the cavity.

The monostatic RCS at 45^{o} (Figure 10) has what seems to be discontinuities around k=3.4, k=6.3, and k=9.7. Though not shown, these RCS "spikes" occur at incident angles of 15^{o}, 30^{o}, and 60^{o} at near the same values of k, and expected for at least all angles in between 15^{o} and 60^{o}.

This phenomena was investigated further by: 1) expanding the curve around the k=3.4 value (Figures 12 and 13) and 2) allowing the depth to vary with k=3.3, k=3.4, and k=3.5 (Figure 14). From Figures 12 and 13, it appears as if the "spike" is at least a smooth curve and may belong in the RCS plots (as

opposed to being a numerical instability). Figure 14 shows that slight changes in k and d around these spikes give large changes in the monostatic RCS at 45°. Again, this indicates that k, d, and θ_i are all separate variables and should be treated as such.

Holding k constant and allowing d to vary produces oscillating plots from a maximum to a minimum and back again. This is because as the depth of the channel is increased, more wavelengths (when the wavelength is held constant) can fit into the channel. An example of this type of plot is given in Figure 15. Figures similar to Figures 5 through 15 are given in Appendix B.

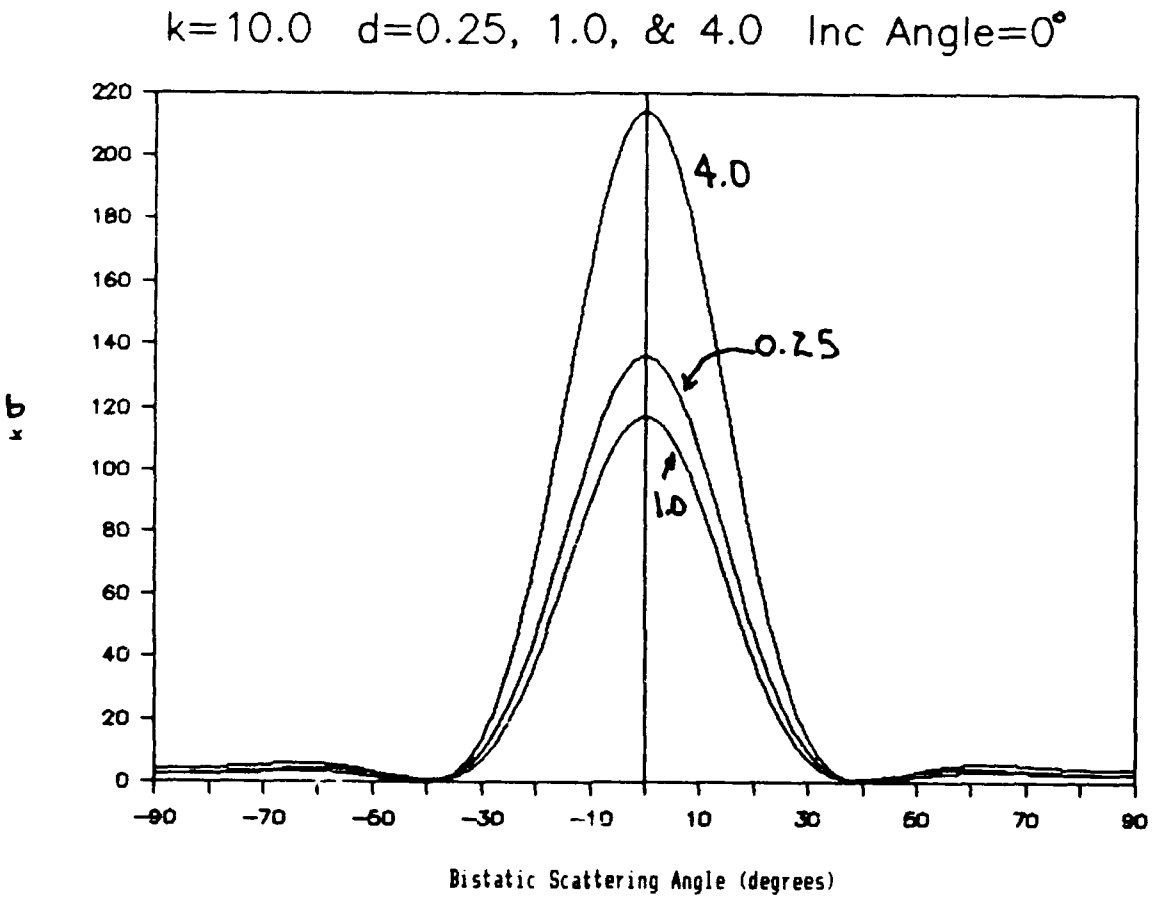

Figure 5. Bistatic RCS with k=10.0, d=0.25, 1.0, and 4.0 with an Incident Angle of 0°.

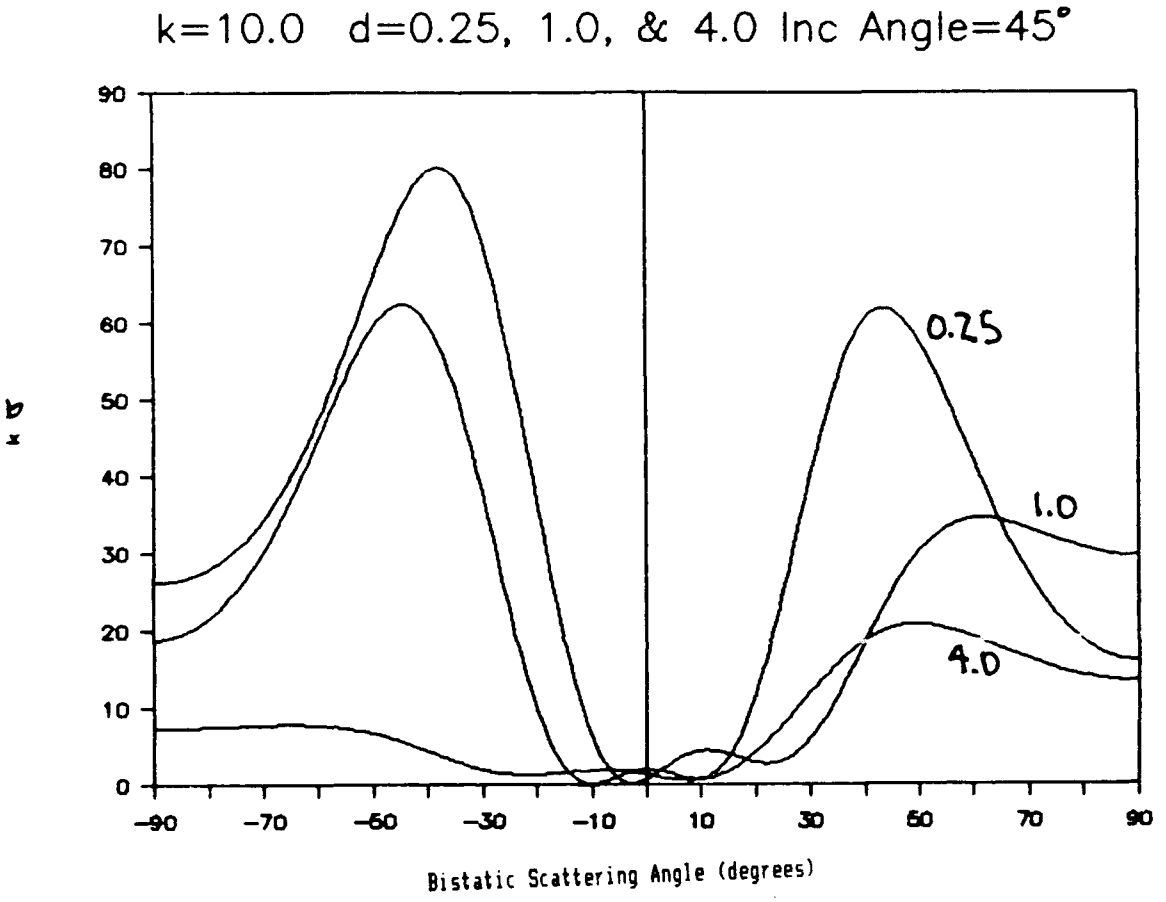

Figure 6. Bistatic RCS with k=10.0, d=0.25, 1.0, and 4.0 with an Incident Angle of 45°.

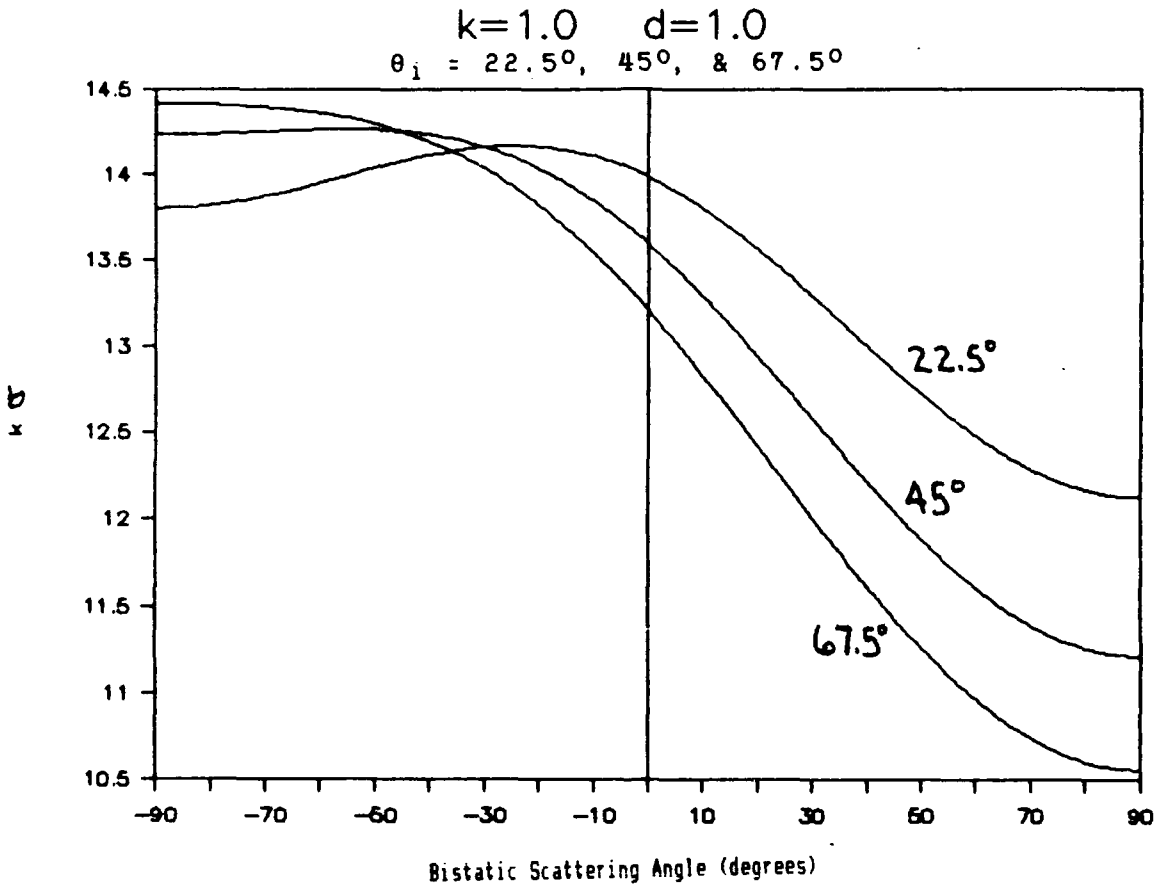

Figure 7. Bistatic RCS with k=1.0 and d=1.0. The Incident Angles are 22.5°, 45°, and 67.5°.

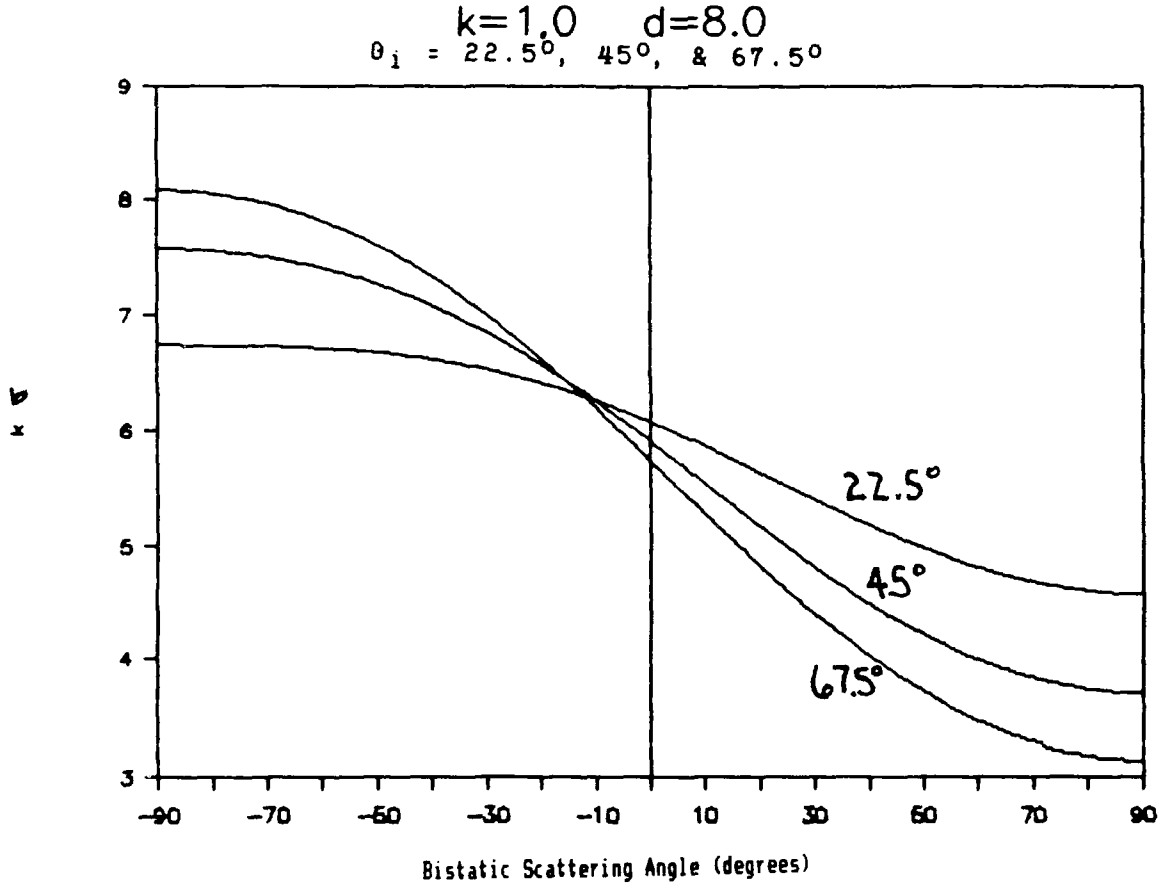

Figure 8. Bistatic RCS with k=1.0 and d=8.0. The Incident Angles are 22.5°, 45°. and 67.5°.

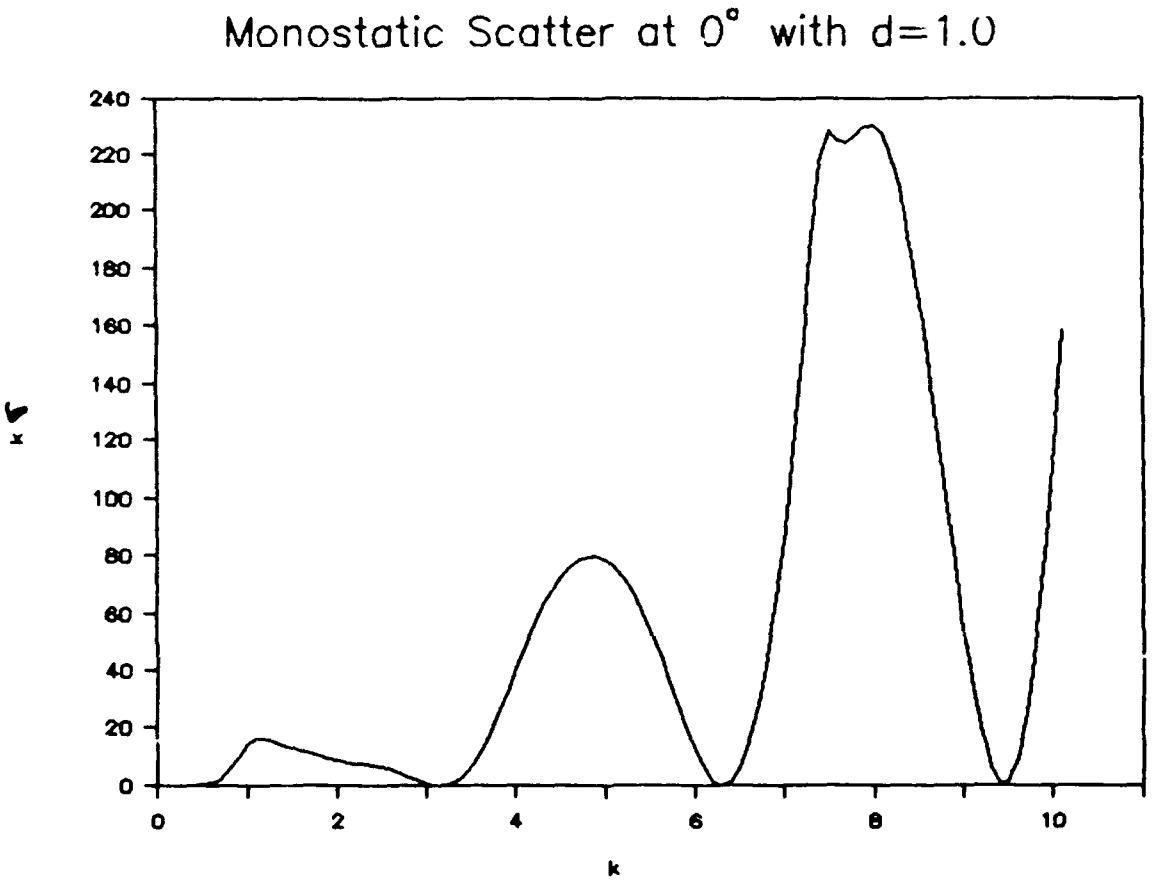

Figure 9. Monostatic RCS at 0° with d=1.0 and a varying wavenumber, k.

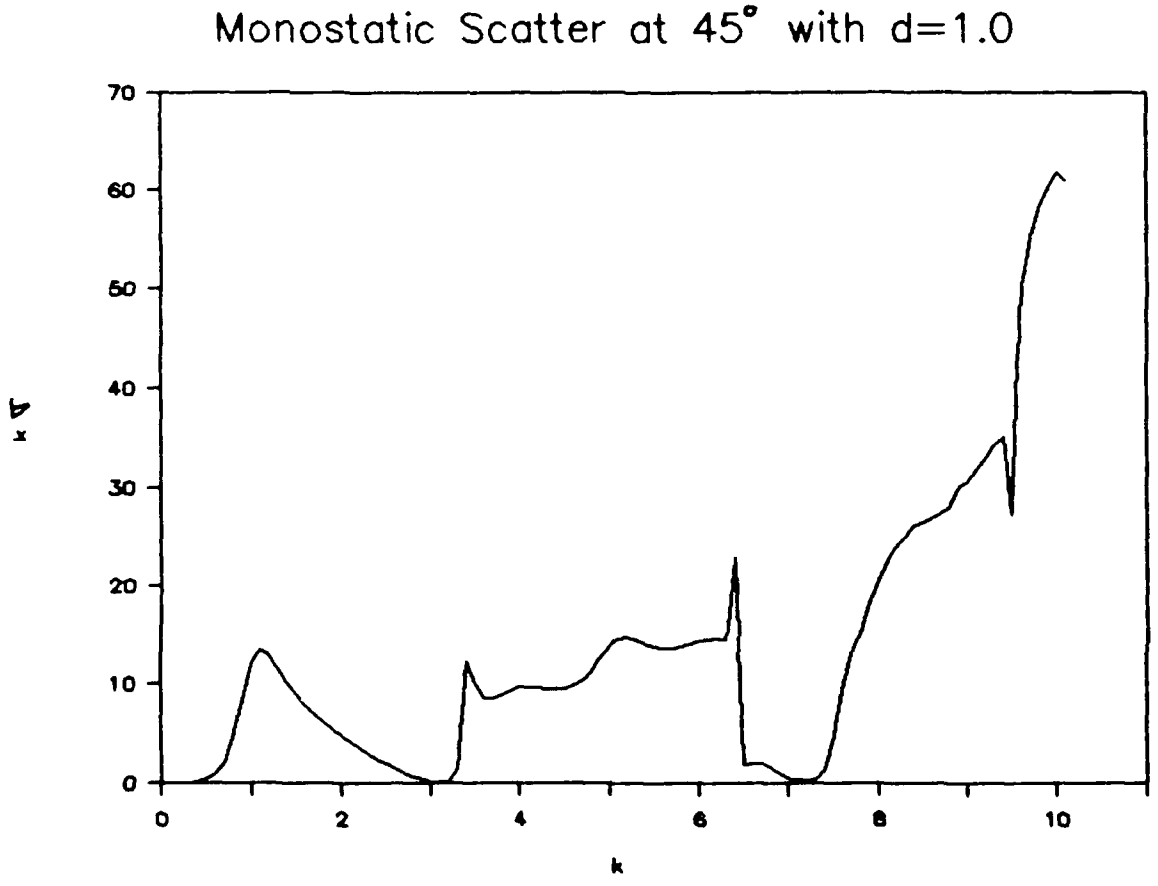

Figure 10. Monostatic RCS at 45° with d=1.0 and a varying wavenumber, k.

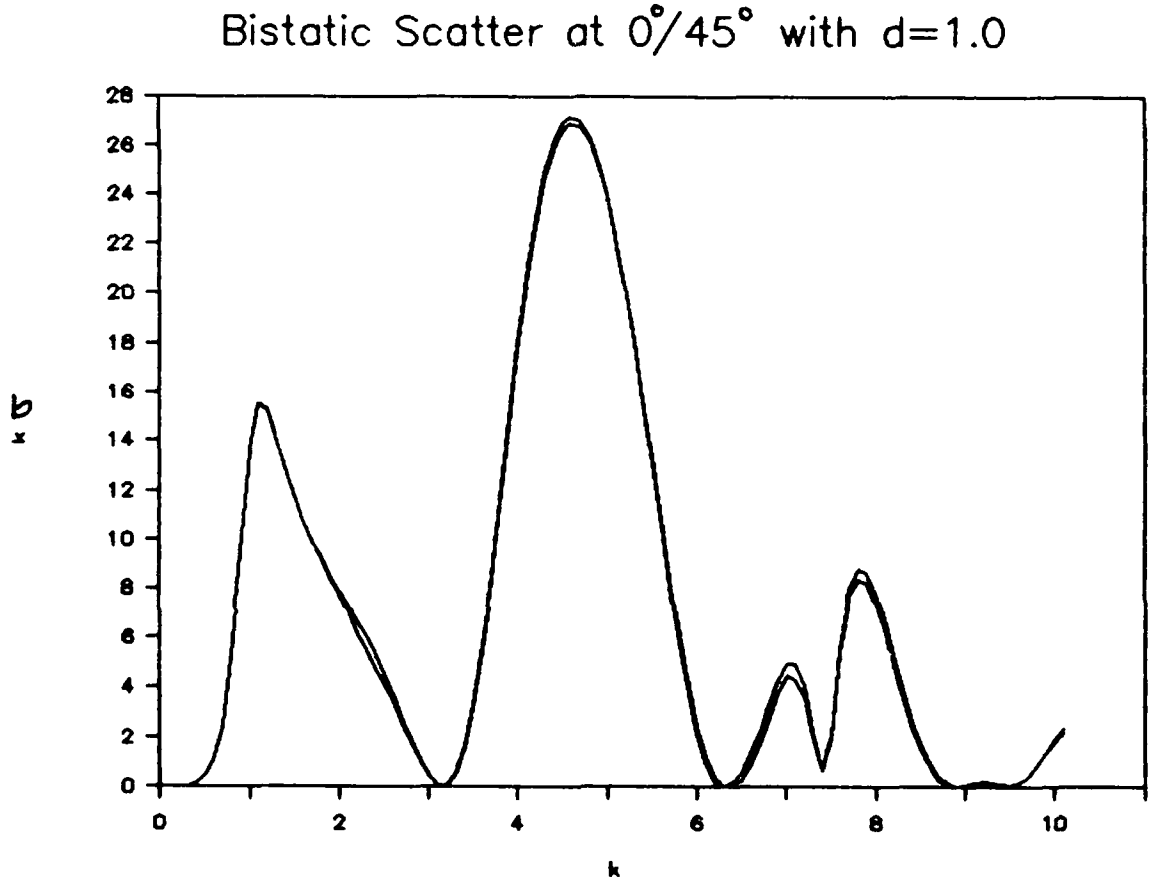

Figure 11. Bistatic RCS at 0°/45° with d=1.0 and a varying wavenumber, k. Reciprocity can easily been seen from these two curves.

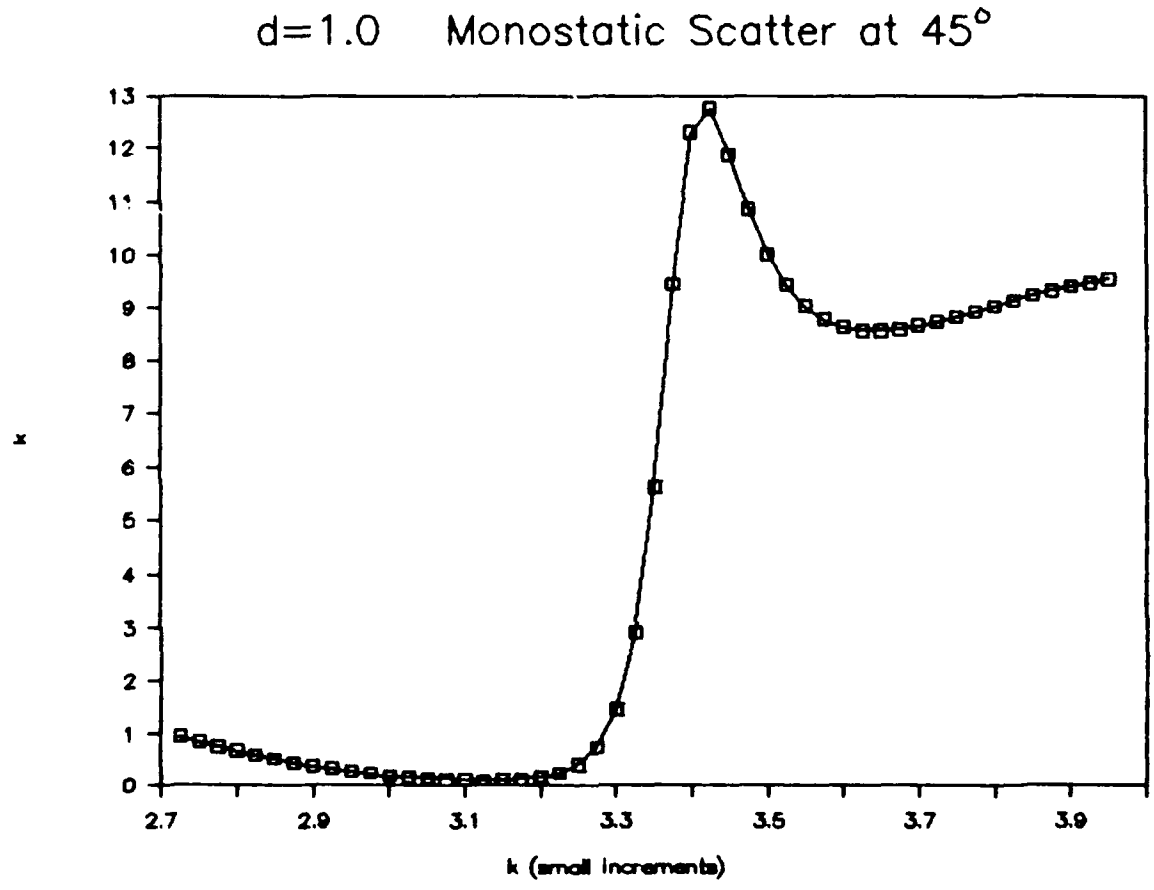

Figure 12. Monostatic RCS at 45° with d=1.0 and a varying wavenumber, k; Small increments of k were taken around the spike in Figure 10.

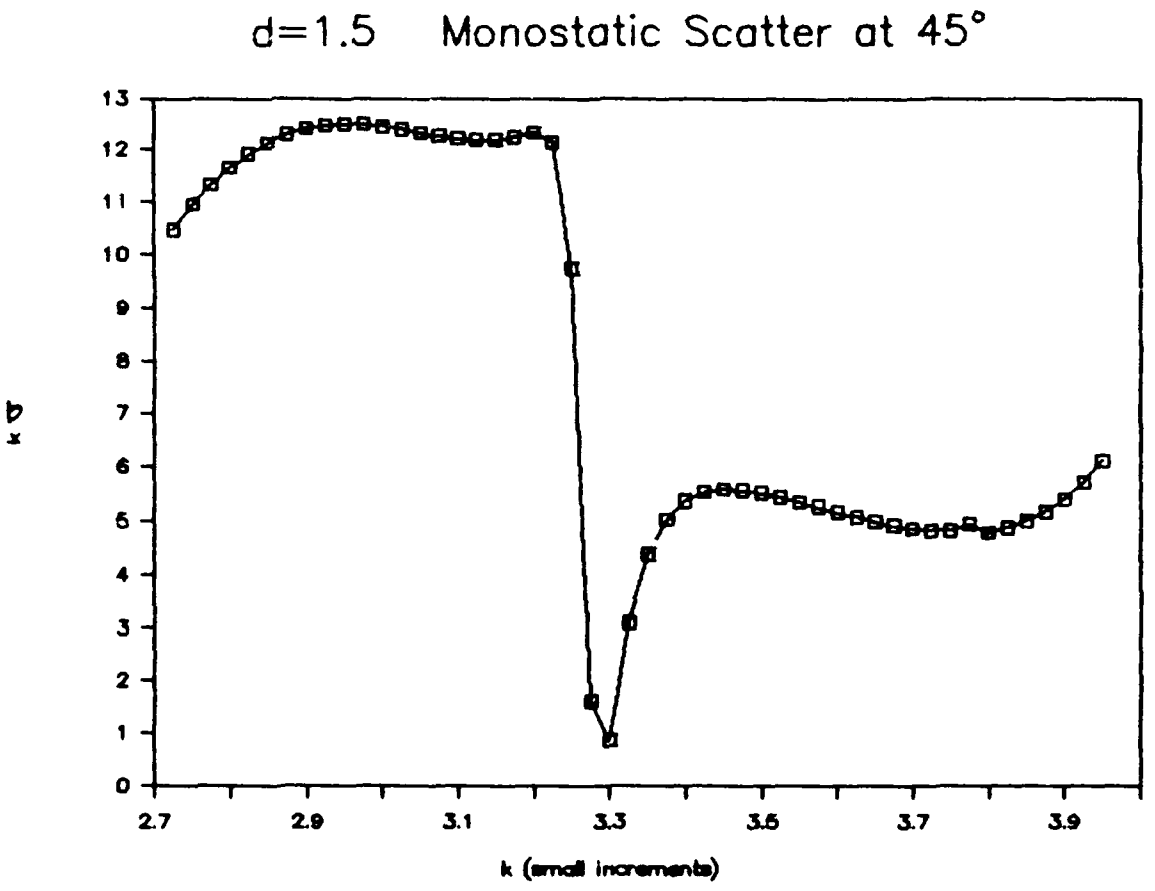

Figure 13. Monostatic RCS at 45° with d=1.5 and a varying wavenumber, k; Small increments of k were taken around the spike in Figure 10.

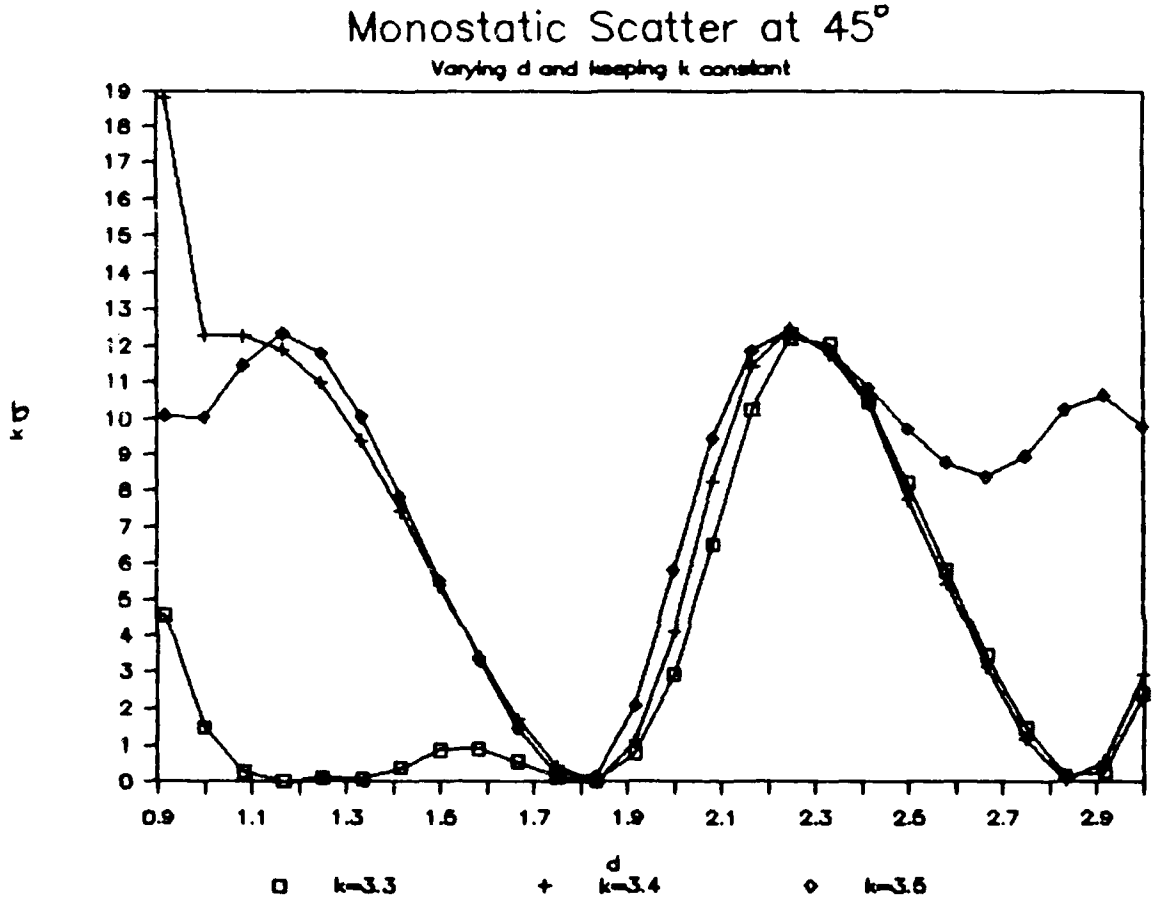

Figure 14. Monostatic RCS at 45° with k=3.3, 3.4, and 3.5 and a varying depth, d; Small increments of d were taken for the three k values around the spike in Figure 10.

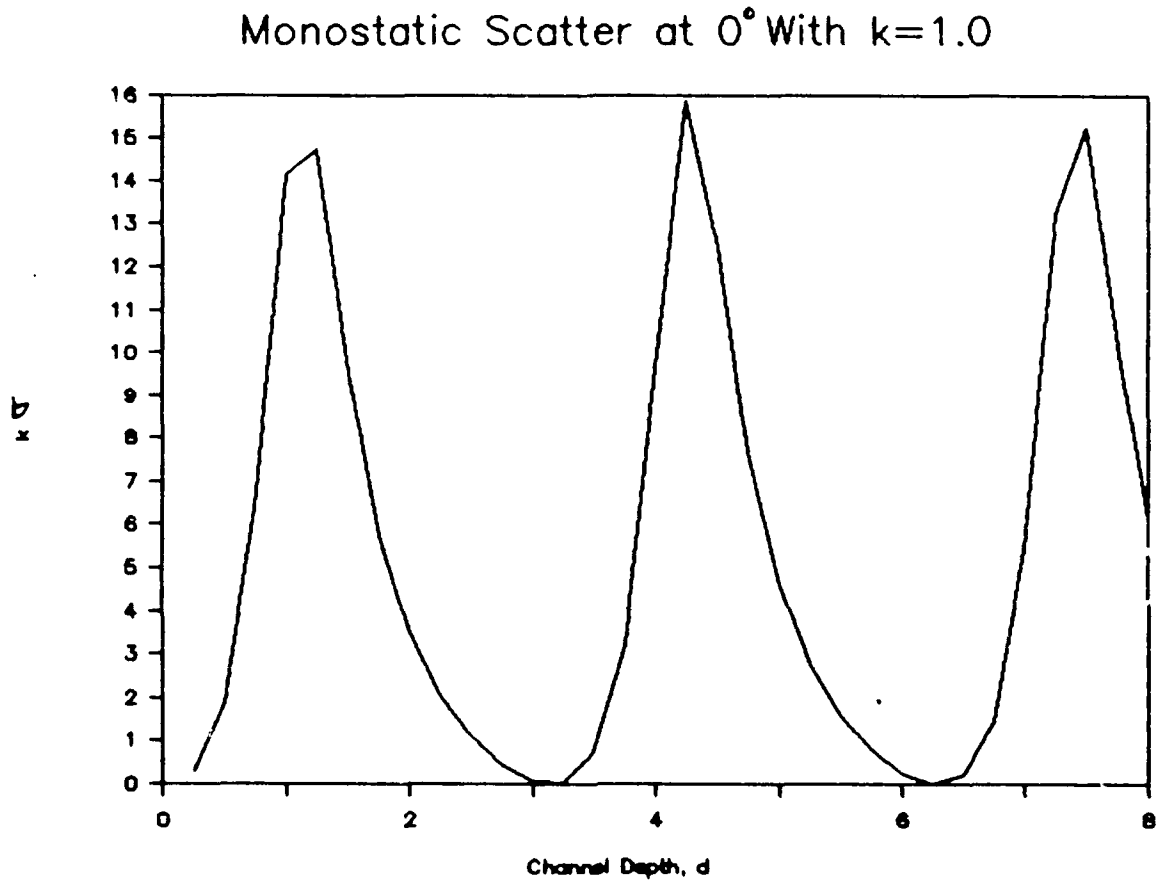

Figure 15. Monostatic RCS at 0° with a fixed k=1.0 and a varying depth, d.

IX. Conclusions and Recommendations

The most important contribution of the thesis is the development of the coupled set of Fredholm integral equations of the second kind for the two-dimensional cavity. The integral equations derived for finding both the electric and magnetic fields and the surface currents and charges are exact. This thesis shows that using the half space Green's function to derive the equations above the plane in Figure 1, the free space Green's function to derive the equations used inside the cavity, and then coupling these equations through the aperture is an accurate way to determine the fields scattered from the channel. It is concluded that the RCSs plotted in Figures 5 through 15 and Appendix B are reasonably accurate. They are not exact in that some approximations were necessary to solve the equations numerically.

The method used to calculate the fields, currents, and charges is an approximation. As the discretization parameter, ΔC, approaches zero, the approximation should better represent the exact solution. However, with more segments, the number of unknowns and equations also increases and therefore so does the computer time required to solve the system of equations. As the number of equations increases, so too does round-off error in the computer. The accuracy that can be obtained using moment methods is therefore limited by round-off error.

In this thesis, the smallest length in the problem (wavelength, channel depth, or width) was broken up into at

least 12 segments. This seems to give reasonable accuracy at a reasonable cost in computer time. Test cases were applied for several different segments per smallest length. (Actually, 4, 5, 6, 8, 10, 12, 14, 16, 20, 24, and 32 segments per smallest length were used.) All of the cases above 8 segments per smallest length gave RCS plots of approximately the same magnitude and shape for all bistatic angles. The time required when using 12 segments per smallest length was only a few minutes longer than when using 10 segments. Though, even at 32 segments per smallest length, the RCS plots seemed to be still converging on an "exact" plot (remember, numerical solutions are limited by round-off error.) The theory and methods used here allow for more accuracy, limited by round-off error, if desired. The user must be willing to give up computer time in order to achieve this accuracy.

Appendix C gives a description of a target designed to obtain RCS measurements of the rectangular cavity. Using this target and the method described in Appendix C, laboratory measurements can be obtained to check the predicted RCS values given in this thesis.

There are several possibilities for further analysis for this problem. These include:

1. Making the measurements on the target described in Appendix C to determine the accuracy of the method described therein.

2. A selection of different shaped cavities than the rectangular one used here. This would require reworking the approximate solutions and new computer programs.

3. A TM (transverse magnetic) incident field instead of the TE case used here. New equations may have to be derived using Dirichlet boundary conditions and an equation similar to Eq (58) could be used in place of Eq (60) and an equation similar to Eq (61) used instead of Eq (59) to get equations similar to Eqs (64) and (65) respectively.

4. A cavity filled with a dielectric. This changes the problem drastically. The free space green's function inside of the cavity will have to be evaluated to determine the affects of filling the cavity with a dielectric.

5. Change the channel to be an open channel, meaning that the depth is infinite. New equations would need to be derived for the inside of the cavity in this case. Perhaps a new Green's function can be explored to eliminate integrating along the now infinitely deep channel sides.

6. Let the cavity be three dimensional. That is, let the cavity have a finite length as well as the finite width, w, and depth, d. This gets closer to an open ended flanged waveguide.

Another contribution from this thesis is that it may now be possible to easily determine the RCS from infinite cylinders, or other two-dimensional objects, containing abrupt "cavity-like" variations in an otherwise smooth surface. If such an object had a trench along the side, such as the rectangular cavity explored in this thesis, or some other cavity, it should be possible to find the RCS of such a cylinder by adding the fields scattered from a perfect cylinder to those scattered from the perturbing cavity and using the result as the scattered field. Such an approximation, based on the cavity solution obtained herein, would better represent the true solution when the curvature near the cavity is small.

Figure 16 shows the proposed method to approximate the scattered RCS from a cylinder with a small rectangular cavity. It should be investigated to ascertain the feasibility of the method.

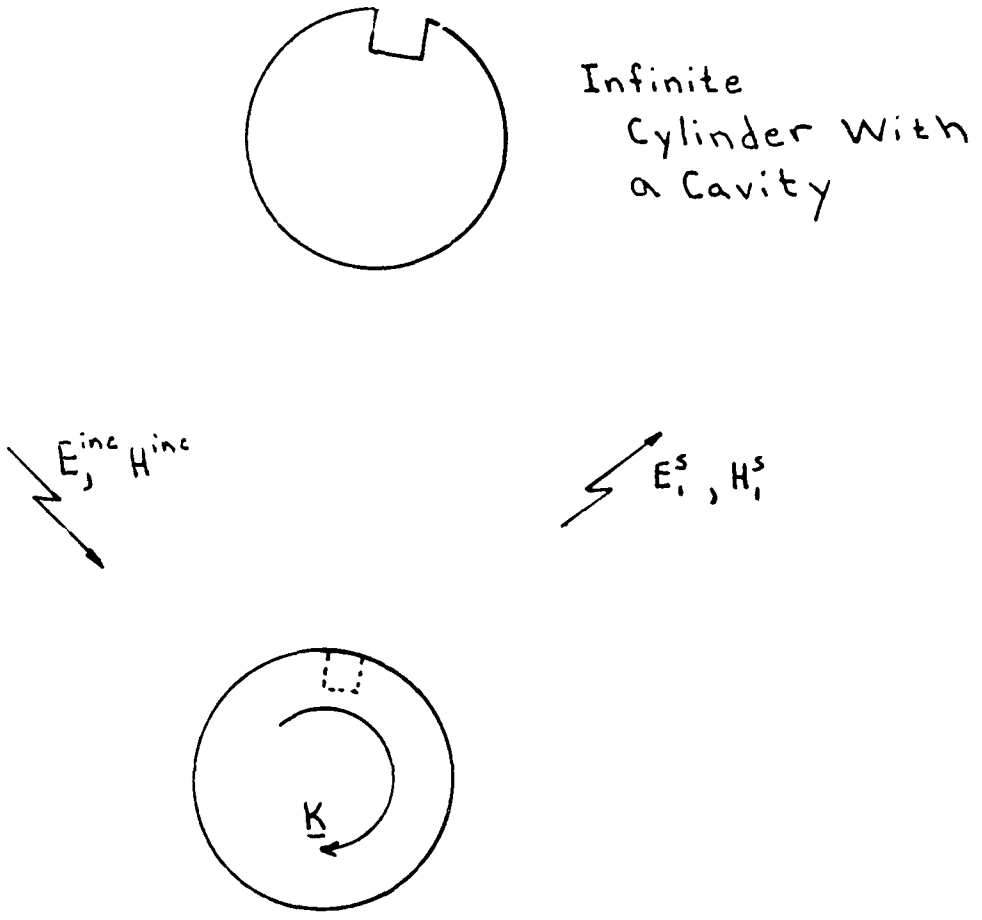

(a) Fields Scattered from a Whole Cylinder Without the Cavity

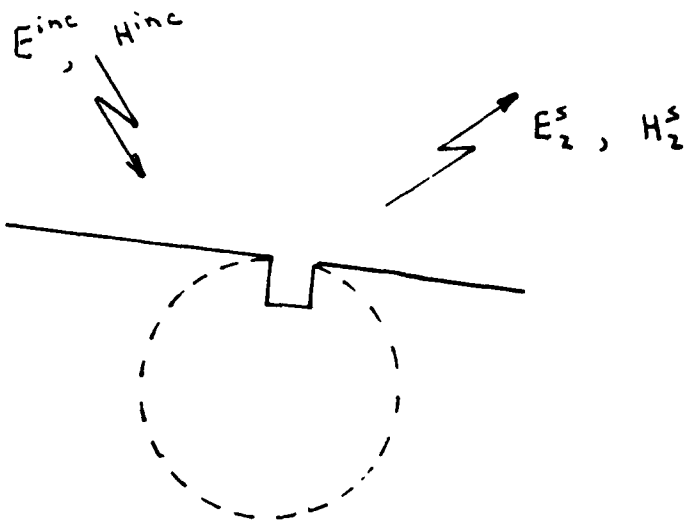

(b) Find the Fields Scattered from the Cavity

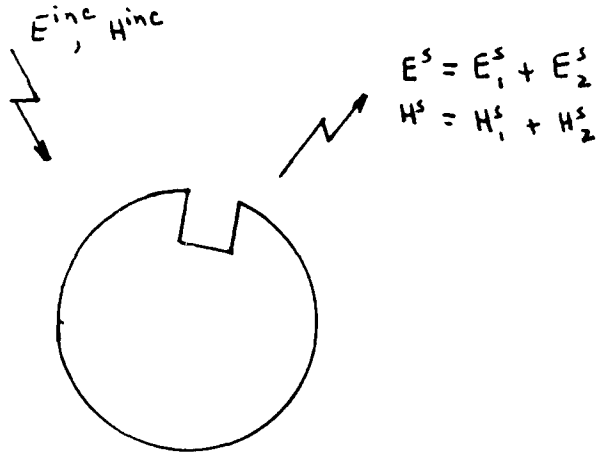

(c) Add the Fields from (a) and (b) to Calculate the RCS

Figure 16. Method for Finding the RCS of an Infinite Cylinder With a Rectangular Cavity by Adding the Fields Scattered From the Perfect Cylinder (a) to Those Scattered From the Cavity (b) to Get the Total Field (c).

The above recommendations for further study are important to fully evaluate the scattered EM fields from objects containing cavities. The information contained in this thesis is a continuation toward that goal.

In the preceding pages, a set of Fredholm integral equations of the second kind using Neumann boundary conditions (the half space Green's function, $G(\underline{x};\underline{x}')$) were derived for the half space above the cavity. These equations were then coupled to a corresponding set of integral equations for inside the cavity and the coupled set was used to find surface currents and charges that could be used to find the scattered fields or the RCS of the cavity. A specific, rectangular, cavity was introduced as a test case and the RCS calculated using a Fortran computer program specifically written for this task. The output of that program was addressed and presented. Finally, specific areas for future analysis were given. Though the analysis, study, and experimentation continues, this thesis has completed.

Appendix A: Computer Program

The following listing is the FORTRAN computer program written to solve the test problem within the thesis.

```
C     This is the program for finding the RCS of a rectangular
C     channel of normalized depth (dw), unity width, and for a
C     wave number (wk) read as input.  This version runs on the
C     AFIT CSC computer system with IMSL commands.  The program
C     must be linked with the IMSL library.  To do this on the
c     CSC
C
C      THE APPROPRIATE LINK STATEMENT IS:
C      LINK FILENAME.OBJ, IMSL$DIR:IMSL/LIB
C
C   This version uses the matrix inverse routine.
C   It reads the input file "DINP.DAT" for the number of
c   different k's (wk) and d's (dw) to be used.  This number is
c   called nin.  The program then runs nin times and prints out
c   the RCS data in 10 significant digits.  The number of
c   segments that the smallest measurement is to be broken into
c   is read from an input file as well as the incoming
c   planewave angles.
c   This version checks for 1/delc as an integer.  As long
c   as npp is divisible by 4, d is a multiple of .25 and
c   k=10, or less than 2pi, this will work.
c
C    Some of the main variables are:
c    J=imaginary operator (squareroot of -1)
c    dw=channel depth normalized to the width
c    wk=wave number normalized to the width
c    delc=width of each line segment after discretization
c    RCS()=Radar Cross Section data that is output
C    XM(1(or 2), N)=The midpoint of the Nth linesegment,  a 1
c    indicates the x point and a 2 indicates the y point
c    CLNM(m,n)=the matrix holding the data for the linear
c    operations on the currents and charges.  (see the Thesis c
c noted above Eq. (109) for details)
C    cout()=the current and charge coefficients
c    g() = the incident fields data (see Eq. 190 in the thesis)
c
c
      IMPLICIT DOUBLE PRECISION A, B, D, E, F, H, O, Q, R, T, U, V, W, X, Y, Z

      IMPLICIT COMPLEX*16 C, J, G, P, S
      DOUBLE PRECISION CONST
      CHARACTER*10 FLNAME
      DIMENSION G(1:500), CLNM(1:500, 1:500), COUT(1:500)
      DIMENSION CWKS(125250), IWKS(500), RCS(1:10, -90:90)
      COMMON J, XM(1:2, 1:500), WK, DELC
```

```
C
C  Set some of the preliminary constants
c
      J=(0.D0,1.D0)
      ONE=1.D0
      CZERO=(0.D0,0.D0)
      PI=3.141592653589D0
c
c  Open files for input (2 and 4) and output (5)
c  unit 5 holds the real and imaginary parts of the current
c  across the aperture for the first incident plane wave
c
      OPEN (UNIT=2,FILE='DINP.DAT',STATUS='UNKNOWN')
      OPEN (UNIT=4,FILE='DIN2.DAT',STATUS='UNKNOWN')
      OPEN (UNIT=5,FILE='CRNT.DAT',STATUS='UNKNOWN')
c
c NIN is the number of times to read the input file for sets of
c k and d (which are wk and dw) and output files to be unit #3
c NPP is the number of points per smallest measurement
c
      READ (2,899) NIN
      READ (2,899) NPP
c
c   RFRST is the first incidence angle, RLST is the last, and
c   RSTEP is the step size to get from RFRST to RLST
c
      READ (4,*) RFRST,RLST,RSTEP
898   FORMAT(F10.3)
899   FORMAT(I4)
C
C     IMAX is the integer to be used latter to store the data
c     generated as RCS data
c
      IMAX=IDINT((RLST-RFRST)/RSTEP+1.5)
      DO 650 ICNT=1,NIN,1
         READ (2,850) WK
         READ (2,851) DW
         READ (2,855) FLNAME
         OPEN (UNIT=3, FILE=FLNAME,STATUS='UNKNOWN')
         WK=DBLE(WK)
         DW=DBLE(DW)
C
C   WAVE is the wavelength
c   RMIN is the smallest of WAVE, DW (depth), and 1 (width)
         WAVE=2.D0*PI/WK
         RMIN=DMIN1(WAVE,DW,ONE)
C
C   Find the discretization size, DELC
c   and then make sure that 1/delc is an integer
c
         DELC=RMIN/DBLE(FLOAT(NPP))
         DELC=1.D0/DBLE(FLOAT(IDINT(1.D0/DELC+0.99975)))
c
```

```
C NMAX will be the matrix size (nmax by nmax).  It is the total
c number of line segments needed to go around the cavity twice
c and across the aperture one extra time.
c The information is written out just to keep track how the
c program is progressing.
c


         NMAX=IDINT((4.D0*DW+5.D0)/DELC +0.5D0)
         WRITE (*,854) WK, DW, DELC, NMAX, FLNAME
         WRITE (3,854) WK, DW, DELC, NMAX, FLNAME
854      FORMAT(1X,3E14.6,2X,I3,A10)
850    FORMAT(F9.6)
851    FORMAT(F4.1)
853    FORMAT(I3)
855    FORMAT(A10)
C
C       FILL THE POSITION MATRIX XM()
C
C       THE "+0.5" INSURES THAT 1.9999 DOES NOT GET TRUNCATED
C
c The MONE through MEIGHT are the last line segments (delc's)
c for each major segment, across the aperture for M, across the
c aperture of K, down S- for K, ...
c
      MONE=IDINT(1.D0/DELC+0.5D0)
      MTWO=2*MONE
      MTHR=MTWO+IDINT(DW/DELC+0.5D0)
      MFOUR=IDINT((3.D0+DW)/DELC+0.5D0)
      MFIVE=MFOUR+IDINT(DW/DELC+0.5D0)
      MSIX=MFIVE+MONE
      MSEVN=MSIX+IDINT(DW/DELC+0.5D0)
      MEIGHT=MSEVN+MONE
C
C The first section is across the aperture (for Mag Crnt)
C
      DO 10,  I=1,MONE,1
         XM(1,I)=-0.5D0+(DBLE(FLOAT(I))-0.5D0)*DELC
         XM(2,I)=0.0D0
10    CONTINUE
C
C The second section is across the aperture for the K vector
C
      DO 12,  I=MONE+1,MTWO,1
         XM(1,I)=0.5D0-DELC*(DBLE(FLOAT(I-MONE))-0.5D0)
         XM(2,I)=0.0D0
12    CONTINUE
C
C Section 3 is for S-
C
      DO 14, I=MTWO+1,MTHR,1
         XM(2,I)=-DELC*(DBLE(FLOAT(I-MTWO))-0.5D0)
         XM(1,I)=-0.5D0
```

```
14     CONTINUE
C
C  Section 4 is for sd
C
       DO 16, I=MTHR+1, MFOUR, 1
          XM(1, I)=-0.5D0+DELC*(DBLE(FLOAT(I-MTHR))-0.5D0)
          XM(2, I)=-DW
16     CONTINUE

C
C  Section 5 is for s+
C
       DO 18,  I=MFOUR+1, MFIVE, 1
          XM(2, I)=-DW+DELC*(DBLE(FLOAT(I-MFOUR))-0.5D0)
          XM(1, I)=0.5D0
18     CONTINUE
C
C  Section 6 is for A for the sigma equations
C
       DO 22,  I=MFIVE+1, MSIX, 1
          XM(1, I)=0.5D0-DELC*(DBLE(FLOAT(I-MFIVE))-0.5D0)
          XM(2, I)=0.0D0
22     CONTINUE
C
C  Section 7 is for s-
C
       DO 24, I=MSIX+1, MSEVN, 1
          XM(2, I)=-DELC*(DBLE(FLOAT(I-MSIX))-0.5D0)
          XM(1, I)=-0.5D0
24     CONTINUE
C
C  Section 8 is for sd
C
       DO 26, I=MSEVN+1, MEIGHT, 1
          XM(1, I)=-0.5D0+DELC*(DBLE(FLOAT(I-MSEVN))-0.5D0)
          XM(2, I)=-DW
26     CONTINUE
C
C  Section 9 is for s+
C
       DO 28,  I=MEIGHT+1, NMAX, 1
          XM(2, I)=-DW+DELC*(DBLE(FLOAT(I-MEIGHT))-0.5D0)
          XM(1, I)=0.5D0
28     CONTINUE
C
C  The position matrix is now filled
C
```

```
C    Next we must fill the CLNM() matrix.
C
C    Set constants
C
       EULER=.5772156649015D0
       CONST=2.D0/WK/PI
       ETA=WK*DELC/4.D0
       SP=-CONST*( DLOG(ETA)-1.D0 )*ETA
       SP=SP+( J/WK - CONST*EULER )*ETA
       ETA3=ETA*ETA*ETA
       SP=SP+ETA3*CONST*( DLOG(ETA) - 1.D0/3.D0 )/3.D0
       SP=SP-ETA3*( CONST*(1.D0-EULER) + J/WK )/3.D0
       C3=-WK*WK
C
C The M is down the side of the matrix (row) and refers to the
C "OBSERVATION" point. The "N" is across the top of the matrix
C  (column) and is the "SOURCE" point.
c
c In appropriate cases, the program must check for self-
C patches, i.e. those cases when the midpoint of the
c observation point is equal to the midpoint of the source
c point.
C
C THE FIRST MAJOR SECTION HAS M ON A(ALPHA)
C
C EQ A  (in the derivation notes)
C
       DO 90,  M=1,MONE,1
C
C N on A(alpha)
C
          DO 40,  N=1,MONE,1
             IF (N .EQ. M) THEN
                 CLNM(M,N)=(0.5D0,0.D0)
                 GOTO 40
             ENDIF
             CLNM(M,N)=CZERO
40        CONTINUE
C
C  N ON A(BETA)
C
          DO 50,  N=MONE+1,MTWO,1
             IF (DABS(XM(1,M)-XM(1,N)) .LT. DELC/3.D0) THEN
                CLNM(M,N)=C3*SP
                GOTO 50
             ENDIF
         CLNM(M,N)=C3*PHI0(XM(1,M),XM(2,M),XM(1,N),XM(2,N))*DELC
50        CONTINUE
C
C  N ON S-(BETA)
C
          DO 60,  N=MTWO+1,MTHR,1
              CLNM(M,N)=CZERO
```

```
60        CONTINUE
C
C  N ON SD(BETA) THROUGH S+(BETA)
C
          DO 65,  N=MTHR+1,MFOUR,1
        CLNM(M,N)=-C3*PHI0(XM(1,M),XM(2,M),XM(1,N),XM(2,N))*DELC
65        CONTINUE
          DO 66,  N=MFOUR+1,MFIVE,1
              CLNM(M,N)=CZERO
66        CONTINUE
C
C  N ON A(GAMMA)
C


          DO 70,  N=MFIVE+1,MSIX,1
             IF (DABS(XM(1,M)-XM(1,N)) .LT. DELC/3.D0) THEN
                CLNM(M,N)=CZERO
                GOTO 70
             ENDIF
           CLNM(M,N)=PHI1X(XM(1,M),XM(2,M),XM(1,N),XM(2,N))*DELC
70        CONTINUE
C
C N ON S-(GAMMA) THROUGH S+(GAMMA)
C
          DO 80,  N=MSIX+1,MSEVN,1
            CLNM(M,N)=PHI1X(XM(1,M),XM(2,M),XM(1,N),XM(2,N))*DELC
80        CONTINUE
          DO 85,  N=MSEVN+1,NMAX,1
CLNM(M,N)=PHI1X(XM(1,M),XM(2,M),XM(1,N),XM(2,N))*DELC
85        CONTINUE
90      CONTINUE
C
C Thus ends the section for M on A(alpha)--the next major c
section is for M on A(beta)
C
C  Eq b divided by 2 to get the 1/2 along the diagonal
C
        DO 130,  M=MONE+1,MTWO,1
C
C  N on A(alpha)
C
          DO 100 N=1,MONE,1
            IF (DABS(XM(1,M)-XM(1,N)) .LT. DELC/3.D0) THEN
                CLNM(M,N)=-SP
                GOTO 100
             ENDIF
           CLNM(M,N)=-PHI0(XM(1,M),XM(2,M),XM(1,N),XM(2,N))*DELC
100       CONTINUE
C
C  N on A(beta)
C
          DO 110,  N=MONE+1,MTWO,1
```

```
               IF (N .EQ. M) THEN
                  CLNM(M,N)=(0.5D0,0.D0)
                  GOTO 110
               ENDIF
               CLNM(M,N)=CZERO
110         CONTINUE
C
C  N on all of the rest of the segments
C
            DO 120, N=MTWO+1,NMAX,1
               CLNM(M,N)=CZERO
120         CONTINUE
130      CONTINUE



C
C  This next major section takes care of the obsrvtn point, M,
C  on s-(beta) through s+(beta) for the source point, N, on
c  A(alpha) and A(beta)
C
C
C  The next major section is for M on s-(beta) and N on all
c  surfaces except for A(alpha) and A(beta)
C
C  Eq c
C
         DO 210, M=MTWO+1,MTHR,1
C
C  N on A(alpha)
C
            DO 140, N=1,MONE,1
              CLNM(M,N)=PHI0(XM(1,M),XM(2,M),XM(1,N),XM(2,N))*DELC
140         CONTINUE
C
C  N on A(beta)
C
            DO 150, N=MONE+1,MTWO,1
             CLNM(M,N)=PHI1Y(XM(1,M),XM(2,M),XM(1,N),XM(2,N))*DELC
150         CONTINUE
C
C  N on s-(beta)
C
            DO 170, N=MTWO+1,MTHR,1
               IF (N .EQ. M) THEN
                  CLNM(M,N)=(0.5D0,0.D0)
                  GOTO 170
               ENDIF
               CLNM(M,N)=CZERO
170         CONTINUE
C
C  N on sd(beta)
C
```

```
          DO 180,  N=MTHR+1, MFOUR, 1
          CLNM(M, N)=-PHI1Y(XM(1, M), XM(2, M), XM(1, N), XM(2, N))*DELC
180       CONTINUE
C
C  N on s+(beta)
C
          DO 190,  N=MFOUR+1, MFIVE, 1
           CLNM(M, N)=PHI1X(XM(1, M), XM(2, M), XM(1, N), XM(2, N))*DELC
190       CONTINUE
C
C  N on A(gamma) through s+(gamma)
C
          DO 200,  N=MFIVE+1, NMAX, 1
             CLNM(M, N)=CZERO
200       CONTINUE
210    CONTINUE

C
C   The next major section is for M on sd(beta)
C
C   Eq d
C
       DO 260,  M=MTHR+1, MFOUR, 1
C
C  N on A(alpha)
C
          DO 141,  N=1, MONE, 1
          CLNM(M, N)=-PHI0(XM(1, M), XM(2, M), XM(1, N), XM(2, N))*DELC
141       CONTINUE
C
C  N on A(BETA)
C
          DO 151,  N=MONE+1, MTWO, 1
          CLNM(M, N)=-PHI1Y(XM(1, M), XM(2, M), XM(1, N), XM(2, N))*DELC
151       CONTINUE

C
C  N on s-(beta)
C
          DO 220,  N=MTWO+1, MTHR, 1
          CLNM(M, N)=PHI1X(XM(1, M), XM(2, M), XM(1, N), XM(2, N))*DELC
220       CONTINUE
C
C  N on sd(beta)
C
          DO 230,  N=MTHR+1, MFOUR, 1
            IF (N .EQ. M) THEN
               CLNM(M, N)=(-0.5D0, 0.D0)
               GOTO 230
            ENDIF
            CLNM(M, N)=CZERO
230       CONTINUE
```

```
C
C  N on s+(beta)
C
          DO 240,  N=MFOUR+1,MFIVE,1
          CLNM(M,N)=-PHI1X(XM(1,M),XM(2,M),XM(1,N),XM(2,N))*DELC
240       CONTINUE
C
C  N on A(gamma) through s+(gamma)
C
          DO 250,  N=MFIVE+1,NMAX,1
              CLNM(M,N)=CZERO
250       CONTINUE
260    CONTINUE
C
C  The next major section is for M on s+(beta)
C
C  Eq e
C
       DO 310,  M=MFOUR+1,MFIVE,1
C
C N on A(alpha)
C
          DO 142,  N=1,MONE,1
           CLNM(M,N)=-PHI0(XM(1,M),XM(2,M),XM(1,N),XM(2,N))*DELC
142       CONTINUE
C
C  N on A(BETA)
C
          DO 152,  N=MONE+1,MTWO,1
          CLNM(M,N)=-PHI1Y(XM(1,M),XM(2,M),XM(1,N),XM(2,N))*DELC
152       CONTINUE
C
C  N on s-(beta)
C
          DO 270,  N=MTWO+1,MTHR,1
          CLNM(M,N)=PHI1X(XM(1,M),XM(2,M),XM(1,N),XM(2,N))*DELC
270       CONTINUE
C
C   N on sd(beta)
C
          DO 280,  N=MTHR+1,MFOUR,1
          CLNM(M,N)=PHI1Y(XM(1,M),XM(2,M),XM(1,N),XM(2,N))*DELC
280       CONTINUE
C
C  N on s+(beta)
C
          DO 290,  N=MFOUR+1,MFIVE,1
             CLNM(M,N)=CZERO
             IF (N .EQ. M) CLNM(M,N)=(-0.5D0,0.D0)
290       CONTINUE
```

```
C
C  N on A(gamma) through s+(gamma)
C
          DO 300,  N=MFIVE+1, NMAX, 1
             CLNM(M, N)=CZERO
300       CONTINUE
310       CONTINUE
C
C  All of the elements for the observation point on the "beta"
c  segments are now filled.
C
C  The next major section is to have M on all the "gamma"
c  segments and the source point, N, on the beta segments.
C
       DO 330,  M=MFIVE+1, NMAX, 1
          DO 320 N=MONE+1, MFIVE, 1
             CLNM(M, N)=CZERO
320       CONTINUE
330    CONTINUE

C
C  Now we again systematically fill M on A(gamma)
C
C  Eq f
C
       DO 390,  M=MFIVE+1, MSIX, 1
C
C  N on A(ALPHA)
C
          DO 340,  N=1, MONE, 1
             IF(DABS(XM(1, M)-XM(1, N)) .LT. DELC/3.D0) THEN
                CLNM(M, N)=CZERO
                GOTO 340
             ENDIF
           CLNM(M, N)=PHI1X(XM(1, M), XM(2, M), XM(1, N), XM(2, N))*DELC
340       CONTINUE
C
C  N on s-(beta) and s+(beta)
C
          DO 342,  N=MTWO+1, MTHR, 1
        CLNM(M, N)=-C3*PHI0(XM(1, M), XM(2, M), XM(1, N), XM(2, N))*DELC
342       CONTINUE
          DO 344,  N=MFOUR+1, MFIVE, 1
       CLNM(M, N)=C3*PHI0(XM(1, M), XM(2, M), XM(1, N), XM(2, N))*DELC
344       CONTINUE
C
C  N on A(GAMMA)
C
          DO 350,  N=MFIVE+1, MSIX, 1
             CLNM(M, N)=CZERO
             IF (N .EQ. M) CLNM(M, N)=(-0.5D0, 0.D0)
350       CONTINUE
```

```
C
C  N on s-(gamma)
C
          DO 360,  N=MSIX+1, MSEVN, 1
          CLNM(M, N)=-PHI1Y(XM(1, M), XM(2, M), XM(1, N), XM(2, N))*DELC
360       CONTINUE
C
C    N on sd(gamma)
C
          DO 370,  N=MSEVN+1, MEIGHT, 1
          CLNM(M, N)=-PHI1Y(XM(1, M), XM(2, M), XM(1, N), XM(2, N))*DELC
370       CONTINUE
C
C    N on s+(gamma)
C
          DO 380,  N=MEIGHT+1, NMAX, 1
          CLNM(M, N)=-PHI1Y(XM(1, M), XM(2, M), XM(1, N), XM(2, N))*DELC
380       CONTINUE
390    CONTINUE
C
C    The next section is for M on s-(gamma)
C
C  Eq g
C
       DO 450,  M=MSIX+1, MSEVN, 1
C
C  N on A(ALPHA)
C
          DO 400,  N=1, MONE, 1
          CLNM(M, N)=PHI1Y(XM(1, M), XM(2, M), XM(1, N), XM(2, N))*DELC
400       CONTINUE
C
C  N on A(BETA)
C
          DO 402,  N=MONE+1, MTWO, 1
         CLNM(M, N)=C3*PHI0(XM(1, M), XM(2, M), XM(1, N), XM(2, N))*DELC
402       CONTINUE
C
C  N on sd(beta)
C
          DO 404,  N=MTHR+1, MFOUR, 1
        CLNM(M, N)=-C3*PHI0(XM(1, M), XM(2, M), XM(1, N), XM(2, N))*DELC
404       CONTINUE
C
C    N on A(GAMMA)
C
          DO 410,  N=MFIVE+1, MSIX, 1
          CLNM(M, N)=PHI1X(XM(1, M), XM(2, M), XM(1, N), XM(2, N))*DELC
410       CONTINUE
```

```
C
C  N on s-(gamma)
C
          DO 420,  N=MSIX+1,MSEVN, 1
             CLNM(M,N)=CZERO
             IF (N .EQ. M) CLNM(M,N)=(-0.5D0,0.D0)
420       CONTINUE
C
C  N on sd(gamma)
C
          DO 430,  N=MSEVN+1,MEIGHT, 1
          CLNM(M,N)=PHI1X(XM(1,M),XM(2,M),XM(1,N),XM(2,N))*DELC

430       CONTINUE
C
C  N on s+(gamma)
C
          DO 440,  N=MEIGHT,NMAX, 1
          CLNM(M,N)=PHI1X(XM(1,M),XM(2,M),XM(1,N),XM(2,N))*DELC
440       CONTINUE
450    CONTINUE
C
C  The next section is for M on sd(gamma)
C
C  Eq h
C
       DO 500,  M=MSEVN+1,MEIGHT, 1
C
C  N on A(ALPHA)
C
          DO 460,  N=1,MONE, 1
             IF (DABS(XM(1,M)-XM(1,N)) .LT. DELC/3.0D0) THEN
                CLNM(M,N)=CZERO
                GOTO 460
             ENDIF
          CLNM(M,N)=-PHI1X(XM(1,M),XM(2,M),XM(1,N),XM(2,N))*DELC

460       CONTINUE
C
C  N on s-(beta)
C
          DO 462,  N=MTWO+1,MTHR, 1
        CLNM(M,N)=C3*PHI0(XM(1,M),XM(2,M),XM(1,N),XM(2,N))*DELC
462       CONTINUE
C
C  N on s+(beta)
C
          DO 464,  N=MFOUR+1,MFIVE, 1
        CLNM(M,N)=-C3*PHI0(XM(1,M),XM(2,M),XM(1,N),XM(2,N))*DELC
464       CONTINUE
```

```
C
C  N on A(gamma) and s-(gamma)
C
          DO 470,  N=MFIVE+1,MSEVN, 1
          CLNM(M,N)=PHI1Y(XM(1,M),XM(2,M),XM(1,N),XM(2,N))*DELC
470       CONTINUE
C
C  N on sd(gamma)
C
          DO 480,  N=MSEVN+1,MEIGHT, 1
             CLNM(M,N)=CZERO
             IF (N .EQ. M) CLNM(M,N)=(-0.5D0,0.D0)
480       CONTINUE
C
C  N on s+(gamma)
C
          DO 490,  N=MEIGHT+1,NMAX, 1
          CLNM(M,N)=PHI1Y(XM(1,M),XM(2,M),XM(1,N),XM(2,N))*DELC
490       CONTINUE
500    CONTINUE
C
C   The last major section!! Is for M on s+(gamma)
C
C  Eq i
C
       DO 550,  M=MEIGHT+1,NMAX, 1
C
C  N on A(ALPHA)
C
          DO 510,  N=1,MONE, 1
         CLNM(M,N)=-PHI1Y(XM(1,M),XM(2,M),XM(1,N),XM(2,N))*DELC
510       CONTINUE
C
C N on A(BETA)
C
          DO 512,  N=MONE+1,MTWO, 1
       CLNM(M,N)=-C3*PHI0(XM(1,M),XM(2,M),XM(1,N),XM(2,N))*DELC
512       CONTINUE
C
C  N on sd(beta)
C
          DO 514,  N=MTHR+1,MFOUR, 1
        CLNM(M,N)=C3*PHI0(XM(1,M),XM(2,M),XM(1,N),XM(2,N))*DELC
514       CONTINUE
C
C   N on A(gamma) and s-(gamma)
C
          DO 520,  N=MFIVE+1,MSEVN, 1
         CLNM(M,N)=-PHI1X(XM(1,M),XM(2,M),XM(1,N),XM(2,N))*DELC
520       CONTINUE
```

```
C
C  N on sd(gamma)
C
         DO 530,  N=MSEVN+1, MEIGHT, 1
        CLNM(M, N)=-PHI1X(XM(1, M), XM(2, M), XM(1, N), XM(2, N))*DELC
530      CONTINUE
C
C  N on s+(gamma)
C
         DO 540,  N=MEIGHT+1, NMAX, 1
            CLNM(M, N)=CZERO
            IF (N .EQ. M) CLNM(M, N)=(-0.5D0, 0.D0)
540      CONTINUE
550   CONTINUE
C
C
C  The CLNM() matrix is now filled.
C
C
       WRITE (*, *) 'LNM MATRIX FILLED...GOING TO INVERT'
C
C The major matrices are now all filled.  The next step is to
C invert the CLNM() matrix.
C
C Using AFIT's IMSL library, one statement will invert CLNM()
C
      CALL DL2NCG(NMAX, CLNM, 500, CLNM, 500, CWKS, IWKS)
      WRITE (*, *) ' MATRIX INVERTED...'
C
C   We next fill the "g()" matrix of known values
C
         DO 601,  L4=1, IMAX, 1
c
c  AL2 is the input angle in degrees
c
            AL2=DBLE(FLOAT(L4))*RSTEP-RSTEP+RFRST
            WRITE(*, 888) AL2
888         FORMAT(5X, F6.2)
c
c  Convert the input angle to radians
c
         THTI=AL2*PI/180.D0
c
c   Fill the G() matrix
c
         DO 560,  I=1, MONE, 1
            G(I)=CZERO
560      CONTINUE
         DO 570,  I=MONE+1, MTWO, 1
            G(I)=CKPO(I, THTI)/2.D0
570      CONTINUE
```

```
          DO 580,  I=MTWO+1, NMAX, 1
             G(I)=CZERO
580       CONTINUE
C
C    Multiply the inverted matrix by the input matrix, G()
C    using the IMSL library function.
C
    CALL DMCRCR(NMAX, NMAX, CLNM, 500, NMAX, 1, G, 500, NMAX, 1, COUT, 500)
c
c    If it's the first input angle, then write out the currents
c
          IF (L4 .EQ. 1) THEN
             DO 700, IM1=1, MONE, 1
                WRITE(*, 860) REAL(COUT(IM1)), DIMAG(COUT(IM1))
                WRITE(5, 860) REAL(COUT(IM1)), DIMAG(COUT(IM1))
860             FORMAT (1X, 2E19.12)
700          CONTINUE
          ENDIF
          WRITE(5,*)'   '
          WRITE (*,*)'   '
c
c   Calculate the RCS using Eq. 121 in the Thesis
c   for each output angle from -90 to 90
c
          DO 600,  L=-90, 90, 1
             THTR=DBLE(FLOAT(L))*PI/180.D0
             CSUM=0.D0
            DO 610,  M=1, MONE, 1
              CSUM=CSUM+COUT(M)*CDEXP(-J*WK*XM(1,M)*DSIN(THTR))
610          CONTINUE
             IF (L .NE. 0) THEN
        CSUM=CSUM*DSIN(WK*DELC*0.5D0*DSIN(THTR))/(WK*DSIN(THTR))
             ENDIF
             IF (L .EQ. 0) THEN
                CSUM=CSUM*DELC/2.D0
             ENDIF
             RCS(L4, L)=4.D0*CDABS(CSUM)*CDABS(CSUM)
600       CONTINUE
601       CONTINUE
c
c   Output the RCS data
c
          DO 603,  L=-90, 90, 1
             WRITE(3, 868) L, RCS(1, L), RCS(2, L), RCS(3, L), RCS(4, L)
868          FORMAT (I4, 4E19.12)
603       CONTINUE
```

```
C
c    Close the output file and go back for the next k and d
c
        CLOSE(UNIT=3)
650     CONTINUE
        CLOSE(UNIT=2)
        CLOSE(UNIT=5)
        CLOSE(UNIT=4)
        END
C
C
c   CKPO is the function that gives the physical optics current
c   across the aperture.  This is actually the H field incident
c   to the aperture.
c
        COMPLEX*16 FUNCTION CKPO(M, THTI)
        IMPLICIT DOUBLE PRECISION A, B, D, E, F, H, O, Q, R, T, U, V, W, X, Y, Z
        IMPLICIT COMPLEX*16 C, J, G, P
        COMMON J, XM(1:2, 1:500), WK, DELC
        CKPO=2.D0*CDEXP(-J*WK*(XM(1,M)*DSIN(THTI)))
        RETURN
        END
C
C
c    PHI0 is the function that gives the Hankle function of the
c    first kind of order 0 for k times r. It is multiplied by
c    j/4 to give the Green's function in two dimensions.
c
        COMPLEX*16 FUNCTION PHI0(X1, Y1, X2, Y2)
        IMPLICIT DOUBLE PRECISION A, B, D, E, F, H, O, Q, R, T, U, V, W, X, Y, Z
        IMPLICIT COMPLEX*16 C, J, G, P
        COMMON J, XM(1:2, 1:500), WK, DELC
        WKR=WK*DSQRT((X1-X2)*(X1-X2)+(Y1-Y2)*(Y1-Y2))
        PHI0=(DBSJ0(WKR)+J*DBSY0(WKR))*J*0.25D0
        RETURN
        END
C
C
c   PHI1X gives the x component of the gradient of PHI0
c
        COMPLEX*16 FUNCTION PHI1X(X1, Y1, X2, Y2)
        IMPLICIT DOUBLE PRECISION A, B, D, E, F, H, O, Q, R, T, U, V, W, X, Y, Z
        IMPLICIT COMPLEX*16 C, J, G, P
        COMMON J, XM(1:2, 1:500), WK, DELC
        R=DSQRT((X1-X2)*(X1-X2)+(Y1-Y2)*(Y1-Y2))
        WKR=WK*R
        PHI1X=J*0.25D0*WK*(X1-X2)*(DBSJ1(WKR)+J*DBSY1(WKR))/R
        RETURN
        END
C
```

```
C
c   PHI1Y gives the y component of the gradient of PHI0
c
      COMPLEX*16 FUNCTION PHI1Y(X1, Y1, X2, Y2)
      IMPLICIT DOUBLE PRECISION A, B, D, E, F, H, O, Q, R, T, U, V, W, X, Y, Z
      IMPLICIT COMPLEX*16 C, J, G, P
      COMMON J, XM(1:2, 1:500), WK, DELC
      R=DSQRT((X1-X2)*(X1-X2)+(Y1-Y2)*(Y1-Y2))
      WKR=WK*R
      PHI1Y=J*0.25D0*WK*(Y1-Y2)*(DBSJ1(WKR)+J*DBSY1(WKR))/R
      RETURN
      END
C
C
```

Appendix B: Numerically Generated Data For the Test Case

The plots contained in this appendix were obtained from the computer program in Appendix A. The program is discussed in Chapter 7 and some of the results are analyzed in the results section, Chapter 8.

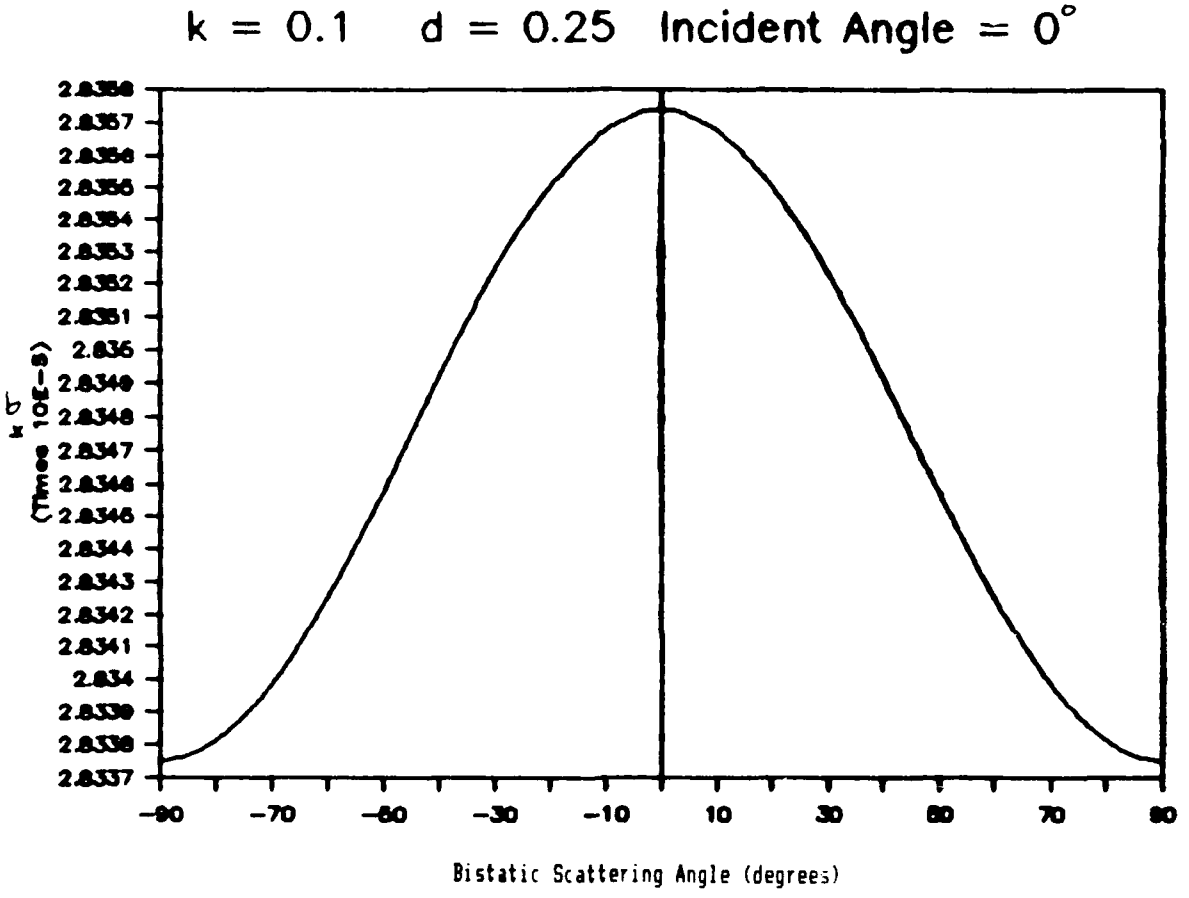

Figure 17. Bistatic RCS of a Rectangular Cavity With a Normalized Wave Number, K, Equal to 0.1, a Cavity Depth, d, of 0.25, and an Incident Plane Wave With $\theta_i = 0^o$.

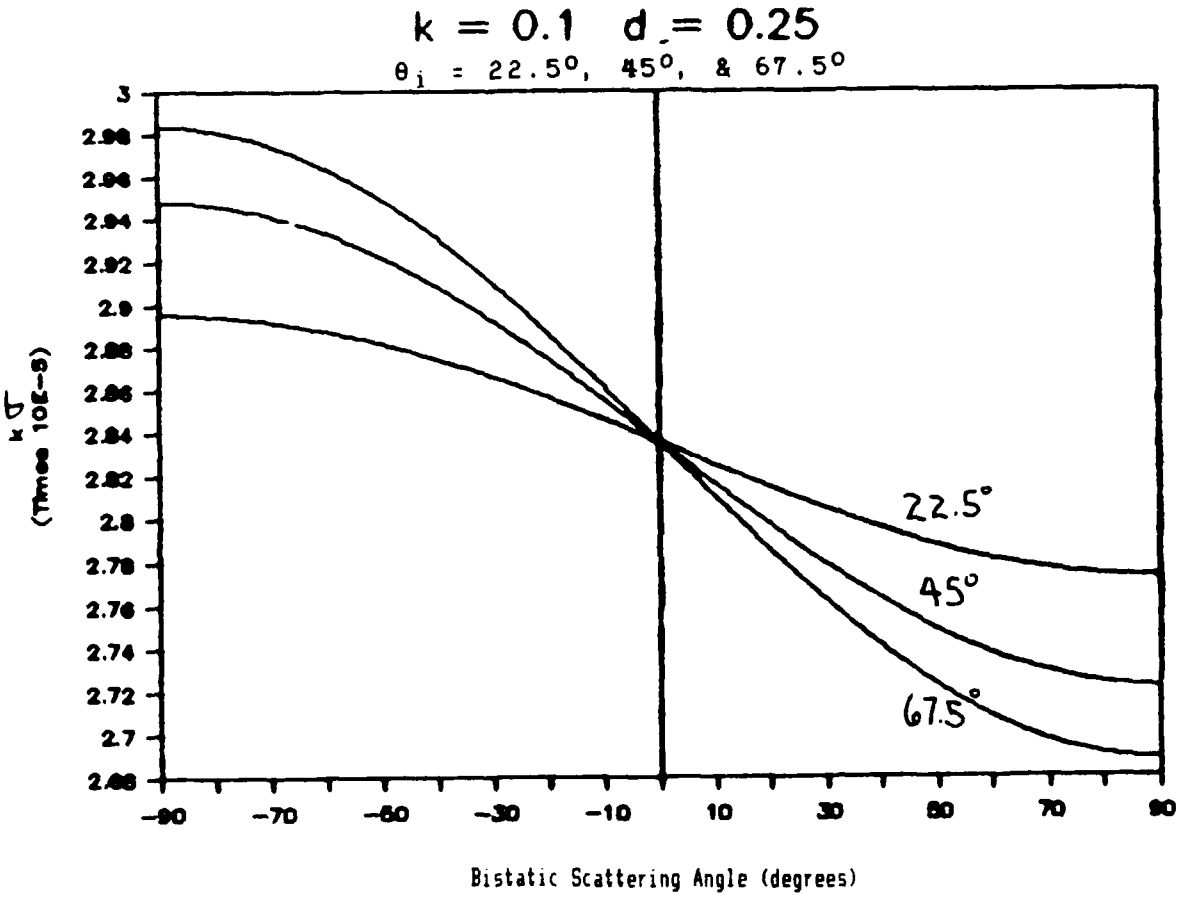

Figure 18. Bistatic RCS of a Rectangular Cavity With a Normalized Wave Number, k, Equal to 0.1, a Cavity Depth, d, of 0.25, and Incident Plane Waves with θ_i = 22.5°, 45.0° and 67.5°.C.

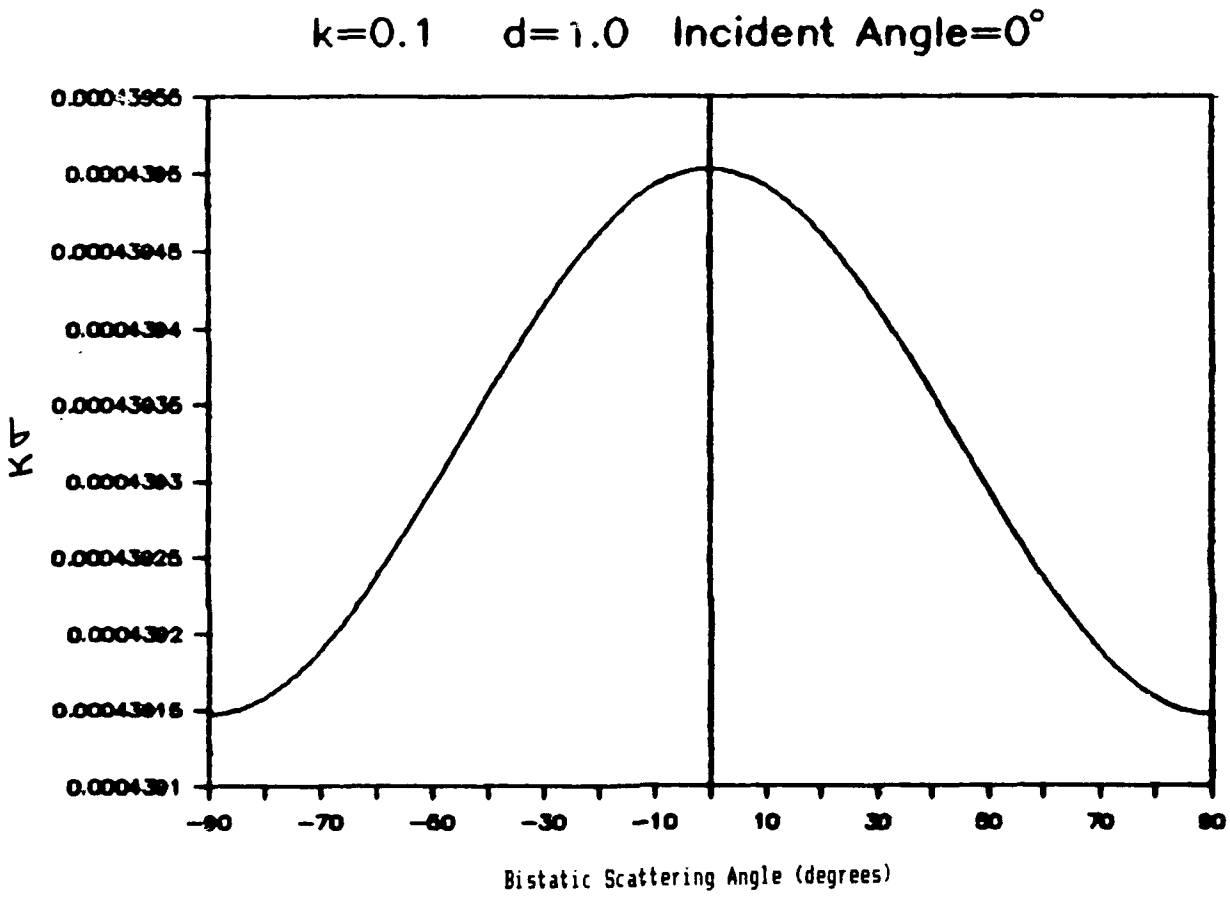

Figure 19. Bistatic RCS of a Rectangular Cavity With a Normalized Wave Number, k, Equal to 0.1, a Cavity Depth, d, of 1.0, and an Incident Plane Wave With $\theta_i = 0^o$.

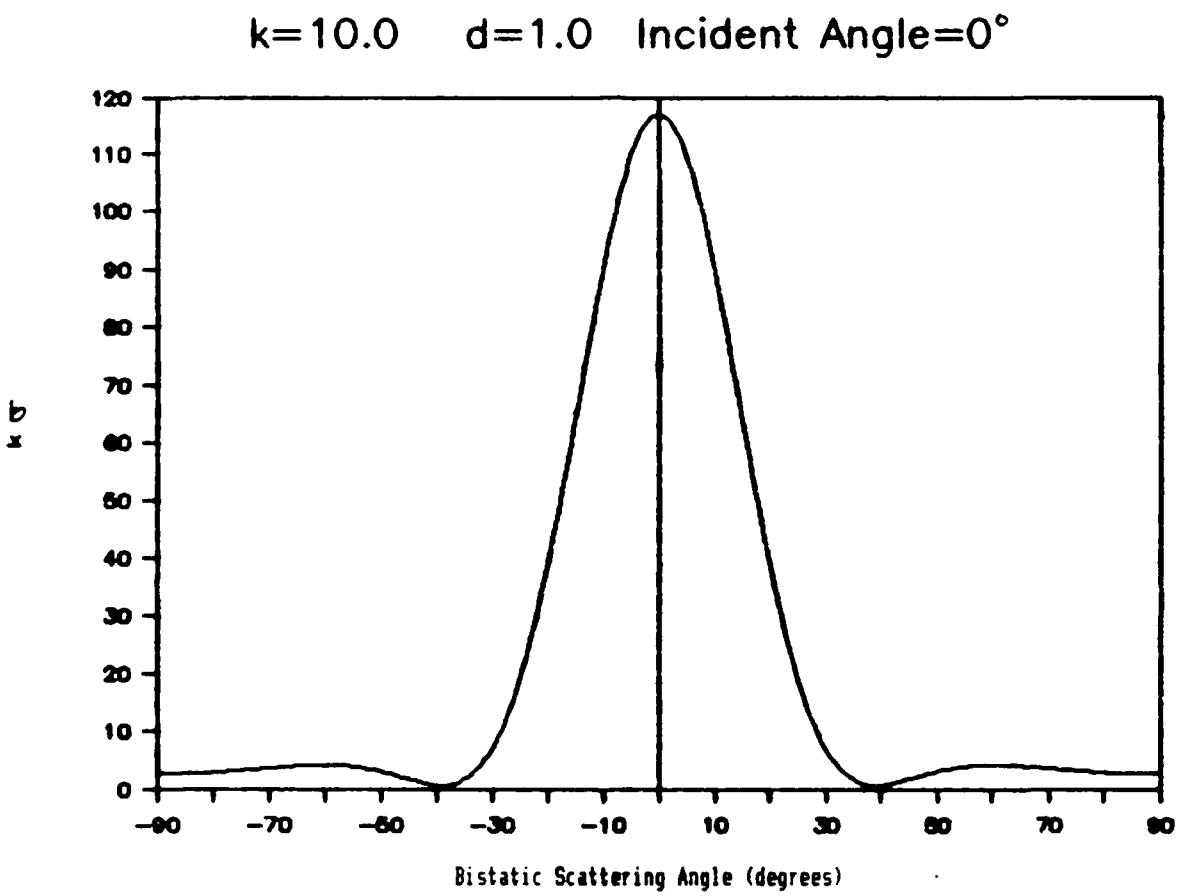

Figure 20. Bistatic RCS of a Rectangular Cavity With a Normalized Wave Number, k, Equal to 10.0, a Cavity Depth, d, of 1.0, and an Incident Plane Wave With $\theta_i = 0^o$.

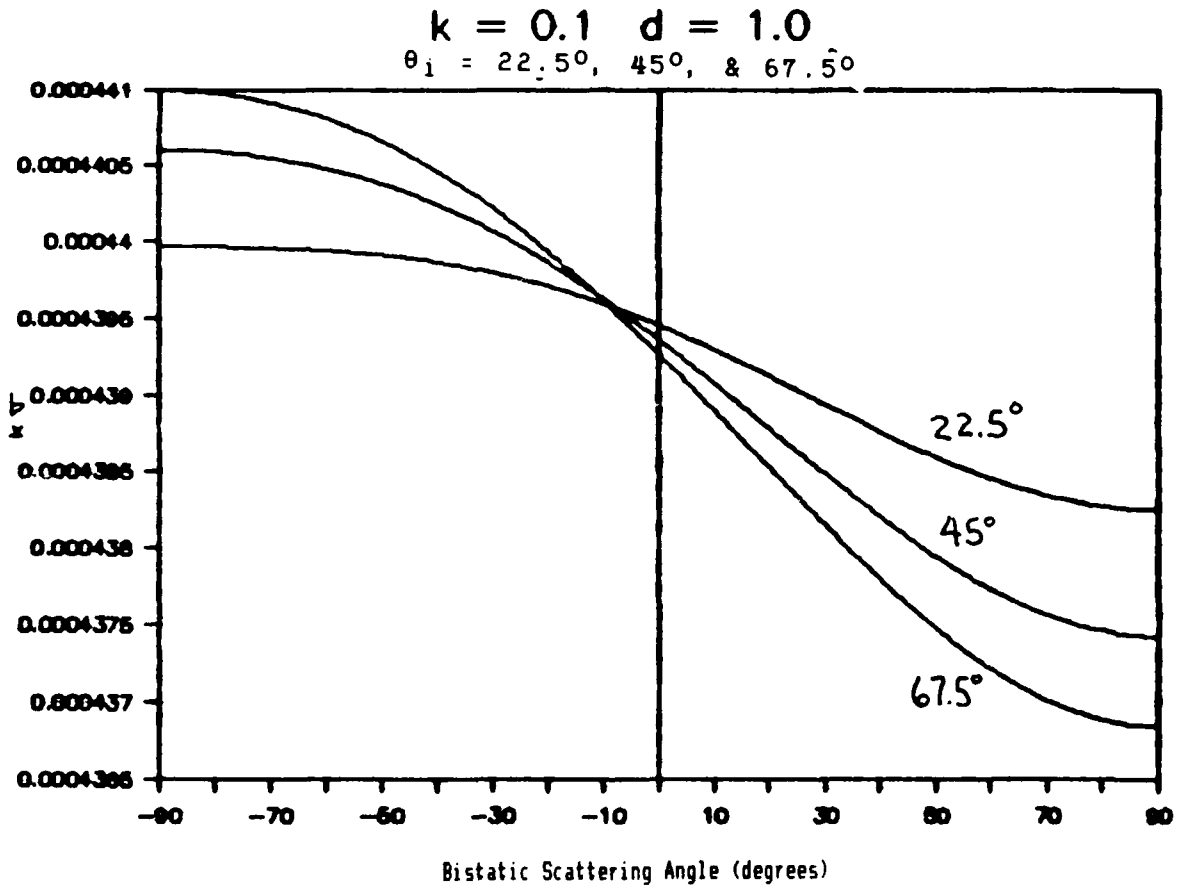

Figure 21. Bistatic RCS of a Rectangular Cavity With a Normalized Wave Number, k, Equal to 0.1, a Cavity Depth, d, of 1.0, and Incident Plane Waves with θ_i = 22.5°, 45.0° and 67.5°.

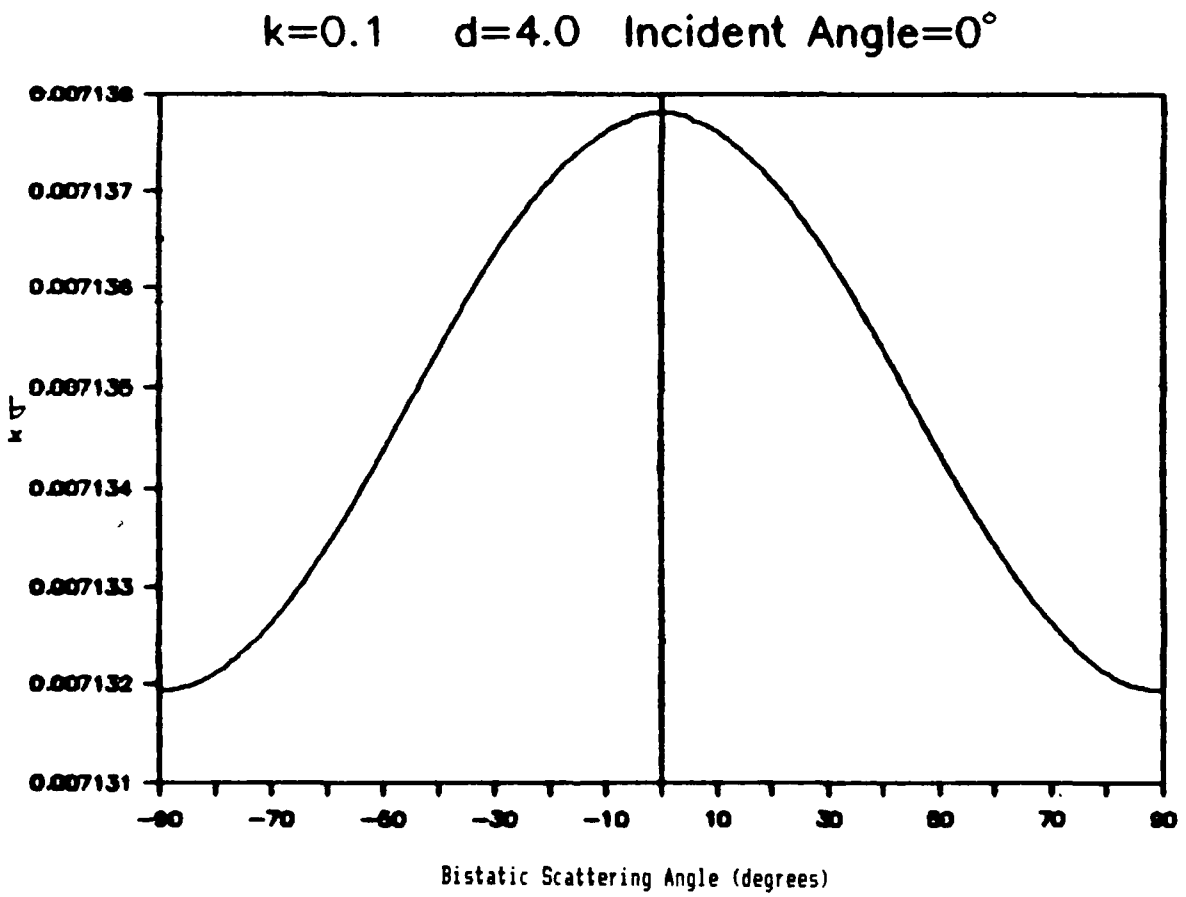

Figure 22. Bistatic RCS of a Rectangular Cavity With a Normalized Wave Number, k, Equal to 0.1, a Cavity Depth, d, of 4.0, and an Incident Plane Wave With $\theta_i = 0^o$.

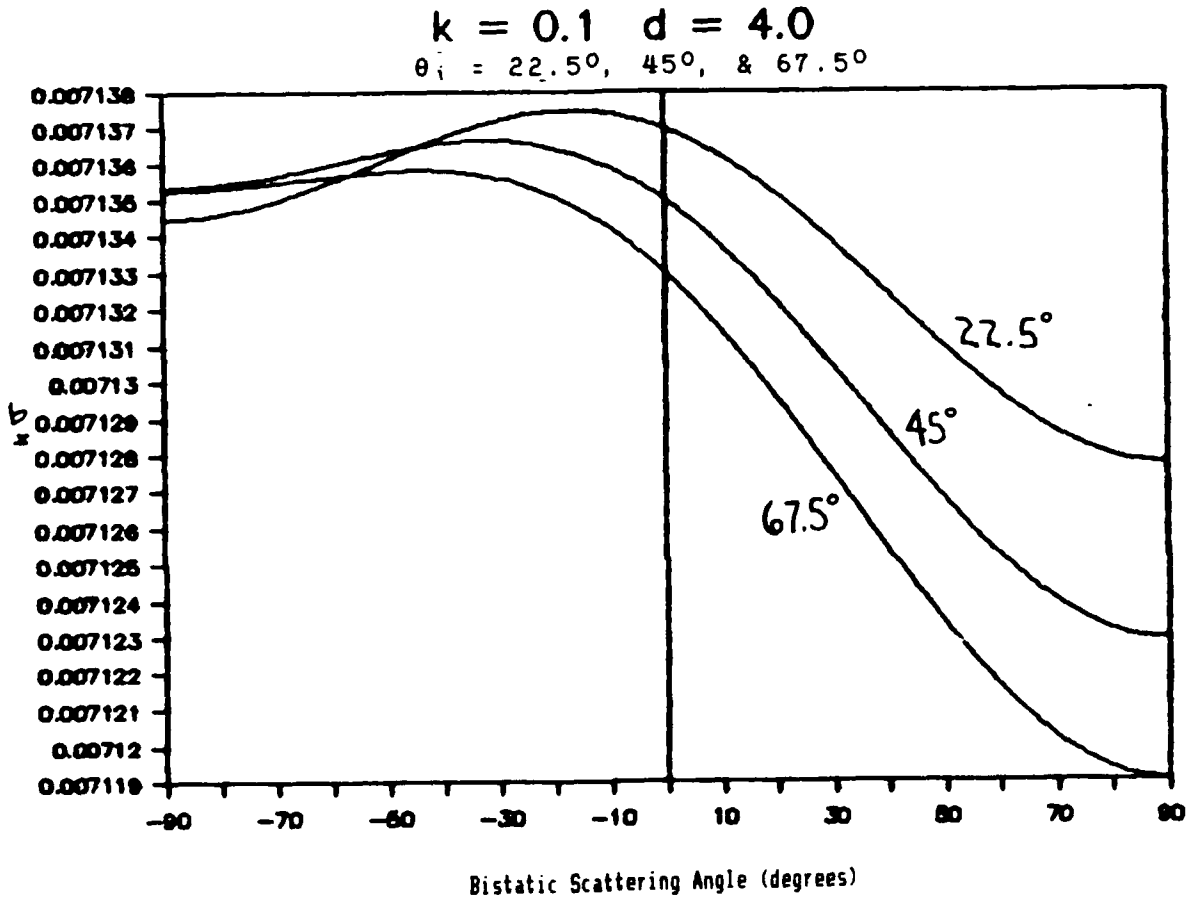

Figure 23. Bistatic RCS of a Rectangular Cavity With a Normalized Wave Number, k, Equal to 0.1, a Cavity Depth, d, of 4.0, and Incident Plane Waves with θ_i = 22.5°, 45.0° and 67.5°.

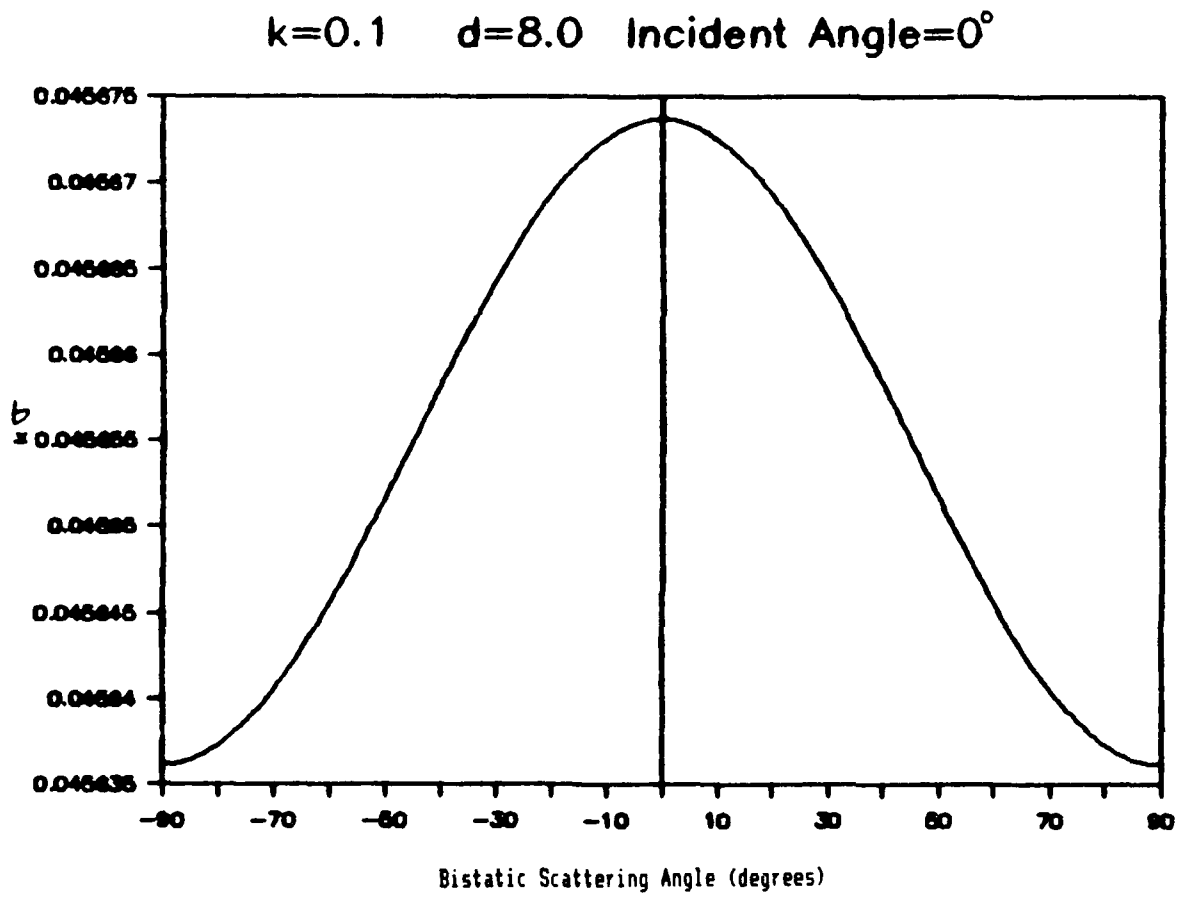

Figure 24. Bistatic RCS of a Rectangular Cavity With a Normalized Wave Number, k, Equal to 0.1, a Cavity Depth, d, of 8.0, and an Incident Plane Wave With $\theta_i = 0^o$.

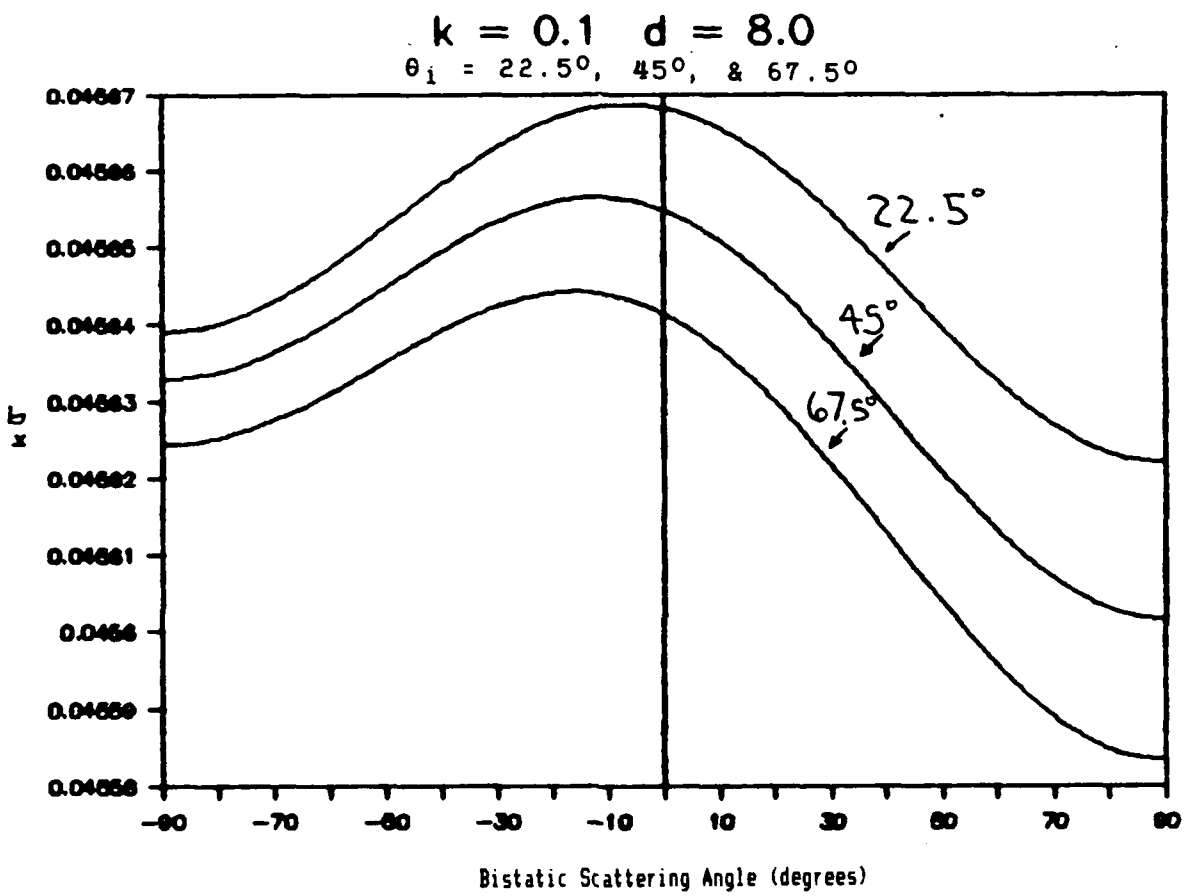

Figure 25. Bistatic RCS of a Rectangular Cavity With a Normalized Wave Number, k, Equal to 0.1, a Cavity Depth, d, of 8.0, and Incident Plane Waves with θ_i = 22.5°, 45.0° and 67.5°.

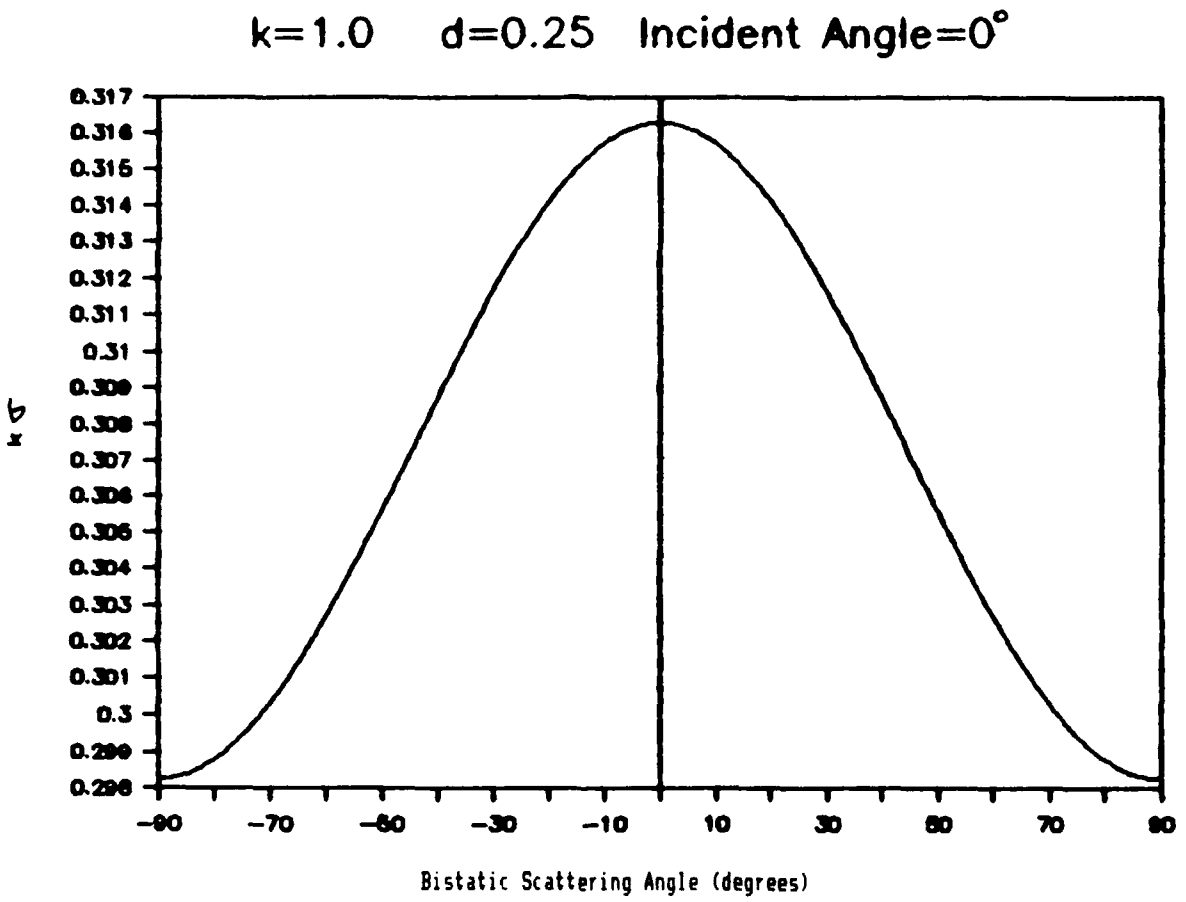

Figure 26. Bistatic RCS of a Rectangular Cavity With a Normalized Wave Number, k, Equal to 1.0, a Cavity Depth, d, of 0.25, and an Incident Plane Wave With $\theta_i = 0^o$.

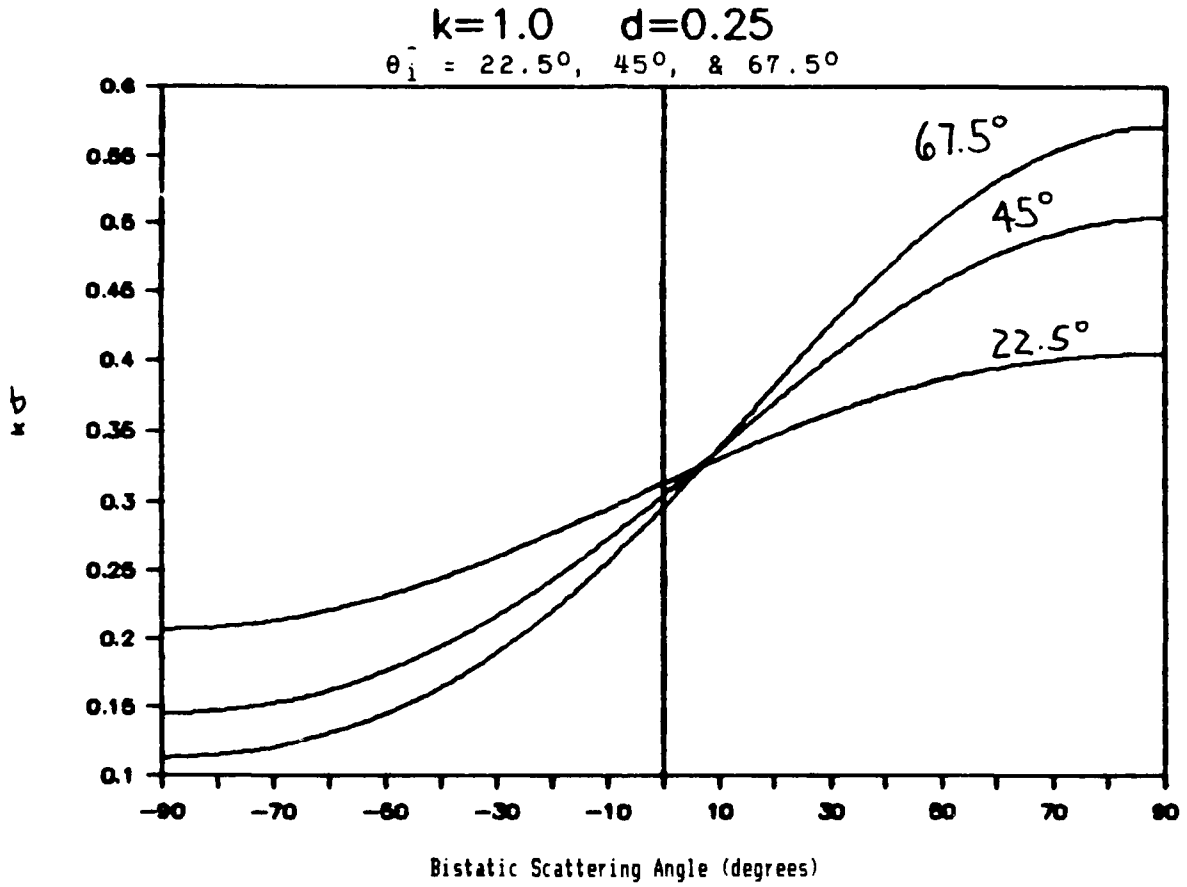

Figure 27. Bistatic RCS of a Rectangular Cavity With a Normalized Wave Number, k, Equal to 1.0, a Cavity Depth, d, of 0.25, and Incident Plane Waves with θ_i = 22.5°, 45.0° and 67.5°.

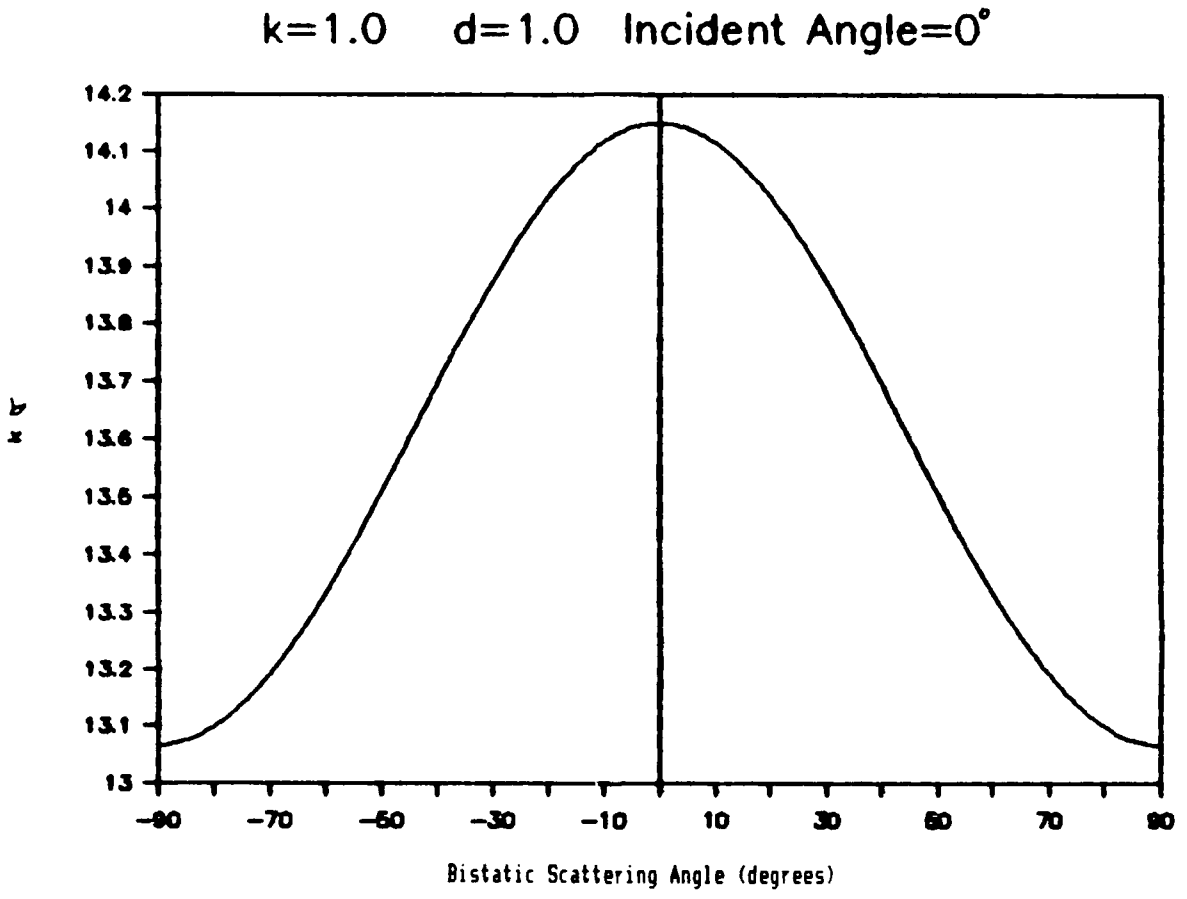

Figure 28. Bistatic RCS of a Rectangular Cavity With a Normalized Wave Number, K, Equal to 1.0, a Cavity Depth, d, of 1.0, and an Incident Plane Wave With $\theta_i = 0^o$.

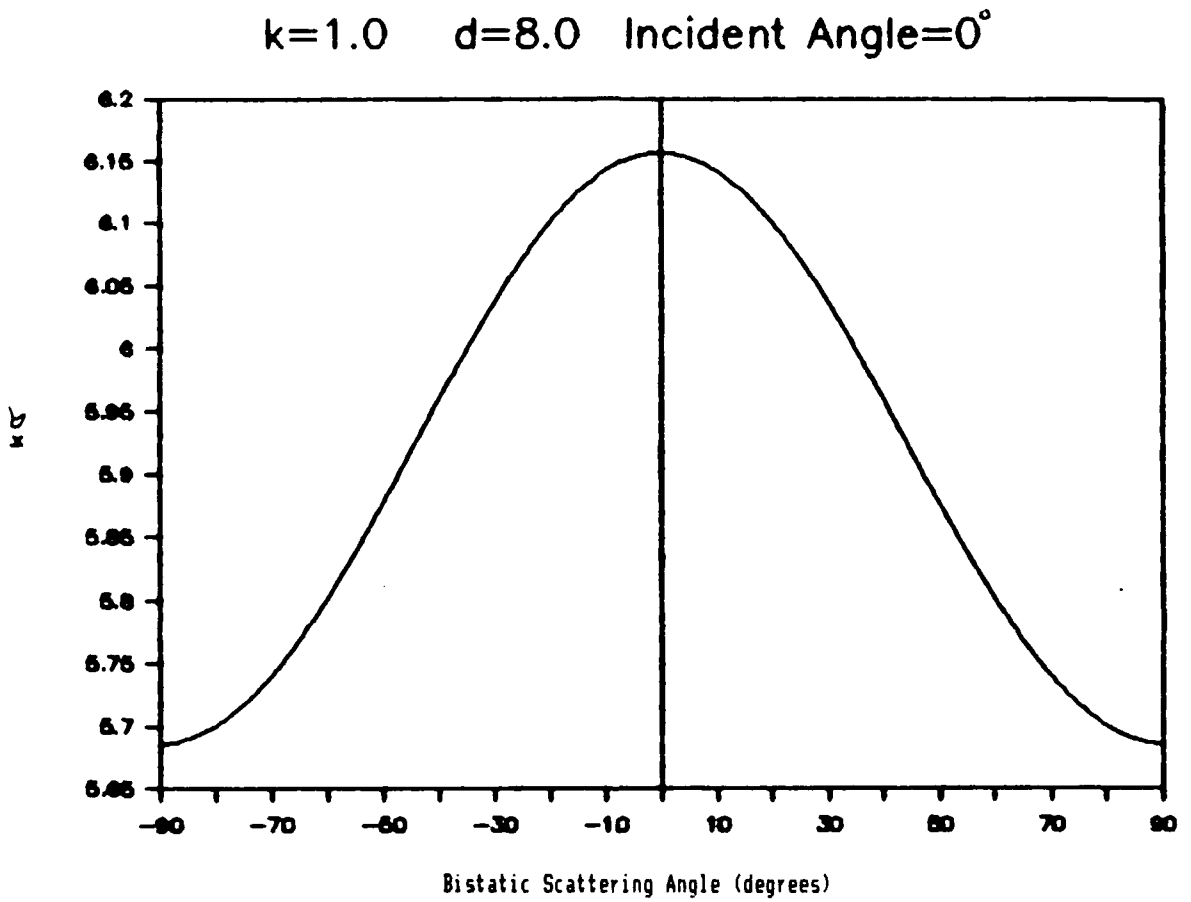

Figure 29. Bistatic RCS of a Rectangular Cavity With a Normalized Wave Number, k, Equal to 1.0, a Cavity Depth, d, of 8.0, and an Incident Plane Wave With $\theta_i = 0^o$.

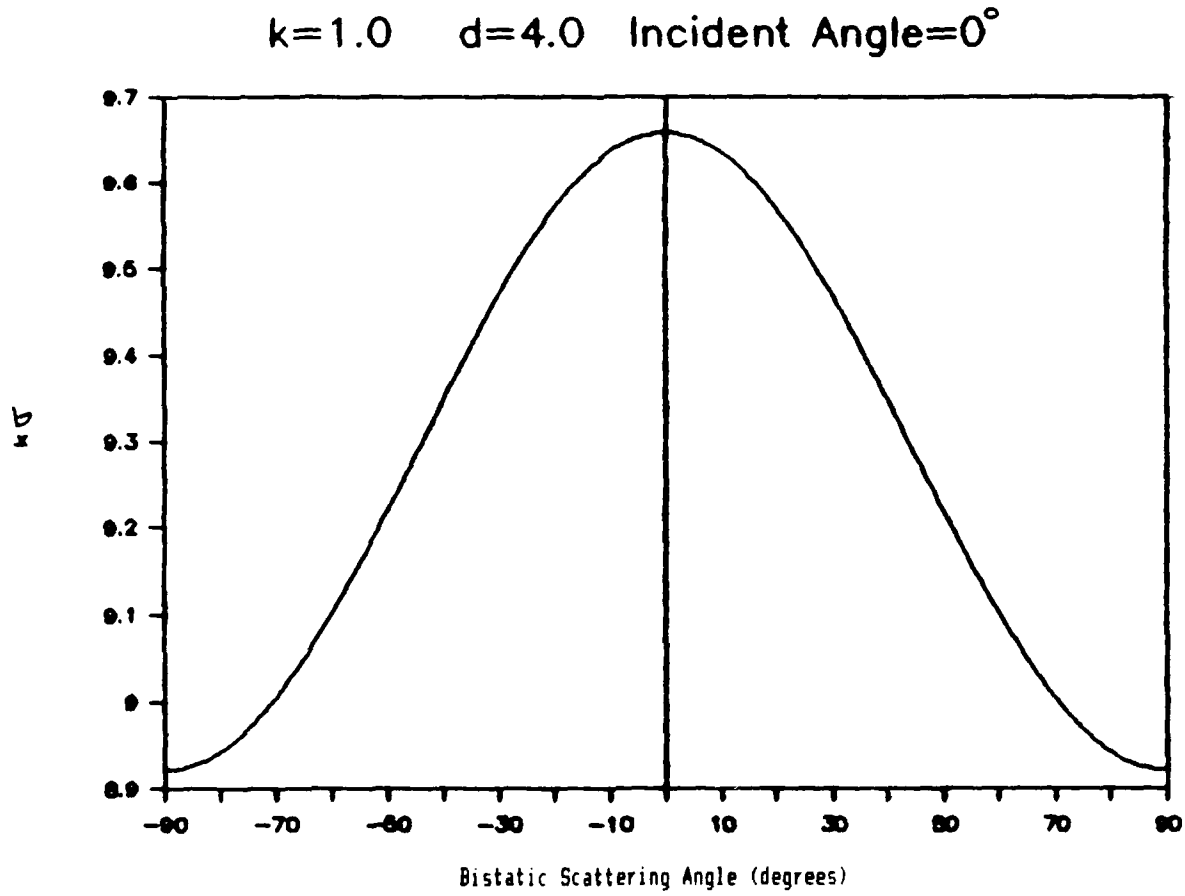

Figure 30. Bistatic RCS of a Rectangular Cavity With a Normalized Wave Number, k, Equal to 1.0, a Cavity Depth, d, of 4.0, and an Incident Plane Wave With $\theta_i = 0^o$.

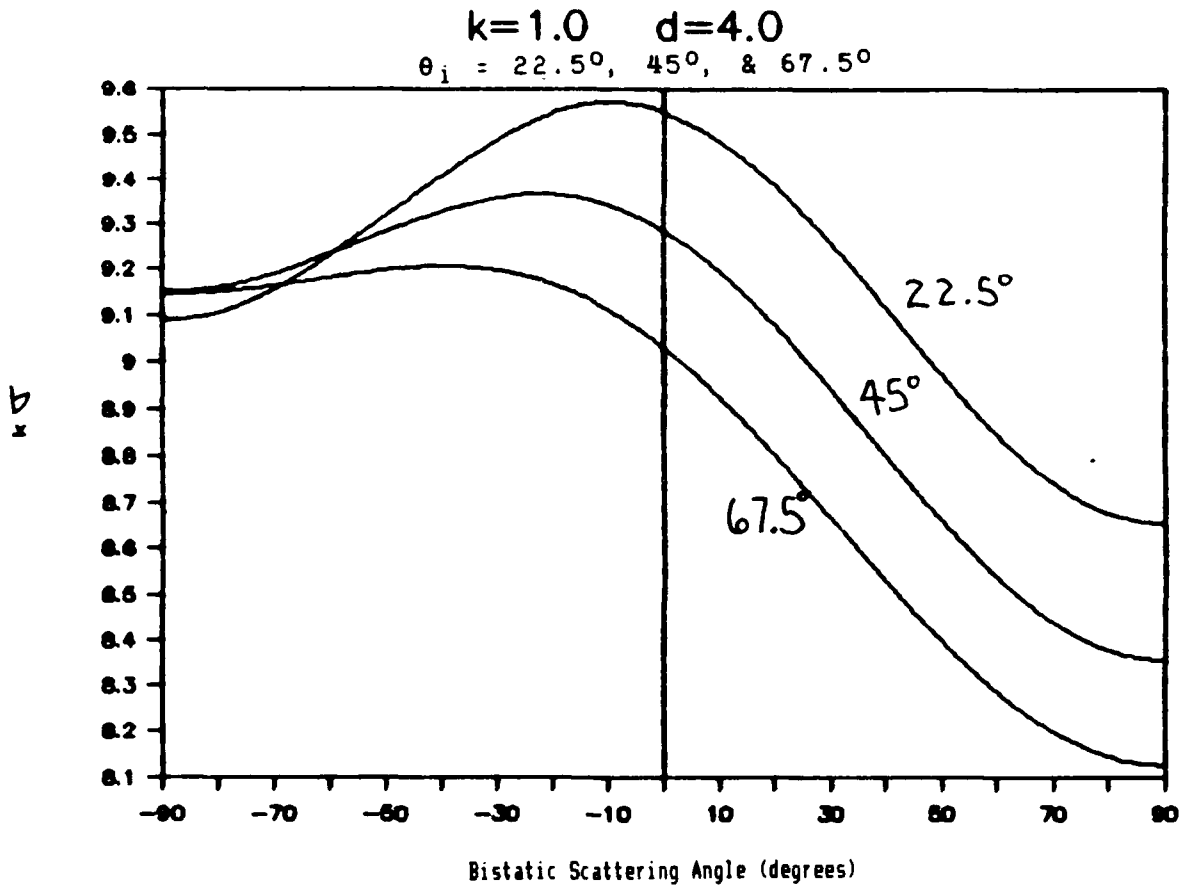

Figure 31. Bistatic RCS of a Rectangular Cavity With a Normalized Wave Number, k, Equal to 1.0, a Cavity Depth, d, of 4.0, and Incident Plane Waves with θ_i = 22.5°, 45.0° and 67.5°.

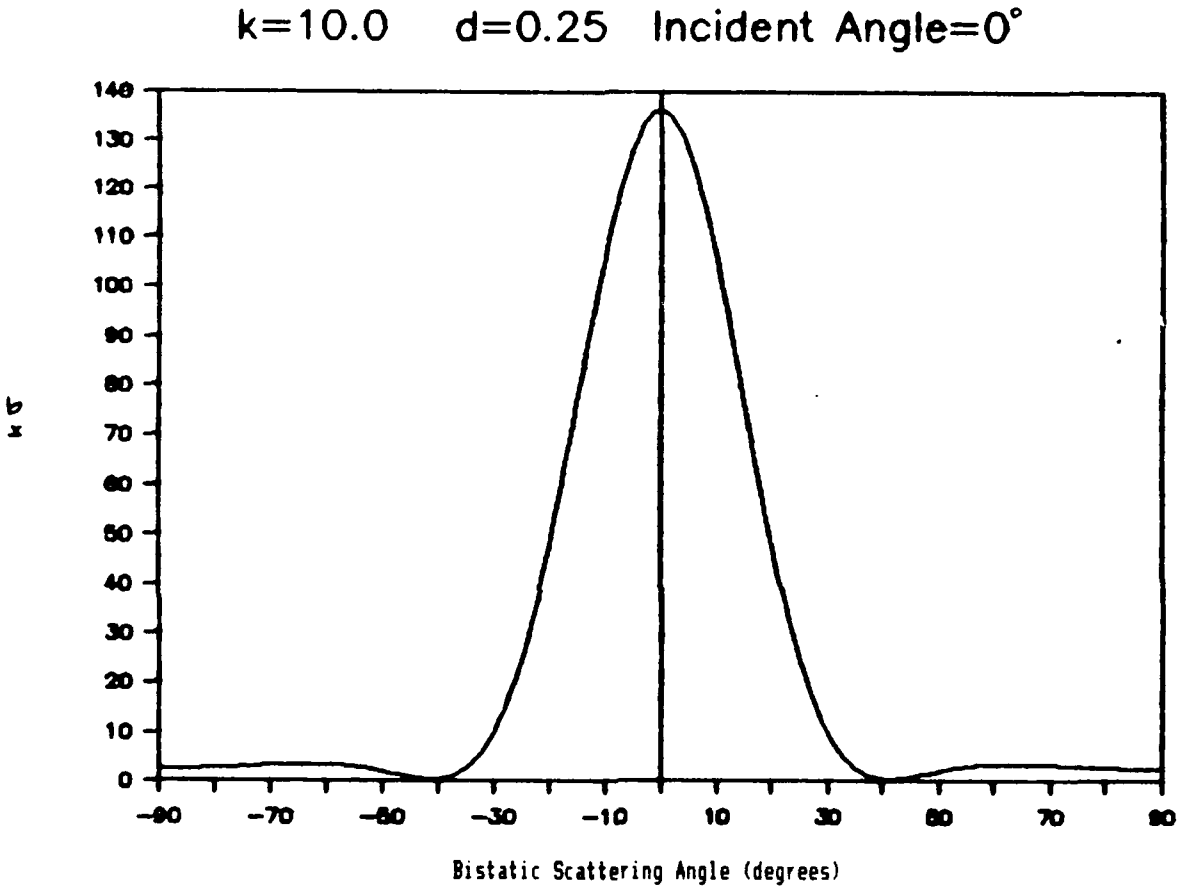

Figure 32. Bistatic RCS of a Rectangular Cavity With a Normalized Wave Number, k, Equal to 10.0, a Cavity Depth, d, of 0.25, and an Incident Plane Wave With $\theta_i = 0^o$.

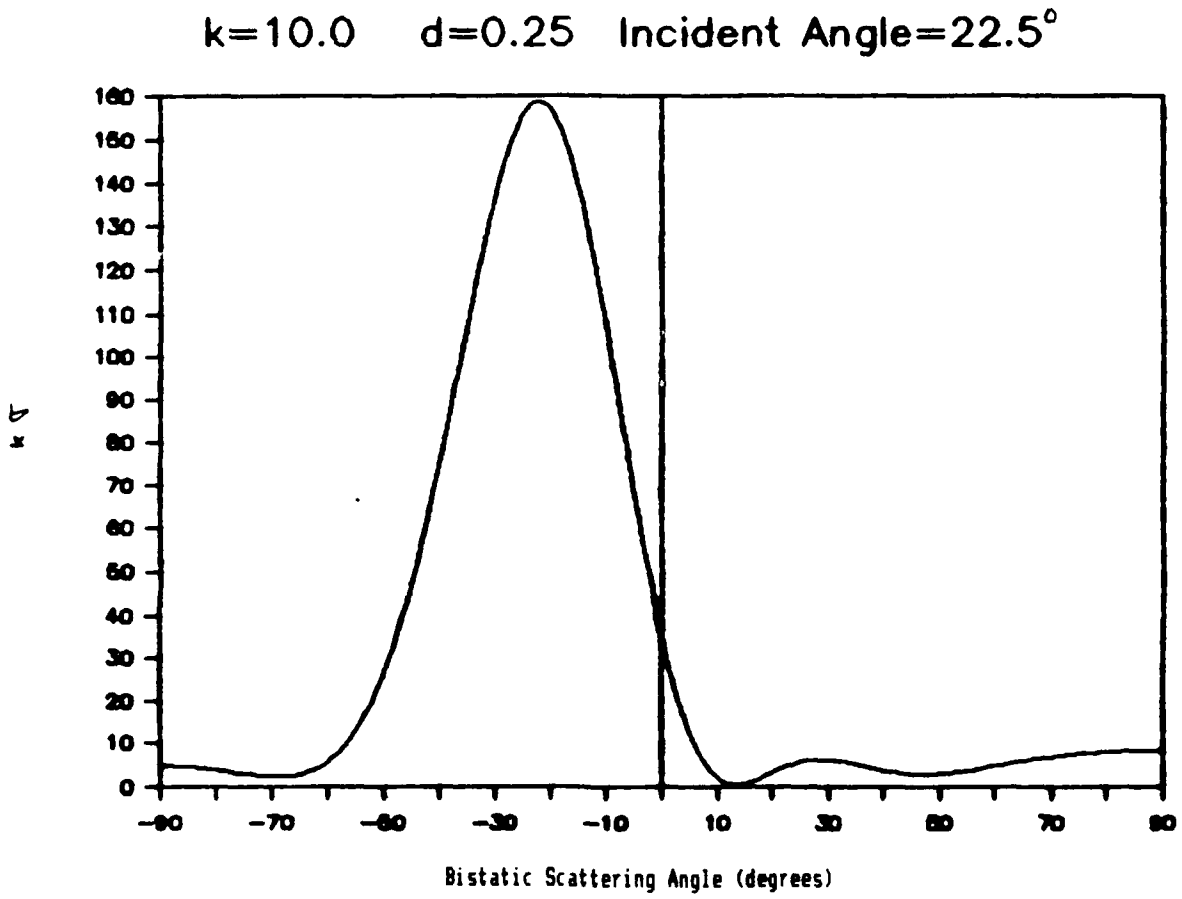

Figure 33. Bistatic RCS of a Rectangular Cavity With a Normalized Wave Number, k, Equal to 10.0, a Cavity Depth, d, of 0.25, and an Incident Plane Wave With θ_i = 22.5°.

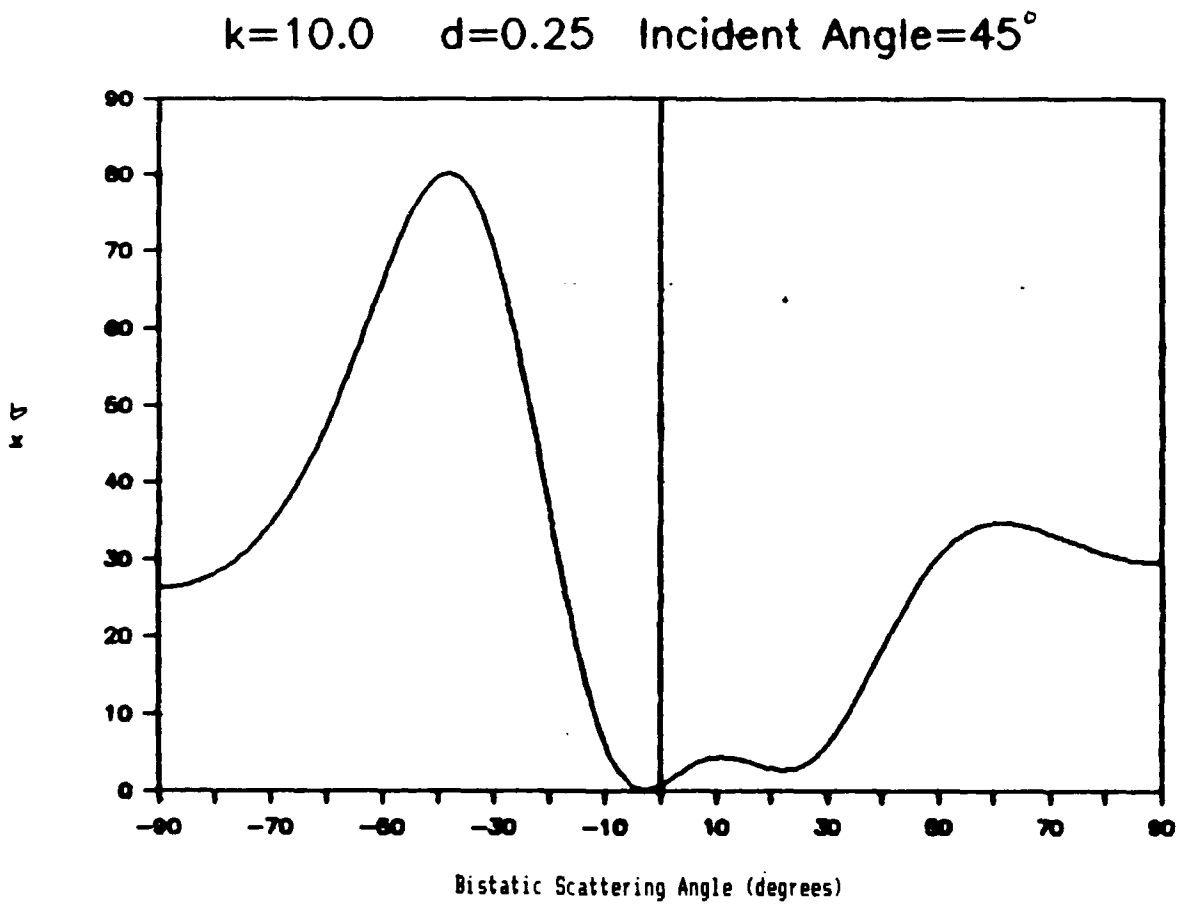

Figure 34. Bistatic RCS of a Rectangular Cavity With a Normalized Wave Number, k, Equal to 10.0, a Cavity Depth, d, of 0.25, and an Incident Plane Wave With $\theta_i = 45^o$.

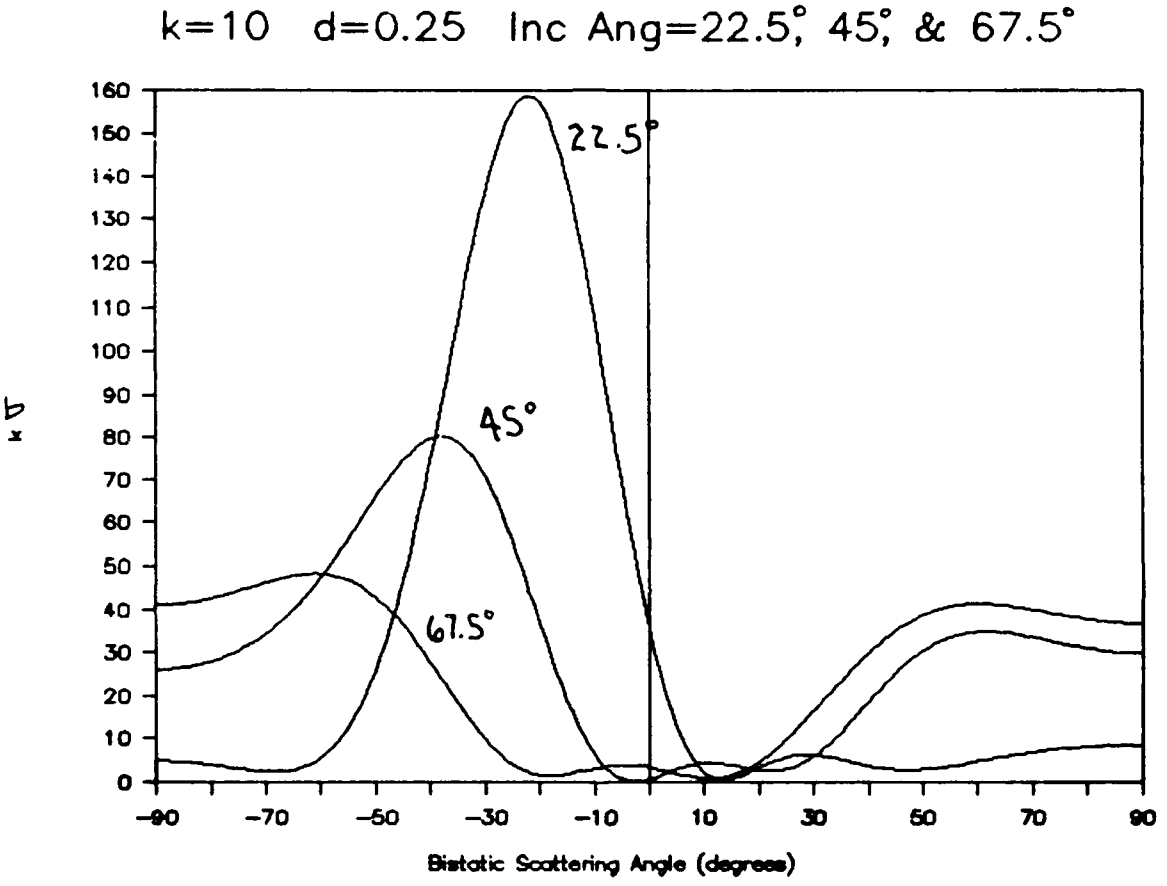

Figure 35. Bistatic RCS of a Rectangular Cavity With a Normalized Wave Number, k, Equal to 10.0, a Cavity Depth, d, of 0.25, and an Incident Plane Wave With θ_i = 22.5°, 45°, and 67.5°.

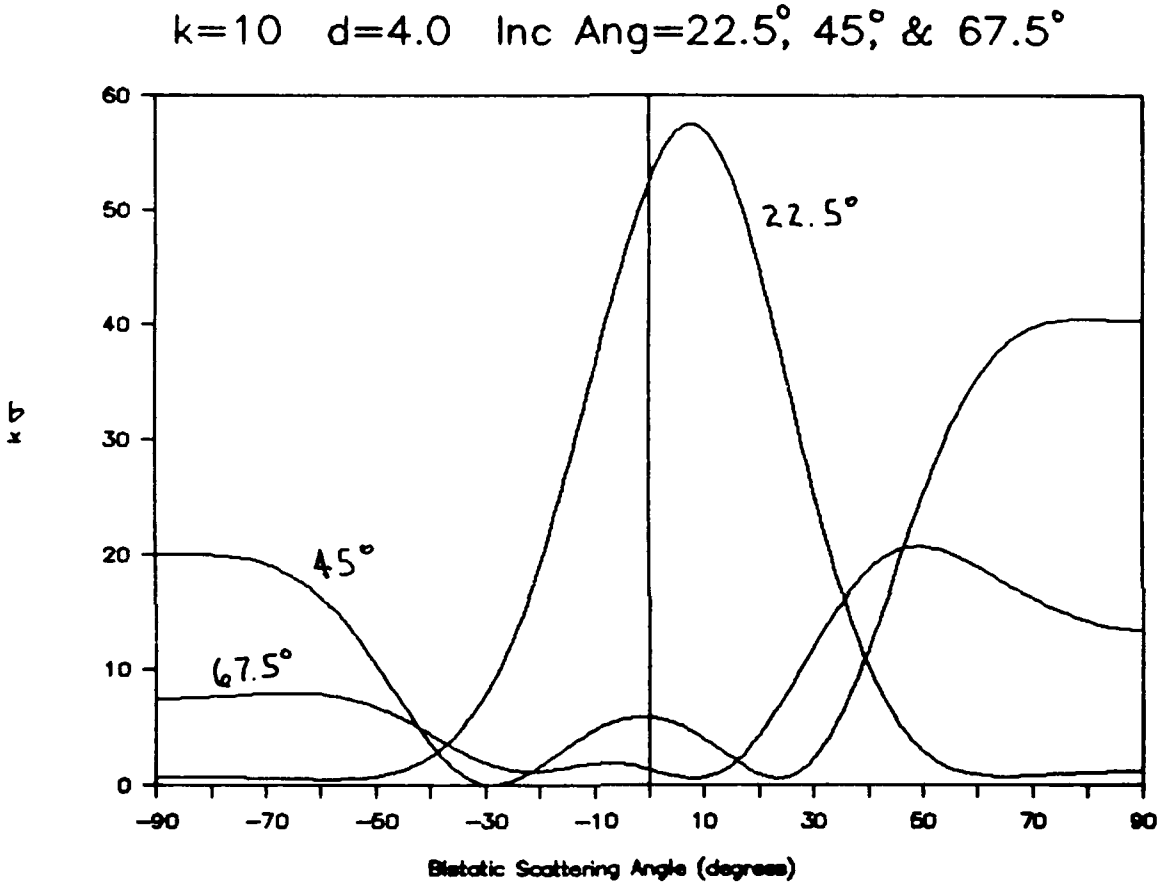

Figure 36. Bistatic RCS of a Rectangular Cavity With a Normalized Wave Number, k, Equal to 10.0, a Cavity Depth, d, of 4.0, and an Incident Plane Wave With θ_i = 22.5°, 45°, and 67.5°.

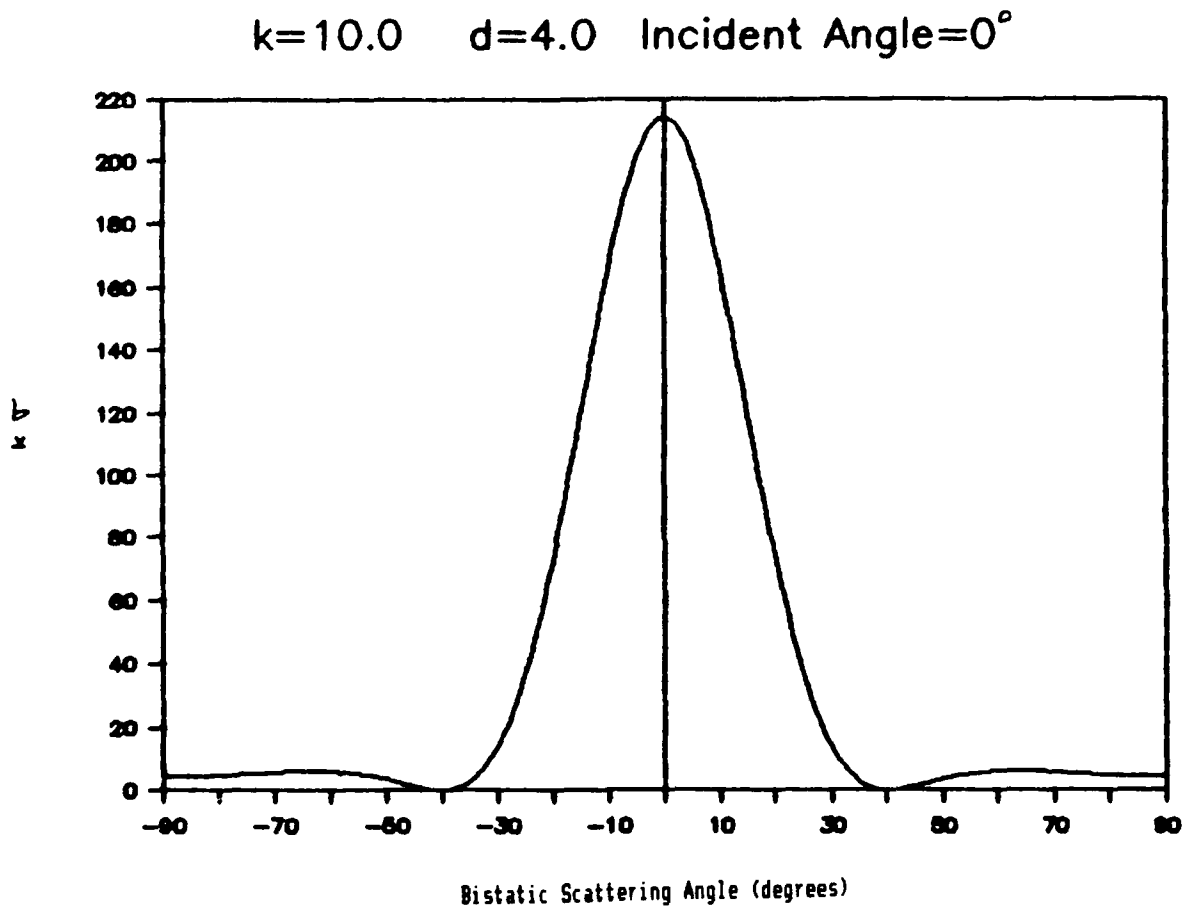

Figure 37. Bistatic RCS of a Rectangular Cavity With a Normalized Wave Number, k, Equal to 10.0, a Cavity Depth, d, of 4.0, and an Incident Plane Wave With $\theta_i = 0^o$.

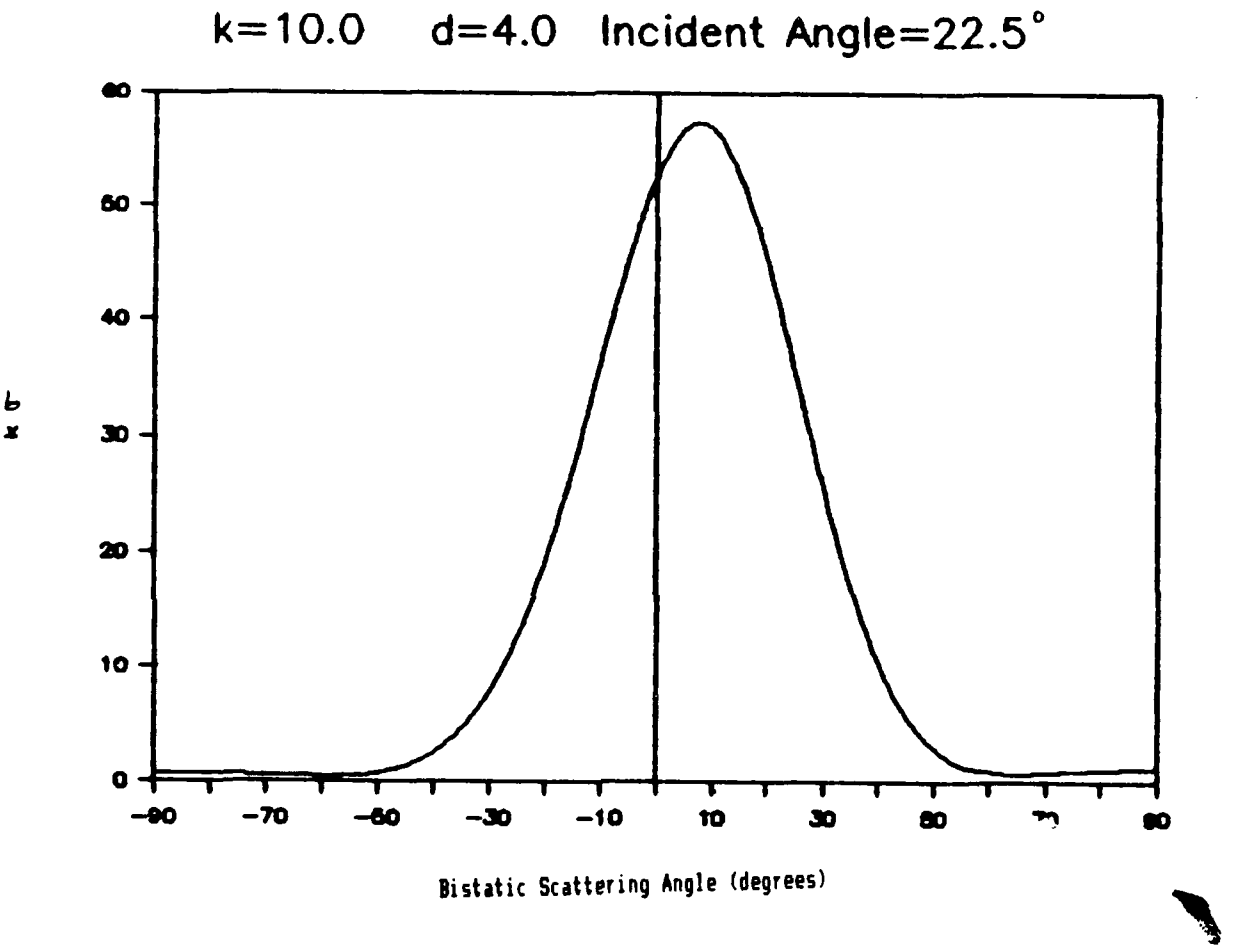

Figure 38. Bistatic RCS of a Rectangular Cavity With a Normalized Wave Number, k, Equal to 10.0, a Cavity Depth, d, of 4.0, and an Incident Plane Wave With θ_i = 22.5°.

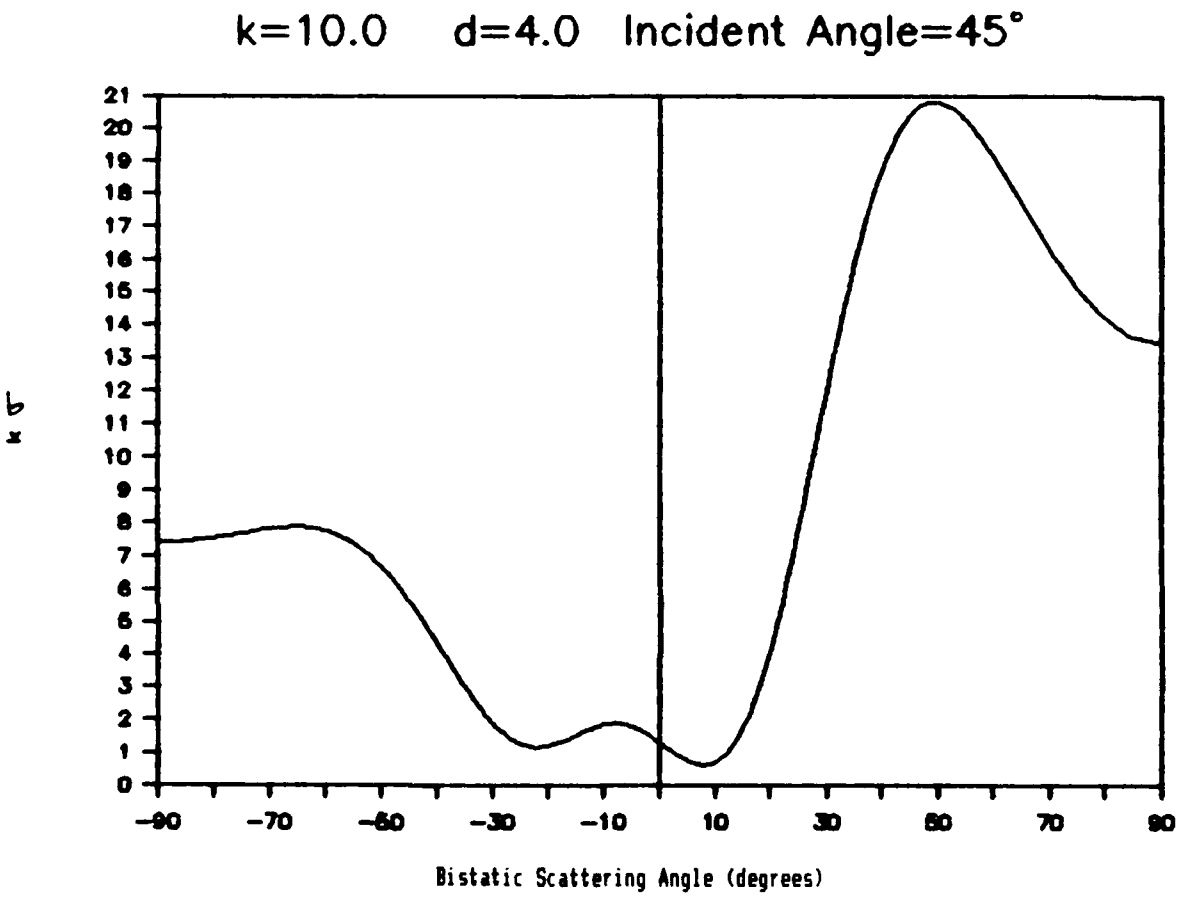

Figure 39. Bistatic RCS of a Rectangular Cavity With a Normalized Wave Number, k, Equal to 10.0, a Cavity Depth, d, of 4.0, and an Incident Plane Wave With θ_i = 45.0°.

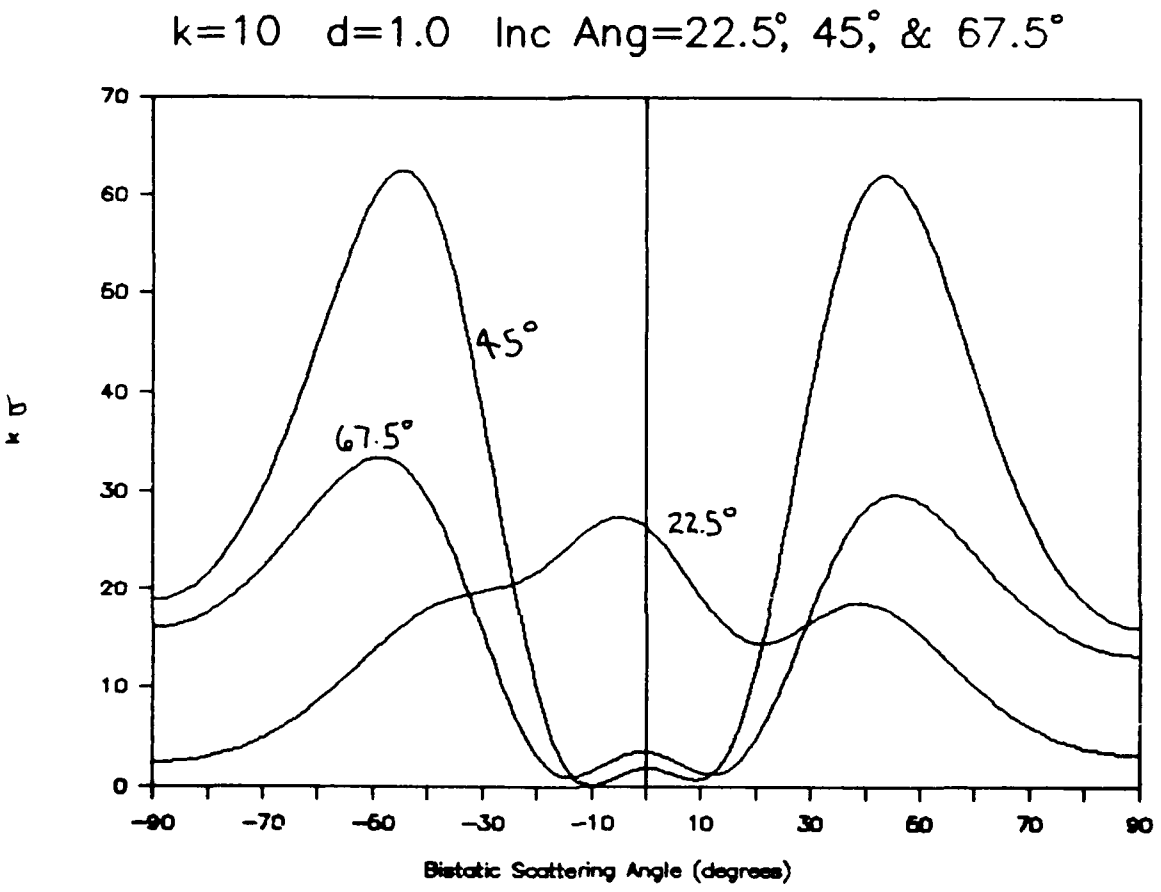

Figure 40. Bistatic RCS of a Rectangular Cavity With a Normalized Wave Number, k, Equal to 10.0, a Cavity Depth, d, of 1.0, and an Incident Plane Wave With θ_i = 22.5°, 45°, and 67.5°.

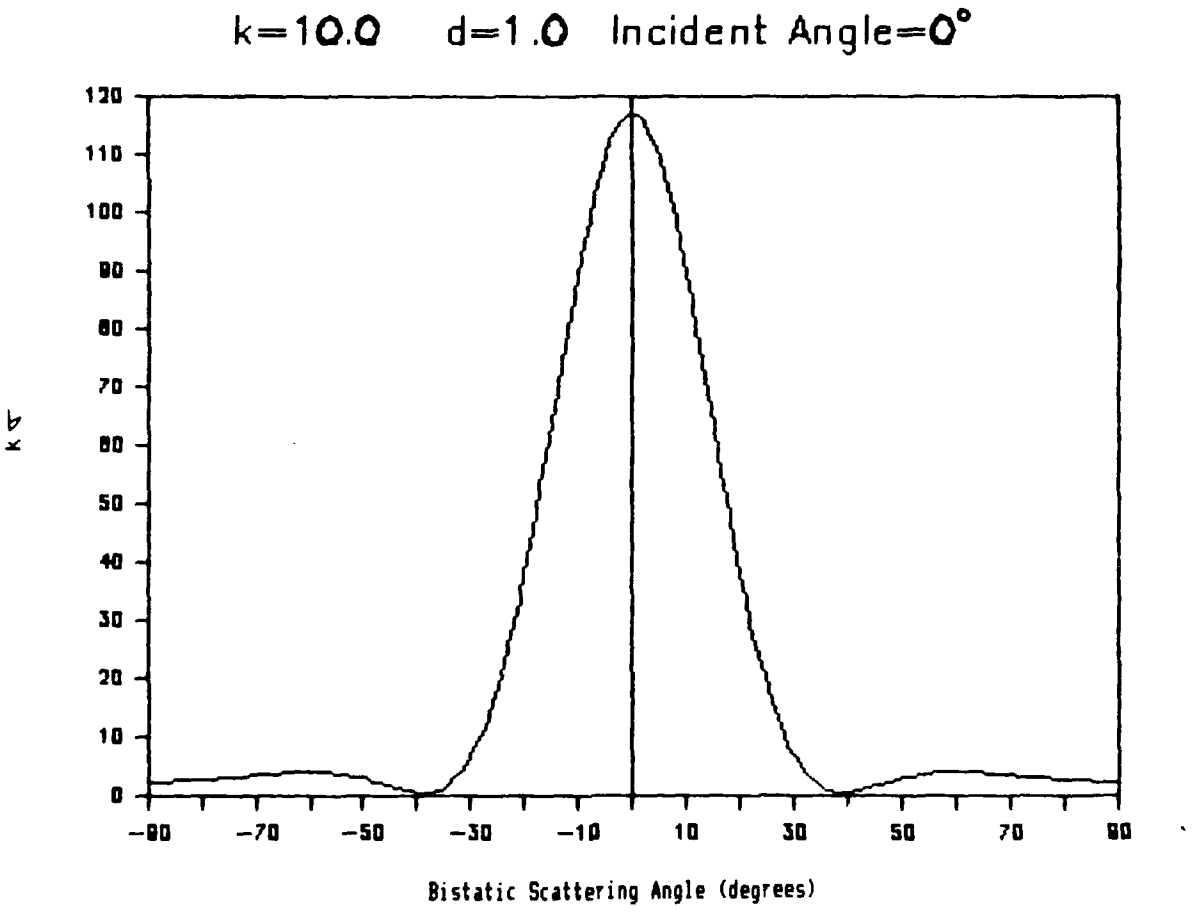

Figure 41. Bistatic RCS of a Rectangular Cavity With a Normalized Wave Number, k, Equal to 10.0, a Cavity Depth, d, of 1.0, and an Incident Plane Wave With $\theta_i = 0^o$.

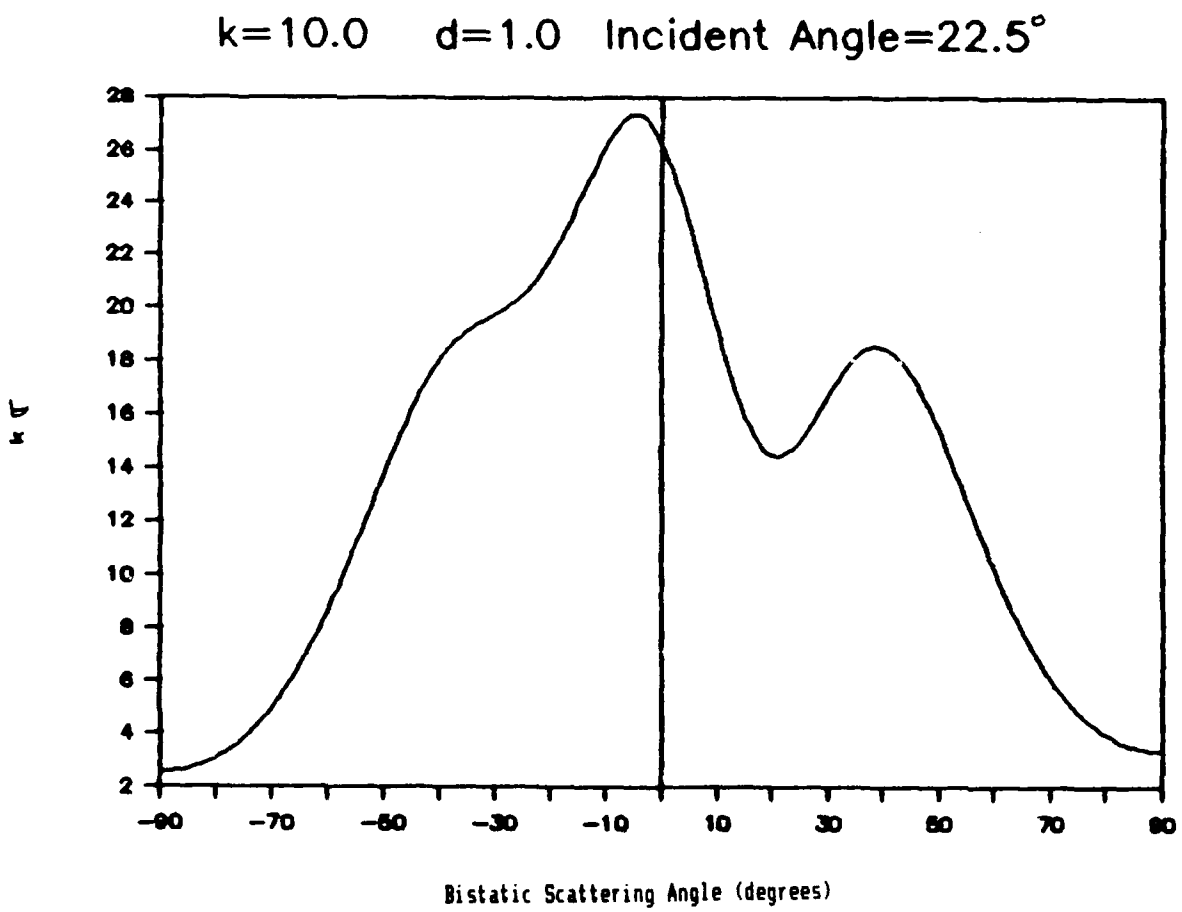

Figure 42. Bistatic RCS of a Rectangular Cavity With a Normalized Wave Number, k, Equal to 10.0, a Cavity Depth, d, of 1.0, and an Incident Plane Wave With θ_i = 22.5°.

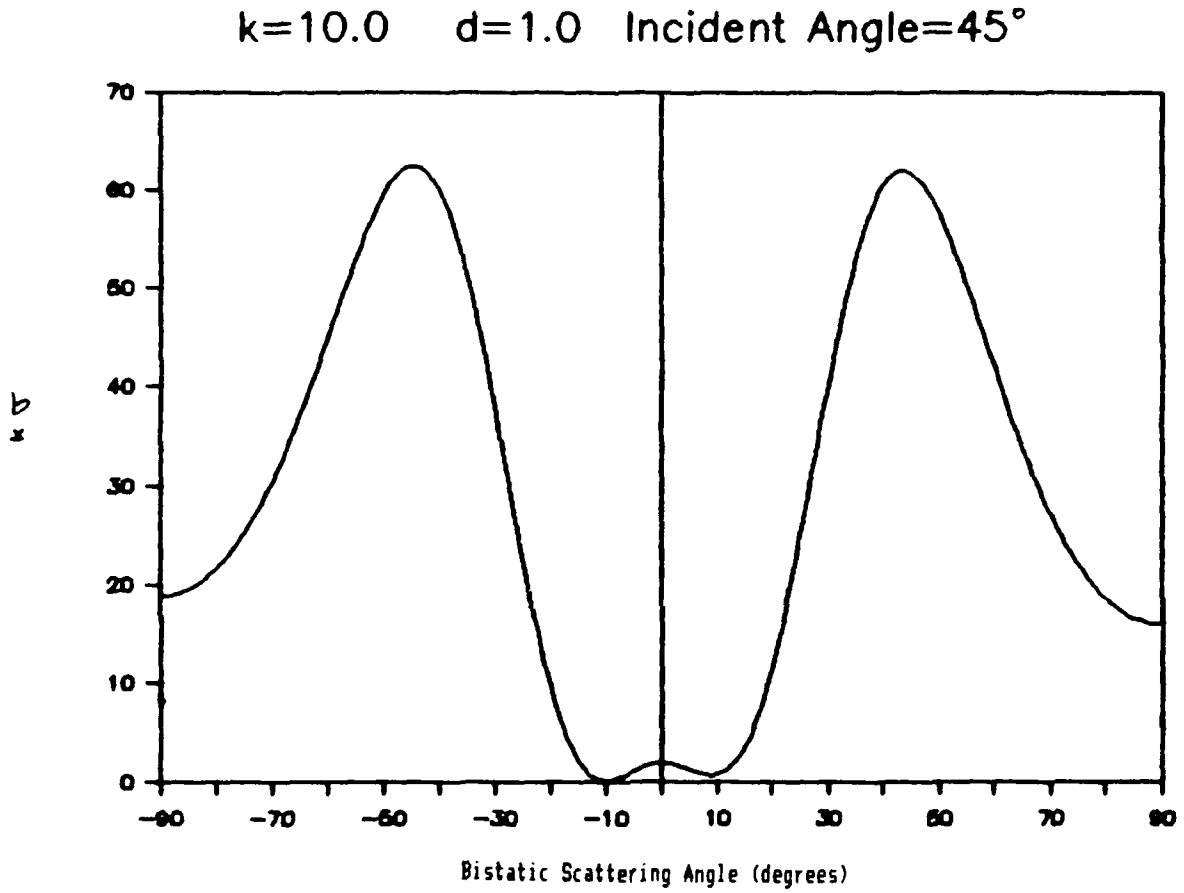

Figure 43. Bistatic RCS of a Rectangular Cavity With a Normalized Wave Number, k, Equal to 10.0, a Cavity Depth, d, of 1.0, and an Incident Plane Wave With θ_i = 45.0°.

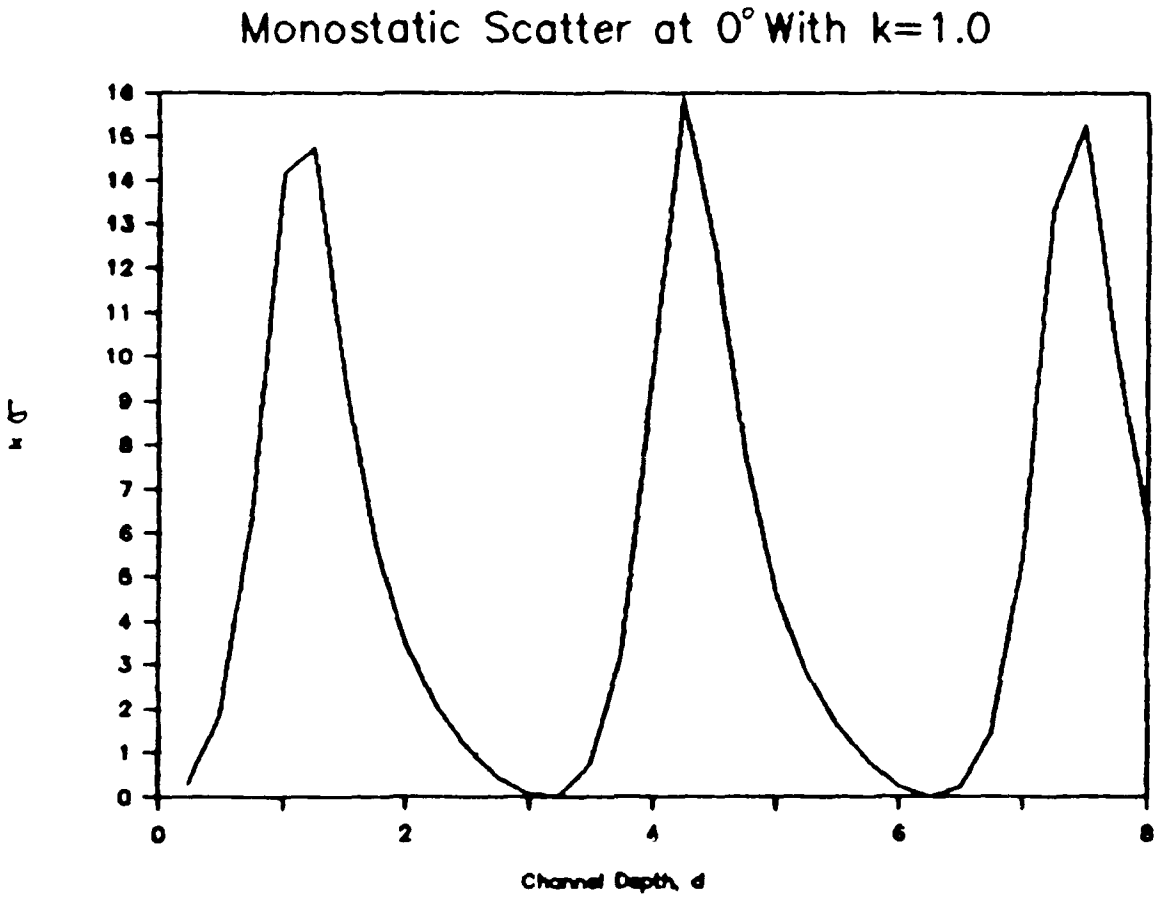

Figure 44. Monostatic RCS at 0° with Varying Depth and k=1.0

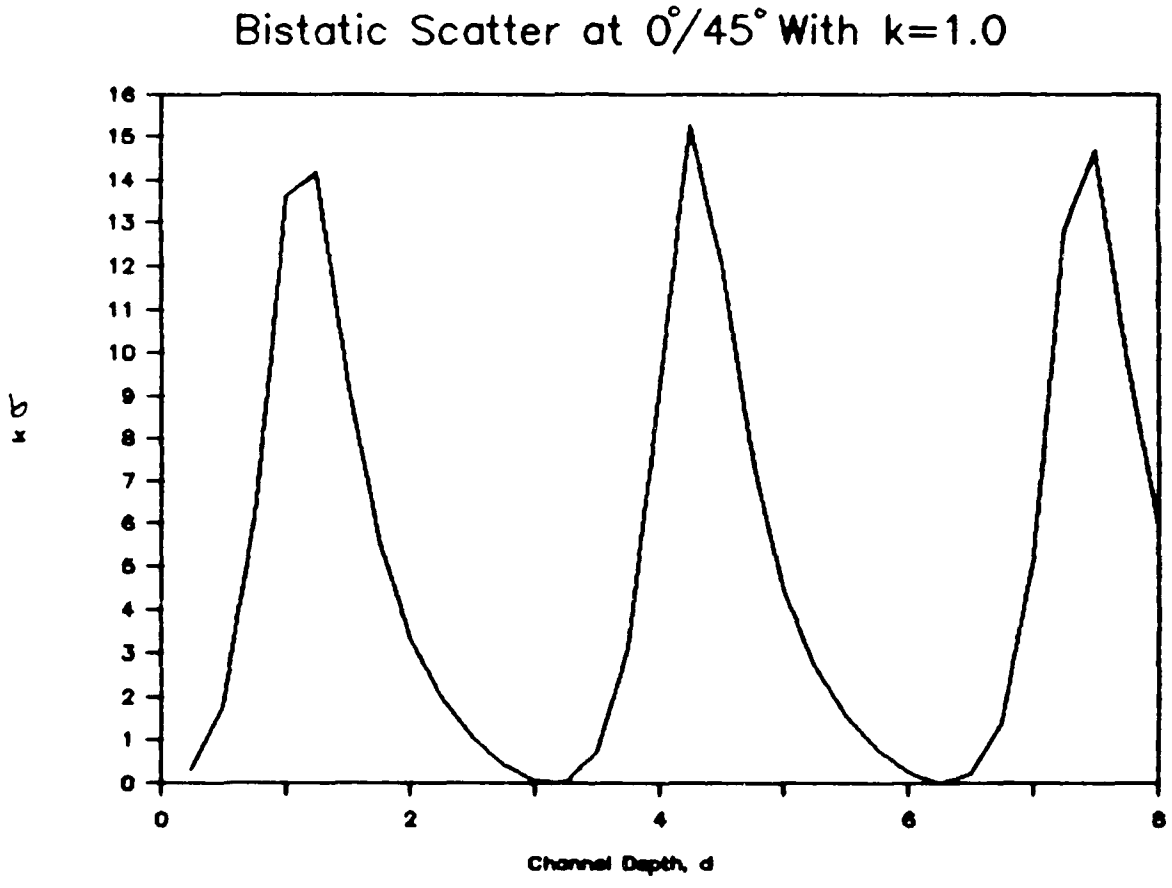

Figure 45. Bistatic RCS at $0^{o}/45^{o}$ with Varying Depth and K=1.0 Reciprocity is demonstrated again.

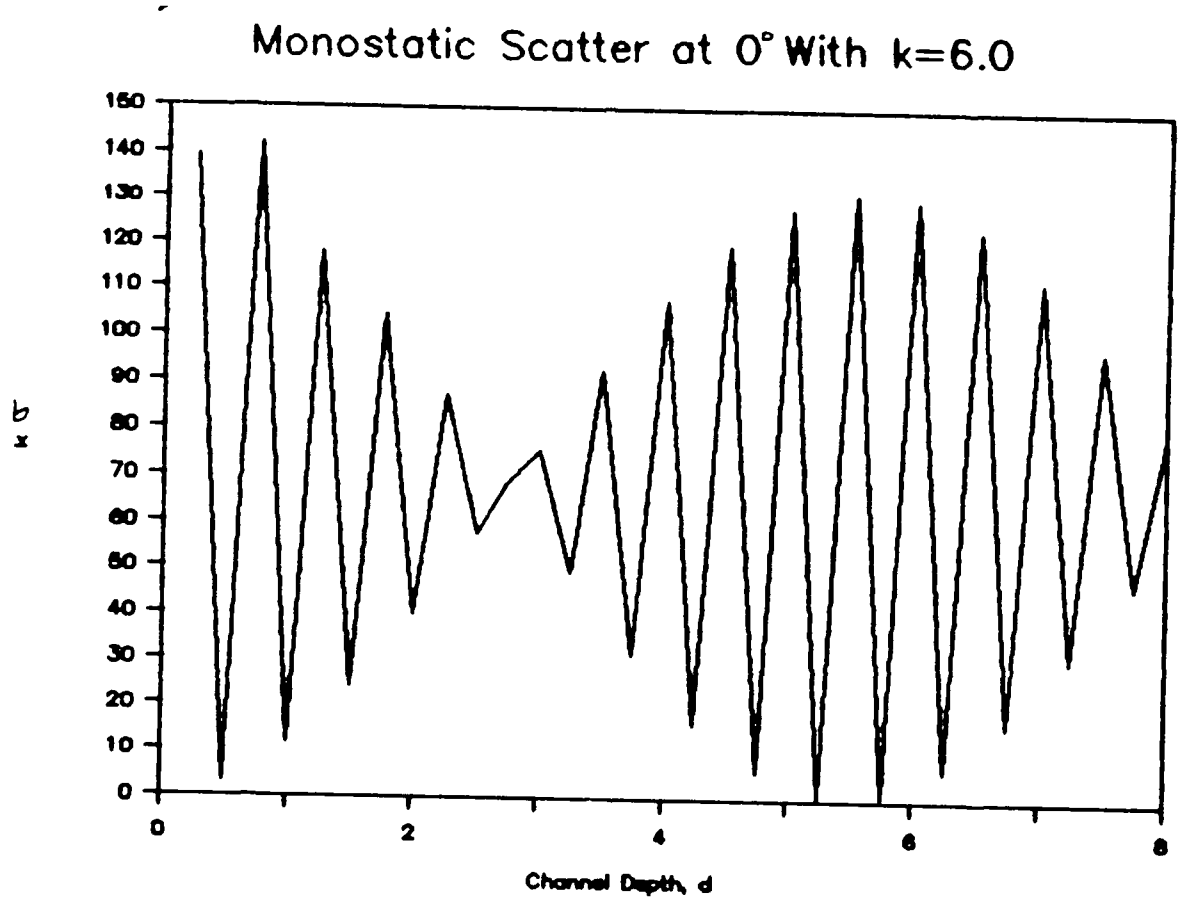

Figure 46. Monostatic RCS at 0° with Varying Depth and k=6.0

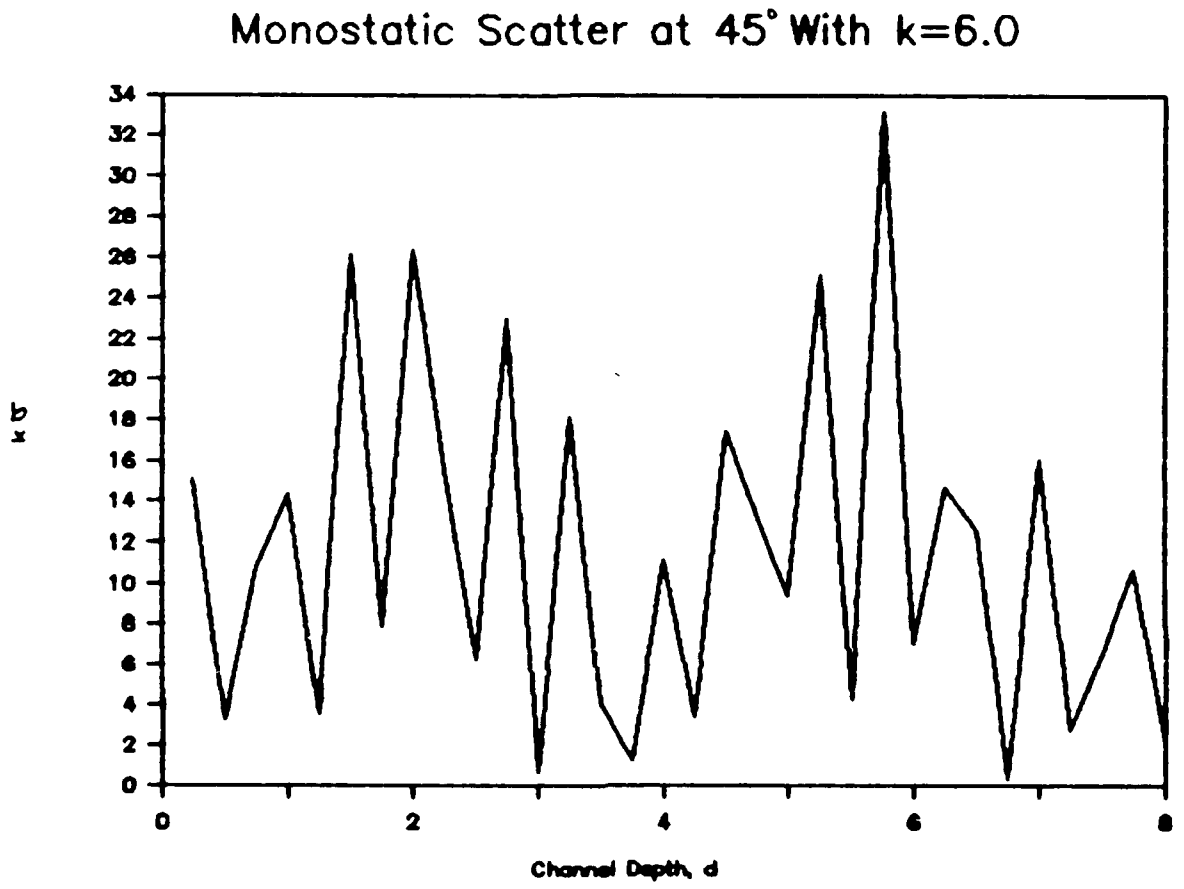

Figure 47. Monostatic RCS at 45° with Varying Depth and k=6.0

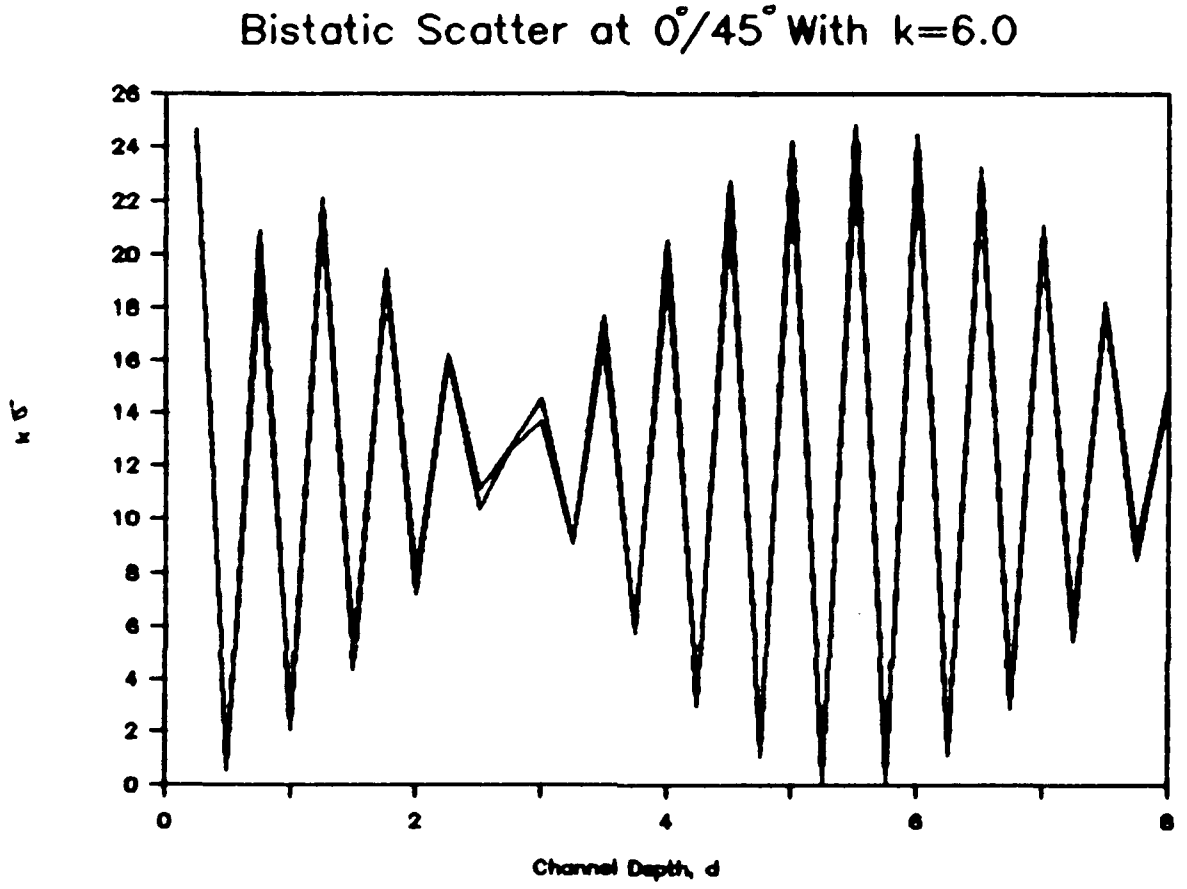

Figure 48. Bistatic RCS at 0°/45° with Varying Depth and k=6.0 Reciprocity is demonstrated once again.

Appendix C: A Model for Obtaining Measurements

A scatterer has been designed for a physical problem related to the example problem attacked in this thesis. Perhaps a follow-on thesis could concentrate on the measurements.

Measuring the fields scattered from the channel is not a trivial matter. The plane on which the incident fields impinge has been assumed, thus far, to be infinite. Such an infinite plane that is also perfectly conducting cannot be constructed. However, some approximations can be made to at least simplify those problems. Further, proper calibrations while making the measurements will also help create accurate measurements.

If the plane containing the channel to be measured cannot be infinite, then it should be very large; but how large? If the edges of the plane are in the far field, then it should be sufficiently large enough for the incident wave to "see" a cavity in an "infinite" plane. The far field is loosely defined as a distance, r, such that (22:21)

$$2\pi r >> \lambda$$

For most practical applications, the far field begins at about 10λ from the scatterer (9). In this problem, the scatterer is the cavity. If the edges of the plane were at least 10λ from the cavity center, they may be considered to be infinite.

The assumption of infinite conductivity needs to be considered when making measurements. Though perfect conductors do exist (i.e. superconductors), it is not yet practical to use them in most applications. A good approximation to a perfect conductor for problems of this type would be any "good" conductor. Aluminum is a good conductor (11). For measurement purposes it can be considered to be a PEC (9). A plane and cavity made of aluminum can therefore be approximated as perfect conductors.

When making the measurements, the system needs to be calibrated to nullify anomalies that may exist within the system (such as transmitter/receiver peculiarities, mounting scatter, etc.). If the system were calibrated using the above plane without the cavity, then most of the edge effects of the plane itself can be subtracted from the measurements along with the system anomalies. This will mostly leave only measurements of the fields due to the cavity alone. This is the same quantity, the integral in Eq (76), that has been calculated and plotted in the earlier sections of this thesis.

Using the described target and the described technique, it should be possible to duplicate the data plotted in the last section. The target has been designed and built and is the property of the Air Force Institute of Technology; to date, no measurements have been made.

In addition to a very large aluminum plane, an adjustable channel width and depth is also desired. Using all of the

above information, a drawing of the target that has been designed and built is given in Figure 49. The measurements given were derived assuming a measuring frequency between 8 GHz and 12.4 GHz but the target may be used at other frequencies due to its adjustability.

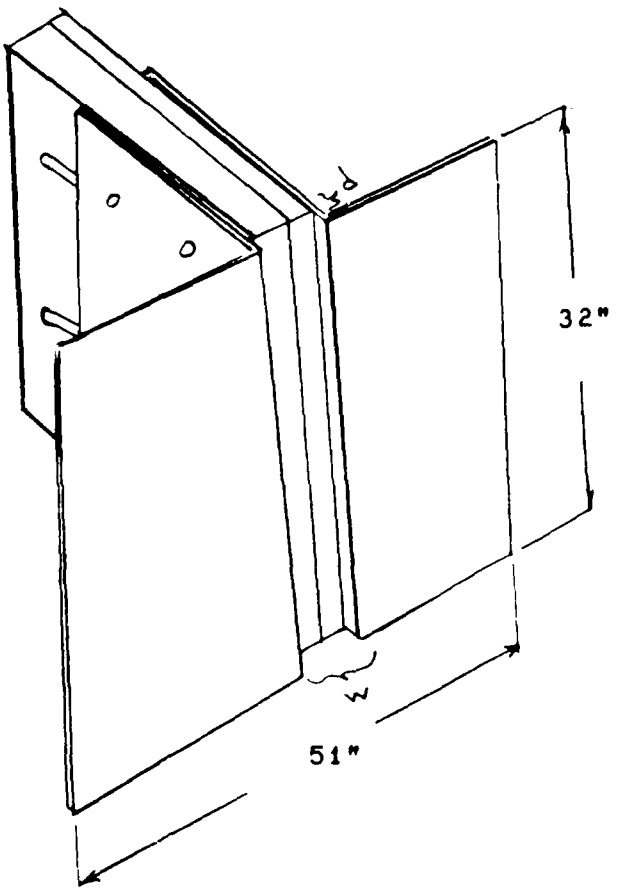

Figure 49. Target Designed to Produce Measurements for Comparison With the Calculated Data. The Target is Made of Aluminum and has Adjustable Rectangular Cavity Width and Depth.

Bibliography

1. Abramowitz, Milton and Irene A. Stegun. Handbook of Mathematical Functions With Formulas, Graphs, and Mathematical Tables. Washington D.C.: National Bureau of Standards Applied Mathematics Series No. 55, March 1965.

2. Ivanov, V.K. "On Linear Problems Which are not Well-Posed," Soviet Mathematics Doklady, Vol. 3, No. 2. (1962).

3. Harrington, Roger F. Field Computation by Moment Methods. Malabar, Florida: Robert E. Krieger Publishing Company, 1968.

4. Harrington, Roger F. Time-Harmonic Electromagnetic Fields. New York: McGraw Hill Book Company, 1961.

5. Harrington, Roger F. and Joseph R. Mautz. "A Generalized Network formulation for Aperture Problems," IEEE Transactions on Antennas and Propagation 870-873 (November, 1976)

6. Jost, Captain Randy J. Classroom lectures in EENG 630, Applications of EM Theory. School of Engineering, Air Force Institute of Technology (AU), Wright-Patterson AFB OH, January-March 1988.

7. Keller, J.B. "Geometrical Theory of Diffraction," Journal of Optical Society of America, 52: 116-130 (February 1962).

8. Kelly, E.J. "Scattering From Conducting Bodies of Revolution: Behavior of the Integral Equations Near Singular Points of Their Kernels," Massachusetts Institute of Technology Lincoln Laboratory, T.R. number 709 (also AD-A149226), (14 November 1984).

9. Knott, Eugene F. and others. Radar Cross Section. Norwood, Massachusetts: Artech House, Inc., 1985.

10. Kouyoumjian, Robert G. and Prabhakar H. Pathak. "A Uniform Geometrical Theory of Diffraction for an Edge in a Perfectly Conducting Surface," Proceedings of the IEEE 1448-1461 (November 1974).

11. Kraus, John D. Electromagnetics. New York: McGraw-Hill Book Company, 1984.

12. Mittra, R. Computer Techniques for Electromagnetics. New York: Pergamon Press, 1973.

13. Pedrotti, Frank L. and Leno S. Pedrotti. Introduction to Optics. Englewood Cliffs, NJ: Prentice-Hall, Inc., 1987

14. Plonus, Martin A. Applied Electromagnetics. New York: McGraw-Hill Book Company, 1978.

15. Poggio, A.J. and E.K. Miller. "Integral Equation Solutions of Three-dimensional Scattering Problems," Computer Techniques for Electromagnetics, Chapter 4, edited by R. Mittra. New York: Pergamon Press, 1973.

16. Ryan, Patricia A. TE Scattering from Short Bumps. MS thesis, Ohio State University School of Engineering, Columbus OH, November, 1987.

17. Sancer, M.I. and others. "Electromagnetic Scattering by an Object Embedded in a Stratified Medium." Air Force Weapons Laboratory TR-80-30 (also AD-A089649) under contract number F29601-78-C-0098 (August 1980).

18. Skinner, Captain Paul and Captain Randy J. Jost. "A Short Tutorial on the Methods of Geometrical Optics for Electromagnetic Scattering," Class handout distributed in EENG 630, Applications of EM Theory. School of Engineering, Air Force Institute of Technology (AU), Wright-Patterson AFB OH, February 1988.

19. Skinner, Captain Paul and Captain Randy J. Jost. "A Short Tutorial on the Methods of Physical Optics for Electromagnetic Scattering," Class handout distributed in EENG 630, Applications of EM Theory. School of Engineering, Air Force Institute of Technology (AU), Wright-Patterson AFB OH, February 1988.

20. Stratton, Julius Adams. Electromagnetic Theory. New York: McGraw-Hill Book Company, 1941.

21. Stutzman, W. L. and G. A. Thiele. Antenna Theory and Design. New York: John Wiley and Sons, 1981

22. Yaghjian, Arthur D., "Application of the Magnetic Field Integral Equation to the Solution for Scattering from Apertures in Perfectly Conducting Bodies," Proposed Thesis Topic from Rome Air Development Center, Air Force Systems Command, Hanscom AFB, MA to The Air Force Institute of Technology, AU, Wright-Patterson AFB, OH. (Undated).

23. Yaghjian, Arthur D. "Augmented Electric and Magnetic Field Integral Equations," Radio Science 16: 987-1001 (November-December 1981).

24. Yaghjian, Arthur D. "Augmented Electric and Magnetic Field Integral Equations," Rome Air Development Center In-House Report, RADC-TR-81-45 (also AD-A-103946), March 1981.

25. Yaghjian, Arthur D. "Broadside Radar Cross Section of the Perfectly Conducting Cube," IEEE Transactions on Antennas and Propagation, AP-33: 321-329 (March 1985).

26. Yaghjian, Arthur D. and others. Personal Interview; Meeting with thesis committee; Discussions on a possible thesis topic. 29 March 1988.

Vita

Ronald R. Fairbanks [redacted] He lived in the small town of Bradner, Ohio until graduating from LaKota High School in 1980. He then enrolled at Ohio Northern University and graduated in 1984 with a Bachelor of Science in Electrical Engineering degree. He went directly to officer training school having joined the USAF one year prior to college graduation. Upon commissioning, the then 2nd Lt Fairbanks was stationed at Wright-Patterson AFB, OH, at the Foreign Technology Division, Systems Directorate, Space Division, Space Subsystems Branch, where he was responsible for evaluating foreign space guidance and control systems. He entered the School of Engineering, Air Force Institute of Technology, in June of 1987. Since that time he has been promoted to Captain, USAF.

[redacted]

SECURITY CLASSIFICATION OF THIS PAGE

REPORT DOCUMENTATION PAGE

Form Approved
OMB No. 0704-0188

1a REPORT SECURITY CLASSIFICATION UNCLASSIFIED	1b RESTRICTIVE MARKINGS
2a SECURITY CLASSIFICATION AUTHORITY	3 DISTRIBUTION/AVAILABILITY OF REPORT Approved for Public Release; Distribution unlimited
2b DECLASSIFICATION/DOWNGRADING SCHEDULE	
4 PERFORMING ORGANIZATION REPORT NUMBER(S) AFIT/MA/GE/88D-1	5 MONITORING ORGANIZATION REPORT NUMBER(S)
6a NAME OF PERFORMING ORGANIZATION School of Engineering School of Mathematics 6b OFFICE SYMBOL (If applicable) AFIT/EN AFIT/MA (ENC)	7a NAME OF MONITORING ORGANIZATION
6c ADDRESS (City, State, and ZIP Code) Air Force Institute of Technology (AU) Wright-Patterson AFB, OH 45433-6583	7b ADDRESS (City, State, and ZIP Code)
8a NAME OF FUNDING/SPONSORING ORGANIZATION RADC/EECT 8b OFFICE SYMBOL (If applicable) RADC/EECT	9 PROCUREMENT INSTRUMENT IDENTIFICATION NUMBER
8c ADDRESS (City, State, and ZIP Code) RADC/EECT Hanscom AFB, MA 01731	10 SOURCE OF FUNDING NUMBERS PROGRAM ELEMENT NO. / PROJECT NO. / TASK NO / WORK UNIT ACCESSION NO

11 TITLE (Include Security Classification)
COUPLED INTEGRAL EQUATION SOLUTION FOR TWO-Dimensional BISTATIC TE SCATTER FROM A CONDUCTING CAVITY BACKED INFINITE PLANE (UNCLASSIFIED)

12 PERSONAL AUTHOR(S)
Ronald R. Fairbanks, Captain, USAF

13a TYPE OF REPORT	13b TIME COVERED	14 DATE OF REPORT (Year, Month, Day)	15 PAGE COUNT
MS Thesis	FROM _____ TO _____	December 1988	158

16 SUPPLEMENTARY NOTATION

17 COSATI CODES		
FIELD	GROUP	SUB-GROUP
12	01	
20	14	

18 SUBJECT TERMS (Continue on reverse if necessary and identify by block number)
Electromagnetic Scatter, Integral Equations, ~~Coupled~~ Fredholm, Two-Dimensional, Cavity, ~~Method~~ of Moments

19 ABSTRACT (Continue on reverse if necessary and identify by block number)

Thesis Advisor: Gregory T. Warhola, Captain, USAF, AFIT/ENC

12 Jan 1989

20 DISTRIBUTION/AVAILABILITY OF ABSTRACT ☒ UNCLASSIFIED/UNLIMITED ☐ SAME AS RPT ☐ DTIC USERS	21 ABSTRACT SECURITY CLASSIFICATION Unclassified
22a NAME OF RESPONSIBLE INDIVIDUAL Gregory T. Warhola, Capt, USAF	22b TELEPHONE (Include Area Code) (513) 255-4185 22c OFFICE SYMBOL AFIT/ENC

DD Form 1473, JUN 86 *Previous editions are obsolete.* SECURITY CLASSIFICATION OF THIS PAGE

Abstract

The purpose of this thesis is to determine the scattered electromagnetic fields and radar cross section from a two-dimensional cavity in a perfectly electric conducting infinite plane. This is accomplished by deriving a coupled set of Fredholm integral equations of the second kind. A set of integral equations outside the cavity and a set of integral equations inside the cavity are coupled together at the interface. The Fredholm integral equations of the second kind for the outside of the cavity use a Green's function with Neumann boundary conditions to avoid an integration over the infinite plane for a transverse electric incident plane wave. An example problem is introduced and numerically solved to test the application of the newly derived equations.